Assessing Forest and Fuels Management Operations Using Integrated Mobile Technologies and Remotely Sensed Data

A Dissertation
Presented in Partial Fulfillment of the Requirements for the
Degree of Doctor of Philosophy
with a
Major in Natural Resources
in the
College of Graduate Studies
University of Idaho
by
Ryer M. Becker

Approved by:
Major Professor: Robert F. Keefe, Ph.D.
Committee Members: Jan U.H. Eitel, Ph.D.; Mark Kimsey, Ph.D.; Randall H. Brooks, Ph.D.
Department Administrator: P. Charles Goebel, Ph.D.

May 2022

Abstract

Position, Navigation and Timing (PNT) technologies have rapidly become an integral part of our everyday lives, through mobile applications, activity sharing, global navigation satellite system (GNSS) supported devices, real-time monitoring of consumer goods and the Internet of Things (IoT). Further, remote sensing data provide unique solutions for aiding PNT methods and techniques in the planning and assessment of active land management through the derivation of site and stand metrics used to develop models. Increased ease of access to a wide range of data sources has supported the expansion of network infrastructures and availability for data sharing and transfer at local and global scales. High-resolution, remotely sensed data and mobile, off-the-grid data collection and interpretation methods provide valuable solutions for production analysis, treatment analysis and data sharing in natural resource management scenarios. Precision forestry and production analytics for industrial forest and fire operations are rapidly transforming through the integration of global navigation satellite system and radio frequency (GNSS-RF) enabled devices, smartphone-based inertial sensors, and high resolution remotely sensed data. Consumer available technologies and data provide the means to collect, share and analyze spatially explicit data using multi-transponder mesh networks and activity recognition models. However, the application of these technologies in operational forest management scenarios for activity recognition and production analysis has received very little attention in formal research. By evaluating operational applications of PNT technologies in forest management, mangers may be able to maximize their effective mobilization effort to manage land and improve on optimization of the operations themselves. Additionally, coupled use of high resolution remotely sensed data with real-time location and activity analytics may provide insight into management effectiveness and post-treatment stand conditions at landscape scales to assist managers in the strategic planning and implementation of future operations.

Acknowledgments

I would like to thank my major professor, Dr. Robert F. Keefe, for his continuous support and encouragement throughout the completion of this dissertation. His mentorship, leadership, and passion for research pushed me to expand my professionalism, strive for excellence, and foster a desire to continue research and academic pursuits into the future. This project would not have reached the level of success it has without his support and contributions. I would also like to thank my committee members; Dr. Randy Brooks, Dr. Mark Kimsey, and Dr. Jan Eitel, for all they have contributed to my development as a scientist and teacher. Their expertise and wisdom have been invaluable throughout the entirety of this project.

This project was funded, in part, by the Joint Fire Sciences Program grant no. 13-1-05-7, the Agriculture and Food Research Initiative Competitive Grant no. 2013-68005-21298 from the USDA National Institute of Food and Agriculture and by the Idaho Forest Utilization Research (FUR) program. The financial support from these programs made this research and my graduate work possible. I would also like to thank all the land managers, contractors, and student employees on the University of Idaho Experimental Forest for helping facilitate field work and sampling. This research would not have been possible without the support of these individuals.

Dedication

This work is dedicated to my incredible wife, Sophie, my family both near and far, and all my dear friends for their endless support and encouragement throughout this process. Thank you all for playing a significant role in making this time in Moscow and at the University of Idaho unforgettable. You have all contributed to my growth and successes as a husband, educator, researcher, and friend. Cheers, to Borrowed Time and future adventures.

A special dedication to my grandpa, Carmon F. Becker, for living a life and leaving a legacy that has and will continue to shape me as a man, husband, father, forester, and steward of nature.

Table of Contents

List of Tables

List of Figures

Statement of Contribution

Ryer M. Becker was primarily responsible for all project development, planning, execution, data analysis, and manuscript completion as required by the graduate committee. Contributions from co-authors included supporting the primary manuscript editing efforts of Mr. Becker. As faculty advisor, Dr. Keefe contributed to initial project planning for all research performed in this dissertation.

Chapter 1: Technological Advancement, Innovation, and Integration in Forest Operations

1.1 Introduction

Emerging technologies and big data are transforming work processes in natural resource management through enhanced analytics. Interest in the rapid integration of advanced technologies provides unique opportunities to advance the field of precision forestry and embrace the continued digitalization of the forest industry. Applications for integrating these technologies and processes into traditional management tasks include production and cost analysis, treatment monitoring, activity recognition, resource mobilization and optimization, and management planning. Advances in mobile technologies and remotely sensed data provide new opportunities to improve the production, sustainability, effectiveness, and safety of forest operations. However, it is necessary to evaluate the specific operational applications of these technologies to ensure their efficient and effective use. Ultimately, the development of advanced solutions to support operational forestry using mobile technologies and remote sensing establishes a foundation for continued development and integration across natural resource management activities and beyond.

1.2 Opportunities for Remotely Sensed Data in Forest and Fire Operations

Remotely sensed data is a significant resource in the planning and implementation efforts of natural resource managers. To address the evolving needs of resource managers, these data provide opportunities to transform how the planning and assessment of management activities are handled. Remote sensing, specifically light detection and ranging (lidar), is currently used extensively in forest, range, and fire management [1]–[7]. However, as increased emphasis is placed on the improved planning and execution of management tasks through the application of precision forestry-based processes, new applications of remotely sensed data must be developed.

With increasingly challenging fire conditions and hazardous fuel loadings, increased effort has been placed on treating forest fuels to reduce the risk of severe wildland fire. Of these fuel treatment options, mechanical treatments using mastication have increased in use [8]. After mastication, the physical characteristics of these resultant fuels is a key driver of fire behavior if these areas eventually burn [8], [9]. Manual field sampling procedures exist for predicting total surface fuel loading but these methods are time consuming and costly, limiting their use for widespread implementation [1], [10]–[12]. Further, these methods depend on sampling performed post-treatment, limiting their utility for the planning and feasibility assessment of treatments prior to use. Previous

work has successfully used remotely sensed data to quantify fuel loads post-treatment, which provides information needed for subsequent fire behavior modelling [13]–[27]. While valuable, these findings are limited to areas where treatments have already occurred, and this limits their benefit when attempting to plan for landscape scale fire behavior modelling and fuel treatments.

With extensive acreage requiring some level of fuel treatment to reduce the risk of severe wildland fire, tools are needed to assist land managers in making decisions regarding the optimal use of mechanical fuel treatments across the landscape prior to implementing treatments. Predicting post-treatment fuel loads prior to treatment to enable landscape scale fire behavior modelling and treatment efficacy is needed. While no processes to predict post-treatment mastication fuel loading from pre-treatment conditions currently exist, remotely sensed data may provide opportunities to perform these landscape scale predictions and support the planning and assessment of mechanical fuel treatments to reduce the risk of severe wildfire in forested landscapes.

The first step in this process is determining if relationships exist between pre-treatment lidar-derived forest metrics and post-treatment surface fuel loading. If relationships exist, this will enable the extrapolation of these relationships at high resolution and provide fuel loading and physical characteristics needed for fire behavior modelling and assessment over large spatial extents. Having the ability to model fire behavior in higher resolution prior to treatment could help managers assess the efficacy of mechanical fuel treatments in management areas to determine whether fuel treatment costs are justified. In Chapter 2, we evaluated whether pre-treatment lidar-derived forest metrics can be used to predict surface fuel loads and associated fuel characteristics following mastication treatments. Masticated fuels were sampled and quantified across varying pre-treatment stand conditions to determine if relationships exist between the masticated fuel loads and lidar-derived forest metrics prior to treatment including trees per hectare, basal area, volume per hectare, and stand density index (SDI). Additionally, relationships between pre-treatment metrics and additional fuel bed characteristics including depth, size class distribution, and bulk density were assessed.

1.3 GNSS-RF and Location Data for Forest and Fire Operations

Along with remotely sensed data, mobile devices provide new opportunities to advance the field of precision forestry and forest digitalization. Global navigation satellite system (GNSS) equipped mobile devices have been widely incorporated into forest operations and management tasks to quantify the production and efficiency of work tasks of forest machines [28]–[38]. While

conventional GNSS devices provide valuable information to support location analytics after the fact, they lack the ability to transfer data in machine-to-machine (m2m) applications.

To overcome this limitation through ad-hoc networking at remote jobsites, more recent studies have evaluated the potential for GNSS devices equipped with radio frequency (RF) communication to enable data sharing and transfer in real-time in remote, off-the-grid environments for logging safety and production analysis [39]–[44]. Preliminary work by Becker and Keefe [39] used GNSS-RF devices to characterize the swing movements of forest machines with real-time data sharing between two GNSS-RF transponders and a receiving unit. The sampling and modelling processes used to develop a basic activity recognition model for machine movements in a controlled setting proved effective in the initial study, but additional work was needed to evaluate and improve on the methodology in operational environments and under forest canopies.

In order to build on the initial GNSS-based equipment activity recognition by Becker and Keefe [39], the third chapter of this dissertation examined the use of GNSS-RF devices to develop activity recognition models for mastication equipment implementing mechanical fuel treatments. In addition to assessing the effectiveness of GNSS-RF devices for modeling the productive cycle elements of mastication equipment, the impact of forest metrics on treatment production and model accuracy was also quantified. Findings from this work show the opportunities and limitations of using consumer-grade devices for real-time data collection, sharing, and subsequent production analysis of mechanical fuel treatments. As the forest industry continues to move toward digitalization, the importance of real-time systems that can quickly and effectively process and communicate big data in real time will increase. The collection, sharing and analysis of complex spatiotemporal data is especially relevant for forestry and fire applications for which access to internet and cellular connectivity is generally unavailable.

1.4 Mobile Devices and Sensor-based Activity Recognition for Forest and Fire Operations

Despite their proven success for some activity recognition applications, the accuracy of the positioning data from GNSS-RF devices is affected by forest canopies and topographic features [30], [31], [37], [45]–[49]. This limits their use in situations where GNSS-based activity recognition (AR) models are expected to accurately capture precise movements and activities of desired individuals or machinery [49]. Other mobile technologies may provide improved accuracy over GNSS-RF devices, specifically smart devices equipped with inertial measurements units (IMUs). Mobile phone IMUs and other sensors provide a high-resolution data source for classifying activities in real time. Mobile

smart devices including smartwatches and smartphones have been widely used in human activity recognition (HAR) given their ubiquity, affordability, ease of use, and powerful computing capabilities [50]–[52]. These activity recognition models are used in healthcare, wellness, intelligent environment, and commerce applications [53]–[61]. There are few examples of developing and evaluating activity recognition models for natural resource applications, e.g. [62]–[66]. Further, no current research has examined the development of a stand-alone smartphone-based activity recognition model for tracked forest machines.

While many newly released forestry machines are equipped with integrated production monitoring systems, these are generally proprietary and specific to equipment manufacturer and equipment type, limiting their use in comparative analysis and synthesis of supply chain logistics data. The development of a stand-alone smartphone-based activity recognition model for forestry equipment could provide a ubiquitous, consumer-available solution. The successful development of initial models could provide proof-of-concept and support the subsequent creation of a library of activity recognition models for a variety of forest management tasks and operational systems. Development of an AR library specific to operational forestry could benefit equipment operators, researchers, and contractors monitoring supply chain and work productivity logistics using readily available devices. For researchers, the models would provide an automated, continuous alternative to traditional time and motion studies, which are time consuming, costly, and generally specific to local site and operator conditions.

To advance science related to equipment activity recognition in forestry, a stand-alone smartphone-based activity recognition model for a tracked mastication machine was developed and tested in Chapter 4. We performed a time and motion study for mastication treatments while simultaneously collecting triaxial gyroscope ($rad^{1}sec^{-2}$), triaxial accelerometer ($m^{1}sec^{-2}$) and sound pressure (dB) data from smartphone-based inertial measurement units (IMU) mounted within the machine cab. Random forest (RF) machine learning algorithms were used to develop the AR models using the smartphone data. RF models were defined by three primary parameters and were examined to determine their impact of activity recognition modelling effectiveness. Forty unique RF algorithms were developed representing all combinations of selected parameters. Model parameters included sampling rate (Hz), sliding window size (seconds), and window overlap (%). After development, these AR models were validated using the time and motion study to determine the best performing combination of sensors, sampling rate, window size, and window overlap. Additionally, the feasibility of merging individual tree inventory data from lidar with these activity recognition models was studied in Chapter 4.

Lidar-derived characterization of stand- and tree-level features has a long history in forest health, biometrics and more recently forest operations research [3], [4], [7], [67]–[75]. Advances in individual tree detection and segmentation from lidar data further increases opportunities to use this data in forest management [17], [76]–[80]. However, these data can also support equipment production estimation and improved precision in supply chain analysis when individual trees and their associated physical characteristics are linked to individual work elements of forestry equipment derived from activity recognition models. This integration of smartphone-based activity recognition with individual-tree lidar products has not previously been studied and provides an opportunity to increase the resolution of production estimation for forest operations and the comparison of pre and post-treatment stand conditions.

1.5 Literature Cited

1. M. J. Falkowski, P. E. Gessler, P. Morgan, A. T. Hudak, and A. M. S. Smith, "Characterizing and Mapping Forest Fire Fuels Using ASTER Imagery and Gradient Modeling," *For. Ecol. Manag.*, vol. 217, pp. 129–146, 2005, doi: 10.1016/j.foreco.2005.06.013.

2. S. E. Reutebuch, H.-E. Andersen, and R. J. McGaughey, "Light Detection and Ranging (LIDAR): An Emerging Tool for Multiple Resource Inventory," *J. For.*, vol. September, pp. 286–292, 2005.

3. A. E. Akay, H. Oğuz, I. R. Karas, and K. Aruga, "Using LiDAR Technology in Forestry Activities," *Environ. Monit. Assess.*, vol. 151, pp. 117–125, 2009, doi: 10.1007/s10661-008-0254-1.

4. M. J. Falkowski, J. S. Evans, S. Martinuzzi, P. E. Gessler, and A. T. Hudak, "Characterizing Forest Succession with Lidar Data: An Evaluation for the Inland Northwest, USA," *Remote Sens. Environ.*, vol. 113, pp. 946–956, 2009, doi: 10.1016/j.rse.2009.01.003.

5. A. T. Hudak *et al.*, "Quantifying Aboveground Forest Carbon Pools and Fluxes from Repeat LiDAR Surveys," *Remote Sens. Environ.*, vol. 123, pp. 25–40, 2012, doi: 10.1016/j.rse.2012.02.023.

6. M. A. Wulder *et al.*, "Lidar Sampling for Large-area Forest Characterization: A Review," *Remote Sens. Environ.*, vol. 121, pp. 196–209, 2012, doi: 10.1016/j.rse.2012.02.001.

7. R. M. Becker, R. F. Keefe, N. M. Anderson, and J. U. H. Eitel, “Use of Lidar-derived Landscape Parameters to Characterize Alternative Harvest System Options in the Inland Northwest,” *Int. J. For. Eng.*, vol. 29, no. 3, pp. 179–191, 2018, doi: 10.1080/14942119.2018.1497255.

8. J. K. Agee and C. N. Skinner, “Basic Principles of Forest Fuel Reduction Treatments,” For. Ecol. Manag., vol. 211, pp. 83–96, 2005, doi: 10.1016/j.foreco.2005.01.034.

9. J. M. Kane, J. M. Varner, and E. E. Knapp, “Novel Fuelbed Characteristics Associated with Mechanical Mastication Treatments in Northern California and Southwestern Oregon, USA,” *Int. J. Wildland Fire*, vol. 18, pp. 686–697, 2009, doi: 10.1071/WF08072.

10. L. A. Arroyo, C. Pascual, and J. A. Manzanera, “Fire Models and Methods to Map Fuel Types: The Role of Remote Sensing,” *For. Ecol. Manag.*, vol. 256, pp. 1239–1252, 2008, doi: 10.1016/j.foreco.2008.06.048.

11. R. E. Keane, R. Burgan, and J. vanWagtendonk, “Mapping Wildland Fuels for Fire Management Across Multiple Scales: Integrating Remote Sensing, GIS, and Biophysical Modeling,” *Int. J. Wildland Fire*, vol. 10, pp. 301–319, 2001, doi: 10.1071/WF01028.

12. M. G. Rollins, R. E. Keane, and R. A. Parsons, “Mapping Fuels and Fire Regimes Using Remote Sensing, Ecosystem Simulation, and Gradient Modeling,” *Ecol. Appl.*, vol. 14, no. 1, pp. 75–95, 2004.

13. N. S. Skowronski, K. L. Clark, M. Duveneck, and J. Hom, “Three-dimensional Canopy Fuel Loading Predicted Using Upward and Downward Sensing LiDAR Systems,” *Remote Sens. Environ.*, vol. 115, pp. 703–714, 2011, doi: 10.1016/j.rse.2010.10.012.

14. H.-E. Andersen, R. J. McGaughey, and S. E. Reutebuch, “Estimating Forest Canopy Fuel Parameters Using LIDAR Data,” *Remote Sens. Environ.*, vol. 94, pp. 441–449, 2005, doi: 10.1016/j.rse.2004.10.013.

15. T. L. Erdody and L. M. Moskal, “Fusion of LiDAR and Imagery for Estimating Forest Canopy Fuels,” *Remote Sens. Environ.*, vol. 114, pp. 725–737, 2010, doi: 10.1016/j.rse.2009.11.002.

16. Y. Chen, X. Zhu, M. Yebra, S. Harris, and N. Tapper, “Development of a Predictive Model for Estimating Forest Surface Fuel Load in Australian Eucalypt Forests with LiDAR Data,” *Environ. Model. Softw.*, vol. 97, pp. 61–71, 2017, doi: 10.1016/j.envsoft.2017.07.007.

17. M. K. Jakubowksi, Q. Guo, B. Collins, S. Stephens, and M. Kelly, “Predicting Surface Fuel Models and Fuel Metrics Using Lidar and CIR Imagery in a Dense, Mountainous Forest,” *Photogramm. Eng. Remote Sens.*, vol. 79, no. 1, pp. 37–49, 2013.

18. M. Mutlu, S. C. Popescu, C. Stripling, and T. Spencer, “Mapping Surface Fuel Models Using Lidar and Multispectral Data Fusion for Fire Behavior,” *Remote Sens. Environ.*, vol. 112, pp. 274–285, 2008, doi: 10.1016/j.rse.2007.05.005.

19. J. A. N. Van Aardt, M. Arthur, G. Sovkoplas, and T. L. Swetnam, “LiDAR-based Estimation of Forest Floor Fuel Loads Using a Novel Distributional Approach,” University of Tasmania, Australia, Oct. 2011, pp. 1–8.

20. M. Mutlu, S. C. Popescu, and K. Zhao, “Sensitivity Analysis of Fire Behavior Modeling with LIDAR-derived Surface Fuel Maps,” *For. Ecol. Manag.*, vol. 256, pp. 289–294, 2008, doi: 10.1016/j.foreco.2008.04.014.

21. H. A. Kramer, B. M. Collins, M. Kelly, and S. L. Stephens, “Quantifying Ladder Fuels: A New Approach Using LiDAR,” *Forests*, vol. 5, pp. 1432–1453, 2014, doi: 10.3390/f5061432.

22. N. Skowronski, K. Clark, R. Nelson, J. Hom, and M. Patterson, “Remotely Sensed Measurements of Forest Structure and Fuel Loads in the Pinelands of New Jersey,” *Remote Sens. Environ.*, vol. 108, pp. 123–129, 2007, doi: 10.1016/j.rse.2006.09.032.

23. M. García, D. Riaño, E. Chuvieco, J. Salas, and F. M. Danson, “Multispectral and LiDAR Data Fusion for Fuel Type Mapping Using Support Vector Machine and Decision Rules,” *Remote Sens. Environ.*, vol. 115, pp. 1369–1379, 2011, doi: 10.1016/j.rse.2011.01.017.

24. B. Koetz, F. Morsdorf, S. van der Linden, T. Curt, and B. Allgower, “Multi-source Land Cover Classification for Forest Fire Management Based on Imaging Spectrometry and LiDAR Data,” *For. Ecol. Manag.*, vol. 256, pp. 263–271, 2008, doi: 10.1016/j.foreco.2008.04.025.

25. O. F. Price and C. E. Gordon, “The Potential for LiDAR Technology to Map Fire Fuel Hazard Over Large Areas of Australian Forest,” *J. Environ. Manage.*, vol. 181, pp. 663–673, 2016, doi: 10.1016/j.jenvman.2016.08.042.

26. M. García *et al.*, “Extrapolating Forest Canopy Fuel Properties in the California Rim Fire by Combining Airborne LiDAR and Landsat OLI Data,” *Remote Sens.*, vol. 9, no. 394, pp. 1–19, 2017, doi: 10.3390/rs9040394.

27. Y. Chen, X. Zhu, M. Yebra, S. Harris, and N. Tapper, “Strata-based Forest Fuel Classification for Wild Fire Hazard Assessment Using Terrestrial LiDAR,” *J. Appl. Remote Sens.*, vol. 10, no. 4, 2016, doi: 10.1117/1.JRS.10.046025.

28. T. McDonald, “Time Study of Harvesting Equipment Using GPS-Derived Positional Data,” Edinburgh University, Edinburgh, Scotland, GIS Technical Papers, 1999.

29. T. P. McDonald, SE. Taylor, and R. B. Rummer, “Deriving Forest Harvesting Machine Productivity from Positional Data,” Milwaukee, Wisconsin, USA, Jul. 2000, pp. 1–8.

30. S. E. Taylor, T. P. McDonald, M. W. Veal, and T. E. Grift, “Using GPS to Evaluate Productivity and Performance of Forest Machine Systems,” Seattle, WA, USA, Jun. 2001, pp. 1–20.

31. M. W. Veal, S. E. Taylor, T. P. McDonald, D. K. McLemore, and M. R. Dunn, “Accuracy of Tracking Forest Machines with GPS,” *Trans. Am. Soc. Agric. Eng.*, vol. 44, pp. 1903–1911, 2001.

32. T. P. McDonald and J. P. Fulton, “Automated Time Study of Skidders Using Global Positioning System Data,” *Comput. Electron. Agric.*, vol. 48, pp. 19–37, 2005, doi: 10.1016/j.compag.2005.01.004.

33. C. F. de Hoop and R. H. Dupré, “Using GPS to Document Skidder Motions- A Comparison with Manual Data Collection,” in *Working Globally – Sharing Forest Engineering Challenges and Technologies Around the World*, Coeur d’Alene, ID, USA, Aug. 2006, pp. 1–11.

34. R. Gallo, S. Grigolato, R. Cavalli, and F. Mazzetto, “GNSS-based Operational Monitoring Devices for Forest Logging Operation Chains,” *J. Agric. Eng.*, vol. 44, no. 2, pp. 140–145, 2013, doi: 10.4081/jae.2013.s2.e27.

35. M. Hejazian, S. Hosseini, M. Lotfalian, and P. Ahmadikoolaei, “Possibility of Global Positioning System (GPS) Application for Time Studies in Forest Machinery,” *Eur. J. Exp. Biol.*, vol. 3, no. 4, pp. 93–98, 2013.

36. R. F. Keefe, J. U. H. Eitel, A. M. S. Smith, and Wade T. Tinkham, “Applications of multi transmitter GPS-VHF in Forest Operations,” presented at the Proceedings of the 47th International Symposium on Forestry Mechanization and 5th International Forest Engineering Conference, Gerardmer, France, Jan. 2014.

37. M. Strandgard and R. Mitchell, “Automated Time Study of Forwarders Using GPS and a Vibration Sensor,” *Croat. J. For. Eng.*, vol. 36, no. 2, pp. 175–184, 2015.

38. T. M. Oliveira, A. M. G. Barros, A. A. Ager, and P. M. Fernandes, “Assessing the Effect of a Fuel Break Network to Reduce Burnt Area and Wildfire Risk Transmission,” *Int. J. Wildland Fire*, vol. 25, pp. 619–632, 2016, doi: 10.1071/WF15146.

39. R. M. Becker, R. F. Keefe, and N. M. Anderson, “Use of Real-Time GNSS-RF Data to Characterize the Swing Movements of Forestry Equipment,” *Forests*, vol. 8, no. 44, pp. 1–15, 2017, doi: 10.3390/f8020044.

40. L. M. Grayson *et al.*, “Accuracy of WAAS-Enabled GPS-RF Warning Signals When Crossing a Terrestrial Geofence,” *Sensors*, vol. 16, no. 912, pp. 1–8, 2016, doi: doi:10.3390/s16060912.

41. A. M. Wempe and R. F. Keefe, “Characterizing Rigging Crew Proximity to Hazards on Cable Logging Operations Using GNSS-RF: Effect of GNSS Positioning Error on Worker Safety Status,” *Forests*, vol. 8, no. 357, pp. 1–17, 2017, doi: 10.3390/f8100357.

42. E. G. Zimbelman, R. F. Keefe, E. K. Strand, C. A. Kolden, and A. M. Wempe, “Hazards in Motion: Development of Mobile Geofences for Use in Logging Safety,” *Sensors*, vol. 17, no. 882, pp. 1–16, 2017, doi: 10.3390/s17040822.

43. S. M. Newman, R. F. Keefe, R. H. Brooks, E. Q. Ahonen, and A. M. Wempe, “Human Factors Affecting Logging Injury Incidents in Idaho and the Potential for Real Time Location-Sharing Technology to Improve Safety,” *Safety*, vol. 4, no. 4, pp. 1–28, 2018, doi: 10.3390/safety4040043.

44. A. M. Wempe, R. F. Keefe, S. M. Newman, and T. B. Paveglio, “Intent to Adopt Location Sharing for Logging Safety Applications,” *Safety*, vol. 5, no. 7, pp. 1–22, 2019, doi: 10.3390/safety5010007.

45. P. Sigrist, P. Coppin, and M. Hermy, “Impact of Forest Canopy on Quality and Accuracy of GPS Measurements,” *Int. J. Remote Sens.*, vol. 20, no. 18, pp. 3595–3610, 1999.

46. P. Bolstad, A. Jenks, J. Berkin, and K. Horne, “A Comparison of Autonomous, WAAS, Real-Time, and Post-Processed Global Positioning Systems (GPS) Accuracies in Northern Forests,” *North. J. Appl. For.*, vol. 22, no. 1, pp. 5–11, 2005.

47. H. Hasegawa and T. Yoshimura, “Estimation of GPS Positional Accuracy Under Different Forest Conditions Using Signal Interruption Probability,” *J. For. Res.*, vol. 12, pp. 1–7, 2007, doi: 10.1007/s10310-006-0245-4.

48. G. J. Devlin and K. McDonnell, “Performance Accuracy of Real-Time GPS Asset Tracking Systems for Timber Haulage Trucks Travelling on Both Internal Forest Road and Public Road Networks,” *Int. J. For. Eng.*, vol. 20, no. 1, pp. 45–49, 2009, doi: 10.1080/14942119.2009.10702575.

49. E. G. Zimbelman and R. F. Keefe, “Real-time Positioning in Logging: Effects of Forest Stand Characteristics, Topography, and Line-of-Sight Obstructions on GNSS-RF Transponder Accuracy and Radio Signal Propagation,” *PLoS ONE*, vol. 13, no. 1, pp. 1–17, 2018, doi: 10.1371/journal. pone.0191017.

50. M. Fahim, I. Fatima, S. Lee, and Y.-T. Park, “EFM: Evolutionary Fuzzy Model for Dynamic Activities Recognition Using a Smartphone Accelerometer,” *Appl. Intell.*, vol. 39, pp. 475–488, 2013, doi: 10.1007/s10489-013-0427-7.

51. O. D. Incel, M. Kose, and C. Ersoy, “A Review and Taxonomy of Activity Recognition on Mobile Phones,” *BioNano Sci.*, vol. 3, pp. 145–171, 2013, doi: 10.1007/s12668-013-0088-3.

52. R. San-Segundo, H. Blunck, J. Moreno-Pimentel, A. Stisen, and M. Gil-Martín, “Robust Human Activity Recognition Using Smartwatches and Smartphones,” *Eng. Appl. Artif. Intell.*, vol. 72, pp. 190–202, 2018, doi: 10.1016/j.engappai.2018.04.002.

53. S. Reddy, M. Mun, J. Burke, D. Estrin, and M. Hansen, “Using Mobile Phones to Determine Transportation Modes,” *ACM Trans. Sens. Netw.*, vol. 6, no. 2, pp. 1–27, 2010.

54. P. Casale, O. Pujol, and P. Radeva, “Human Activity Recognition from Accelerometer Data Using a Wearable Device,” 2011, pp. 289–296. doi: 10.1007/978-3-642-21257-4_36.

55. L. Chen, J. Hoey, C. D. Nugent, D. J. Cook, and Z. Yu, “Sensor-Based Activity Recognition,” *IEEE Trans. Syst. Man Cybern.*, vol. 42, no. 6, pp. 790–808, 2012, doi: 10.1109/TSMCC.2012.2198883.

56. A. M. Khan, M. H. Siddiqi, and S.-W. Lee, “Exploratory Data Analysis of Acceleration Signals to Select Light-Weight and Accurate Features for Real-Time Activity Recognition on Smartphones,” *Sensors*, vol. 13, pp. 13099–13122, 2013, doi: 10.3390/s131013099.

57. R. Khusainov, D. Azzi, I. E. Achumba, and S. D. Bersch, “Real-Time Human Ambulation, Activity, and Physiological Monitoring: Taxonomy of Issues, Techniques, Applications, Challenges and Limitations,” *Sensors*, vol. 13, pp. 12852–12902, 2013, doi: 10.3390/s131012852.

58. A. Bayat, M. Pomplun, and D. A. Tran, “A Study on Human Activity Recognition Using Accelerometer Data from Smartphones,” *Procedia Comput. Sci.*, vol. 34, pp. 450–457, 2014.

59. M. Shoaib, S. Bosch, O. D. Incel, H. Scholten, and P. J. M. Havinga, “Complex Human Activity Recognition Using Smartphone and Wrist-Worn Motion Sensors,” *Sensors*, vol. 16, no. 426, pp. 1–24, 2016, doi: 10.3390/s16040426.

60. M. Gjoreski, H. Gjoreski, M. Luštrek, and M. Gams, “How Accurately Can Your Wrist Device Recognize Daily Activities and Detect Falls?,” *Sensors*, vol. 16, no. 800, pp. 1–21, 2016, doi: 10.3390/s16060800.

61. W. S. Lima, E. Souto, K. El-Khatib, R. Jalali, and J. Gama, “Human Activity Recognition Using Inertial Sensors in a Smartphone: An Overview,” *Sensors*, vol. 19, no. 3213, pp. 1–29, 2019, doi: 10.3390/s19143213.

62. S. A. Borz, N. Talagai, M. Cheta, A. V. Gavilanes Montoya, and D. D. Castillo Vizuete, “Automating Data Collection in Motor-manual Time and Motion Studies Implemented in a Willow Short Rotation Coppice,” *Bioresources*, vol. 13, no. 2, pp. 3236–3249, 2018.

63. R. Gallo, R. Visser, and F. Mazzetto, “Developing an Automated Monitoring System for Cable Yarding Systems,” *Croat. J. For. Eng.*, vol. 42, no. 2, pp. 213–225, 2021, doi: 10.5552/crojfe.2021.768.

64. M. Pierzchała, K. Kvaal, K. Stampfer, and B. Talbot, “Automatic Recognition of Work Phases in Cable Yarding Supported by Sensor Fusion,” *Int. J. For. Eng.*, vol. 29, no. 1, pp. 12–20, 2018, doi: 10.1080/14942119.2017.1373502.

65. R. F. Keefe, E. G. Zimbelman, and A. M. Wempe, “Use of Smartphone Sensors to Quantify the Productive Cycle Elements of Hand Fallers on Industrial Cable Logging Operations,” *Int. J. For. Eng.*, pp. 1–12, 2019, doi: 10.1080/14942119.2019.1572489.

66. E. G. Zimbelman and R. F. Keefe, “Development and Validation of Smartwatch-based Activity Recognition Models for Rigging Crew Workers on Cable Logging Operations,” *PLoS ONE*, vol. 16, no. 5, pp. 1–25, 2021, doi: 10.1371/journal. pone.0250624.

67. C. A. Silva *et al.*, “Predicting Stem Total and Assortment Volumes in an Industrial Pinus taeda L. Forest Plantation Using Airborne Laser Scanning Data and Random Forest,” *Forests*, vol. 8, no. 254, pp. 1–17, 2017, doi: 10.3390/f8070254.

68. C. A. Silva, C. Klauberg, A. T. Hudak, L. A. Vierling, S. J. Fennema, and A. P. D. Corte, "Modeling and Mapping Basal Area of Pinus taeda L. Plantation Using Airborne LiDAR Data," *Ann. Braz. Acad. Sci.*, vol. 89, no. 3, pp. 1895–1905, 2017, doi: 10.1590/0001-3765201720160324.

69. M. V. N. d'Oliveira, S. E. Reutebuch, R. j. McGaughey, and H.-E. Andersen, "Estimating Forest Biomass and Identifying Low-intensity Logging Areas Using Airborne Scanning Lidar in Antimary State Forest, Acre State, Western Brazilian Amazon," *Remote Sens. Environ.*, vol. 124, pp. 479–491, 2012, doi: 10.1016/j.rse.2012.05.014.

70. P. Ellis, B. Griscom, W. Walker, F. Gonçalves, and Tina Cormier, "Mapping Selective Logging Impacts in Borneo with GPS and Airborne Lidar," *For. Ecol. Manag.*, vol. 365, pp. 184–196, 2016, doi: 10.1016/j.foreco.2016.01.020.

71. R. A. Slesak and T. Kaebisch, "Using Lidar to Assess Impacts of Forest Harvest Landings on Vegetation Height by Harvest Season and the Potential for Recovery Over Time," *Can. J. For. Res.*, vol. 46, pp. 869–875, 2016, doi: 10.1139/cjfr-2015-0517.

72. M. Alam, M. Acuna, and M. Brown, "Self-Levelling Feller-Buncher Productivity Based on Lidar-Derived Slope," *Croat. J. For. Eng.*, vol. 34, no. 2, pp. 273–281, 2013.

73. A. Kato and P. Schiess, "LIDAR Derived Tree Parameters for Optimal Cable logging System Design," Corvallis, OR, USA, Apr. 2007, pp. 173–179.

74. H. R. Heinimann and J. Breschan, "Pre-Harvest Assessment Based on LiDAR Data," *Croat. J. For. Eng.*, vol. 33, no. 2, pp. 169–180, 2012.

75. M. Maltamo, M. Hauglin, E. Næsset, and T. Gobakken, "Estimating Stand Level Stem Diameter Distribution Utilizing Harvester Data and Airborne Laser Scanning," *Silva Fenn.*, vol. 53, no. 3, pp. 1–19, 2019, doi: 10.14214/sf.10075.

76. M. Z. A. Rahman, B. G. H. Gorte, and A. K. Bucksch, "A New Method for Individual Tree Measurement from Airborne LiDAR," College Station, Texas, USA, Oct. 2009, pp. 1–10.

77. K. Kandare, H. O. Ørka, J. C.-W. Chan, and M. Dalponte, "Effects of Forest Structure and Airborne Laser Scanning Point Cloud Density on 3D Delineation of Individual Tree Crowns," *Eur. J. Remote Sens.*, vol. 49, pp. 337–359, 2016, doi: 10.5721/EuJRS20164919.

78. L. Luo, Q. Zhai, Y. Su, Q. Ma, M. Kelly, and Q. Guo, "Simple Method for Direct Crown Base Height Estimation of Individual Conifer Trees Using Airborne LiDAR Data," *Opt. Express*, vol. 26, no. 10, pp. 1–17, 2018, doi: 10.1364/OE.26.00A562.

79. X. Yu, J. Hyyppä, M. Holopainen, and M. Vastaranta, “Comparison of Area-Based and Individual Tree-Based Methods for Predicting Plot-Level Forest Attributes,” *Remote Sens.*, vol. 2, pp. 1481–1495, 2010, doi: 10.3390/rs2061481.

80. C. A. Silva *et al.*, “Imputation of Individual Longleaf Pine (Pinus palustris Mill.) Tree Attributes from Field and LiDAR Data,” *Can. J. Remote Sens.*, vol. 42, no. 5, pp. 554–573, 2016, doi: 10.1080/07038992.2016.1196582.

Chapter 2: Prediction of Fuel Loading Following Mastication Treatments in Forest Stands in North Idaho, USA

Published In:

Becker, R.M, Keefe, R.F. Prediction of fuel loading following mastication treatments in forested stands in north Idaho, USA. *Sustainability*. **2020**, *12*(17), 7025. DOI: 10.3390/su12177025.

2.1 Abstract

Fuel reduction in forests is a high management priority in the western United States and mechanical mastication treatments are implemented commonly to achieve that goal. However, quantifying post-treatment fuel loading for use in fire behavior modeling to forecast treatment effectiveness is difficult due to the high cost and labor requirements of field sampling methods and high variability in resultant fuel loading within stands after treatment. We evaluated whether pre-treatment lidar-derived forest stand characteristics at 20 m × 20 m resolution could be used to predict post-treatment surface fuel loading following mastication. Plot-based destructive sampling was performed immediately following mastication at three stands in the Nez Perce Clearwater National Forest, Idaho, USA, to correlate post-treatment surface fuel loads and characteristics with pre-treatment lidar-derived forest metrics, specifically trees per hectare (TPH) and stand density index (SDI). Surface fuel loads measured in the stand post-treatment were consistent with those reported in previous studies. A significant relationship was found between the pre-treatment SDI and total resultant fuel loading ($p = 0.0477$), though not between TPH and fuel loading ($p = 0.0527$). SDI may more accurately predict post-treatment fuel loads by accounting for both tree number per unit area and stem size, while trees per hectare alone does not account for variations of tree size and subsequent volume within a stand. Conditions within treated stands and fuels produced during mastication are highly variable and may explain the lack of relationship between fuel classes and loading. Root-mean-square errors of 36 and 46 percent of the random forest lidar models for SDI and TPH may limit the ability to predict the highly variable fuel loads produced from mastication. Use of lidar to predict fuel loading after mastication is a useful approach for managers to understand the efficacy of fuel reduction treatments by providing information that may be helpful for determining areas where treatments can be most beneficial.

2.2 Introduction

Due to the variability of species, management objectives, spatial configuration of management areas, regulatory restrictions, landowner funding availability, fuels characteristics, and other geographic and vegetative factors, developing a one-size-fits-all approach for wide-scale fire management is challenging [1]–[4]. However, forests with high fire risk must be actively managed [5]. Over the previous century, forest management practices such as fire exclusion have resulted in historically uncharacteristic stand attributes in many forests in the western United States, including dense, small-diameter stands with increased surface fuel loads [5], [6]. Fuel reduction in stands that have lacked prior density management is a high priority in many areas of the western United States, especially on federal lands. Understanding the unique challenges and selecting strategies to best suit the needs of each management area, typically applied through one or more treatments applied at the stand level, is vital to long-term management success [2]. Properly designed and implemented fuel treatments have been found to increase fire resilience and resistance while simultaneously changing the behavior of wildfires that impact treated areas [5], [7]–[9].

Given the variability of management factors, including forest composition, topography, climatic conditions, and management history, not all silvicultural and fuel reduction treatments are feasibly implemented. In its most basic form, creating fire resilient stands generally involves three objectives: reducing surface fuels, reducing ladder fuels, and reducing crown density [5]. The complexity of planning fuel treatments for influencing the behavior of large fires must also account for spatial configuration and density of treatments when determining how to effectively and efficiently treat landscapes [4]. Fuel treatment programs have been implemented across the Western United States and include prescribed burning and mechanical treatments such as regeneration harvest, precommercial and commercial thinning, and mastication. The risk of fire escape, smoke restrictions, and poor public perception may limit the feasibility of large-scale prescribed burning efforts [10]. The need to meet particular site and climatic conditions to successfully implement prescribed burning often results in limited availability of windows in prescription, unlike mechanized treatments, that are less dependent on these factors [2]. To mimic the changes to forest structure created by fire, mechanical treatments are widely used to reduce crown fire risk, particularly in the Wildland Urban Interface (WUI) [10]. Mechanical treatments modify the vertical distribution of fuels and reduce overall canopy fuels to levels that are less susceptible to crown fires and rapid fire spread, without the risks associated with prescribed burning.

In many cases, stands that are at risk for severe fire are overstocked and may have high levels or mortality, which reduces the merchantable stand volume component and reduces the profitability

of commercial timber harvest in the context of salvage harvesting. Alternative mechanical fuel treatment options, including mastication and chipping, are used in these instances when revenue from timber harvest may not be a core management objective, but fuel loads nevertheless need to be reduced. In these operations, which occur commonly on federal lands, fuels generated are left on site, unlike final harvest and commercial thinning treatments, where harvested materials are most commonly removed, treated at the landing, or treated in piles within the unit. The size of mechanical fuel treatments is dependent on the overall management objectives of the area. Mastication may target relatively small, high fire risk areas possessing dangerous fuel loads, where harvesting is not feasible. Alternatively, larger mastication operations may be used to reduce canopy density and ladder fuels while simultaneously reducing competition, removing undesirable trees, and preparing the stand for future harvest. Mastication entails the grinding, shredding, chunking, or by other means reducing the size of both standing and downed materials via boom-mounted mulching attachments of excavators, skid-steers, or other machines [11]–[13]. The risk of active crown fires is reduced by altering the vertical distribution and continuity of forest fuels and compacting them on the forest floor as irregularly shaped chips, though dead surface fuel loads are increased in the process [10], [14]. Changes in physical properties of woody material resulting from mastication can influence fire behavior, including the rate of spread, flame length, and intensity [14]. According to Agee and Skinner [5], reducing surface fuels, increasing live crown height, retaining large, fire resistant trees, and decreasing crown bulk density are all important factors in producing fire-resistant stands. Altering the amount and condition of ladder fuels similarly influences fire intensity and burn severity [12]. When implemented correctly, mechanized fuel treatments address all points, excluding the reduction of surface fuel.

Despite the widespread use of mastication treatments [15] and past research, the spatial variability of masticated fuel beds has not been previously studied [10], [11]. Studies have found surface fuel loadings in mulched treatments to range from 16 to 65 Mg ha-1, with woody fuels concentrated in the 1-h and 10-h time-lag classes, which have average diameters <2.54 cm [10], [14], [16]–[18]. Relative to untreated stands, mulched fuel beds with fuels concentrated in these classes have reduced rate of spread and flame lengths, but increased smoldering and flaming duration [10]. Quantifying masticated fuel loads is challenging, however, given the wide variability in masticated fuel physical structures and site, ecosystem, and regional fuel characteristics [15]. In masticated stands, fuel loads are also highly variable, leading to challenges when predicting and modeling loading and fire behavior. Fuel loads rely heavily on multiple factors, including vegetation type, pretreatment stand conditions, machinery and mastication attachment, operator and the treatment objectives, and desired conditions post-treatment [10], [14]–[17]. As a result, the spatial heterogeneity

of fuels within and across masticated stands remains unclear [15]. Several studies have successfully used fuel depth and/or fuel coverage in mulched areas to estimate surface fuel loads [10], [14], [17], [18]. These techniques provide total surface fuel estimates more easily and accurately than planar transect sampling, but still require visiting the site following treatments. While less labor-intensive than past methods, the widespread assessment of surface fuel loading following mastication still requires in-person site visitation and assessment, which can be time-intensive and is only possible post-treatment. Efficient and effective methods to map post-treatment fuel loadings using pre-treatment conditions across stand, site, forest, and broader extents could provide valuable information to landowners when developing fuel management programs and evaluating their potential cost-effectiveness.

Fuel mapping is a difficult and often infeasible process across broad spatial and temporal scales due to high fuel variability, and costs and time constraints associated with field sampling [19]–[22]. Given the additional variability of masticated fuel loads, prediction models will likely need to focus on relatively small geographic extents and account for various forest characteristics. Micro-site predictions may better address site and forest variability and result in more accurate models. To better understand fuel loads resulting from treatments, it is important to first determine what forest conditions existed prior to mastication. On large landscape and regional scales, it is infeasible to perform a forest inventory to determine pre-treatment conditions due to labor and cost restrictions. Therefore, remotely sensed data, specifically lidar, has been repeatedly shown to provide large-scale forest metric predictions and enable the future extrapolation of models [23]. Lidar has been used in part or entirely for assessing forest fuels characteristics including canopy [24]–[26], surface fuel loading [27]–[31], ladder fuels [32], [33] and parameters including overall loading, spatial distribution, composition, vertical and horizontal arrangement, bulk density, and hazard ratings [34]–[38]. The authors were unable to find any relevant studies for lidar applications in masticated surface fuel loadings. Additionally, no models have currently been developed to predict post-mastication surface fuel loads from pre-treatment lidar-derived stand conditions.

In this study, we evaluate whether pre-treatment lidar-derived forest metrics can be used to predict surface fuel loads and associated fuel characteristics following mastication treatments. Masticated fuels were assessed across varying pre-treatment stand conditions to determine if relationships exist between the masticated fuel loads and lidar-derived forest metrics prior to treatment. Additionally, relationships between pre-treatment metrics and additional fuel bed characteristics including depth, size class distribution, and bulk density were assessed. Masticated fuels were sorted and quantified based on time-lag classes to determine if pre-treatment stand

characteristics impact these distributions within sample plots. If remotely sensed forest metrics relate directly to mastication fuel characteristics, these models could be used to predict fuel loading and fuel bed characteristics for areas of similar forest composition, prior to mastication treatments. This information provides valuable insight to natural resources managers when selecting potential forest and fuel treatment options, ensuring both the economic and ecological sustainability of mechanical fuel treatments and other concurrent forest operations. Economically and ecologically unsustainable fuel treatments are financially and operationally infeasible, unsuccessful in achieving the desired operational, environmental and management results, and lead to the inefficient and ineffective use of limited financial resources. Understanding the potential impacts of mastication treatments based on existing forest conditions will help assess areas where this treatment option can be implemented cost-effectively when coupled with existing fire behavior models.

2.3 Methods and Materials

2.3.1 Study Site

The study sites were located in three stands in the Nez Perce-Clearwater National Forest, in north central Idaho, following fuel treatments to gather data pertaining to the resultant surface fuel loads. These treatments were part of the larger Orogrande timber sale and consisted of approximately 38 hectares (95 acres) of mechanical fuel treatment. The management units were predominantly mixed conifer forest type with slopes averaging 25% throughout the units. Mastication was successfully implemented in the three stands as a management alternative to timber harvest. The three stands treated for this study were originally planned for timber harvest. Harvesting was found to be financially infeasible due to the low value of harvested products and long-haul distances to the mill. The prescription developed for the project was intended to release remaining trees to increase timber value for future harvest while simultaneously decreasing stand density and increasing canopy base height to reduce the risk of crown fire using mastication. According to forest personnel, the management approach used in this project was its first application on the Nez Perce-Clearwater National Forest. The machine used to perform the mechanical fuel treatment was a Takeuchi TB290 compact excavator with a Fecon Bull Hog mastication head (Figure 2.1). The machine weighs 8685 kg, is 2.2 m wide and 2.9 m long at the undercarriage, has a maximum reach of 7.4 m, and creates only 37.9 kPa of ground pressure when equipped with 450-mm-wide rubber tracks.

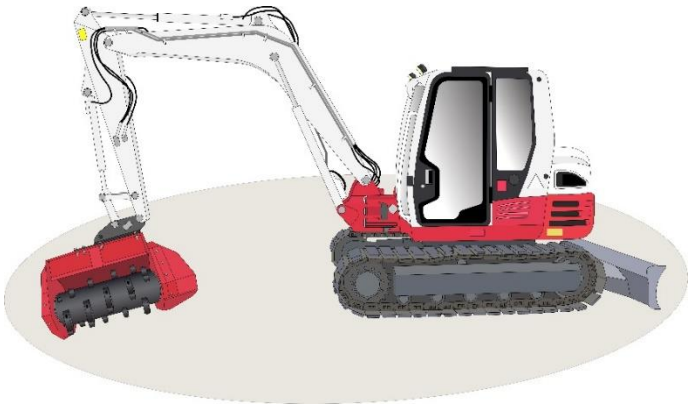

Figure 2.1. Mini-excavator with a horizontal shaft masticator head used in mastication treatments.

The treatment prescription for the stands included a target range for post-treatment stocking level. For the units in this study, the operator was instructed to leave 40 to 80 trees per hectare after treatment while removing only stems less than 18 cm (7 inches) in diameter. Further, all dead and down material up to 30 cm (12 inches) were masticated [39]. Post-treatment surface fuel sampling occurred in the masticated portions of three replicate stands: 117 (13 hectares), 120 (15 hectares), and 147 (10 hectares), within the management boundary. Due to many downed trees in stand 147, meeting the prescription specification for dead and downed material was not operationally feasible. Therefore, the mastication intensity for downed trees was reduced after stand 147 was partially treated. This prescription adjustment was used for treating the remainder of stand 147 and for the entirety of stands 117 and 120 [39] (Figure 2.2).

Figure 2.2. Visual comparison of treated stands and a representation of surface fuels in stand 147 before (left pane) and after (right pane) adjustments to treatment intensity.

2.3.2 Lidar Processing and Sample Plot Selection

The Orogrande timber sale and the three stands (117, 120, 147) were within the extent of the 18,450-hectare (45,600-acre) Crooked River lidar acquisition flown in 2012 with a pulse density return of ≥4 points per square meter (Figure 1.3). Field sampling inventory data from 91 20 × 20-m (1/10 acre) plots were run through the USFS Forest Vegetation Simulator [40] to summarize stand composition and structure. These forest inventory data were part of a previous sampling effort and were collected using field methods described in Falkowski et al. (2005) [22]. Random forest models [41], [42] describing trees per hectare, total volume (m^3ha^{-1}), basal area (m^2/ha^{-1}), and stand density index (SDI) were then developed using lidar metrics encompassing identical extents to the field sampling plots. These methods are consistent with those described in Becker et al. [43]. All random forest development and metric predictions were performed in the open source statistical analysis program, R, using the randomForest package [42], [44].

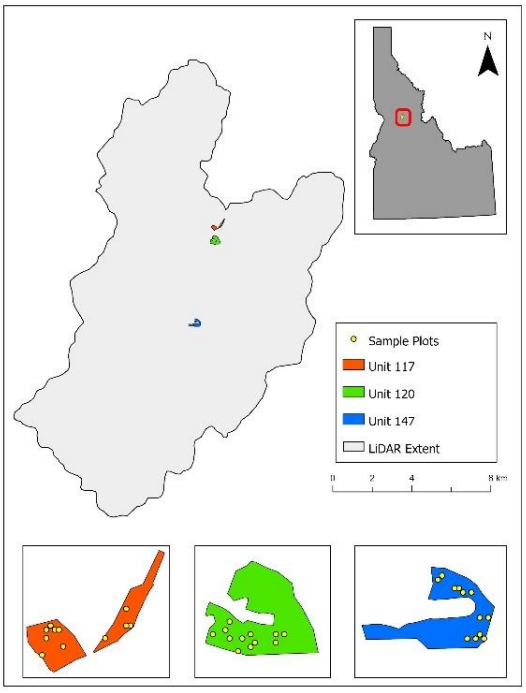

Figure 2.3. Crooked River lidar acquisition area and Orogrande T.S. mastication stands located in the Nez Perce-Clearwater National Forest, Idaho, USA.

Random forest ensemble learning algorithms were used because they provide excellent classification results, speed of processing, ability to reduce bias, and correlation and reduce overfitting compared to other classification and regression trees (CART) models, making them a widely used machine learning solution [45]–[48]. Random forest produces multiple decision trees using bagging and randomly selected subsets of training samples and variables to provide a majority

vote from which a prediction is made. The default number of trees (n_{tree} = 500) and the default number of variables split at each node (m_{try} = square root of the total number of input variables) were used when building random forest models for each forest characteristic. 177 lidar metrics were available to develop each unique random forest algorithm, but only a subset of metrics were used in the final models, based on importance, defined using rfUtilities [49]. Random forest models were built using 2/3 of the data and validated using the remaining 1/3 of the data.

The entire Crooked River lidar acquisition was processed using the USDA lidar processing software FUSION version 3.60 to create an identical post-processed data structure as the initial 91 sampled plots [50]. This enabled the random forest models to be applied directly to the whole area to develop predicted metrics in 20 × 20-m pixels. Stand metrics derived from the lidar analysis included trees per hectare (TPH), total cubic foot volume (m^3 ha^{-1}), total basal area (m^2 ha^{-1}), and stand density index. SDI has been used in even-aged monocultures, and more recently in uneven-aged, mixed species stands to assess stand density as a function of quadratic mean diameter and stem density [51]–[55]. This metric was selected in addition to TPH to provide a more descriptive indication of stand density. The trees per hectare vector map was then stratified into four classes: 0–247; 248–494; 495–740; 741+. These classes were used to select sample plots within the study stands. Trees per hectare classes were used to stratify the selection of a broad distribution of relative stocking in sampled areas prior to mastication.

2.3.3 Field Sampling Procedures

Twelve plots were sampled within each of the three stands, with three representing each of the four levels of pre-treatment trees per hectare derived from the lidar data. The 20 × 20-m pixels chosen for sampling were randomly selected from all available pixels of the trees per hectare class within the stand boundaries. The resulting sampled pixels amounted to 36, with nine plots representing each of the four classes of pre-treatment trees per hectare. Trees per hectare was selected as the stand metric by which to select sample plots, due to the mastication treatment prescription being based on a goal trees per hectare post-treatment. All mastication treatments and sampling of fuel loading occurred during summer 2017.

Center points within the 20 × 20-m pixels were determined via ArcMap, and the resultant coordinates were used to locate the field plot centers. A simple method of plot center relocation was established to address situations where plot centers occur in areas that prohibited the sampling of fuel loading including tree stumps, roadways, rock outcroppings, and exposed mineral soil due to machinery movement. In these instances, plot centers were moved due north 3 m. If needed, plots

were moved due west from original plot centers 3 m if the movement due north did not resolve the issue with the obstruction. A variation on destructive plot-based sampling was used to quantify fuel characteristics and fuel loading following mastication treatments within the three stands at each of the 36 plots [10], [14], [17].

Within each of the 36 sampled plots, fuel size classes were sampled in four quadrats. Once the plot center was located via GPS coordinates, 5-m vectors extending directly north, south, east, and west of the plot center were marked and established as the corner points for the quadrats. For instances in which uncharacteristic site conditions occurred within the quadrats, the frame was reflected over the transect. If this quadrat reflection did not resolve the issue and fuel collection within the quadrat was still not possible, the quadrat was excluded from sampling overall. Situations that would permit quadrat reflection over the transect or exclusion included buried logs, stumps, and rock outcroppings. In addition to the collection of fuels within the 25-cm squared quadrats, the fuel depth of masticated fuels was measured at two locations along the 5-m vectors (2.5 m and 5 m) and at the overall plot center (Figure 2.4). To measure fuel depths, a cross-section of the forest floor was cleared using a trowel, and the depths were manually recorded. For the depths of the woody/masticated material, any branch or piece of woody debris above the measurement point was included in the depth measurement. Where site conditions prevented the measuring of fuel depths, the depth was measured 0.5 m from the original measurement point moving away from the plot center along the transect. If the depth was still not measurable at the second location, the measurement was omitted. Each of the 36 plots contained four separate fuel collection quadrats and nine fuel depth measurements.

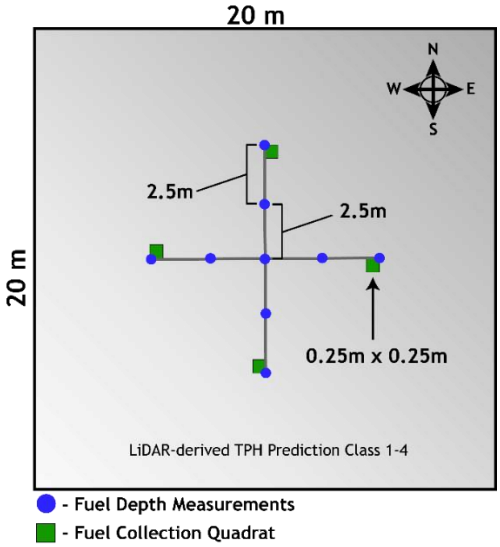

Figure 2.4. Destructive plot-based sampling design used for surface fuel collection and field measurements.

Frames made of PVC pipe measuring 25 cm by 25 cm were built to establish the sampling area extent. Within the 25 × 25-cm collection quadrats, all fuel down to bare mineral soil was gathered, and any pieces extending outside the collection frame were trimmed using hand shears, and thus only pieces completely within the frame were collected (Figure 2.5). All fuels collected were stored in paper bags labeled by their collection point and were brought back to the lab for detailed fuel composition analysis. Within the sampling quadrats, downed trees and logs were not sampled due to their irregular occurrence and collection difficulty for returning to the lab.

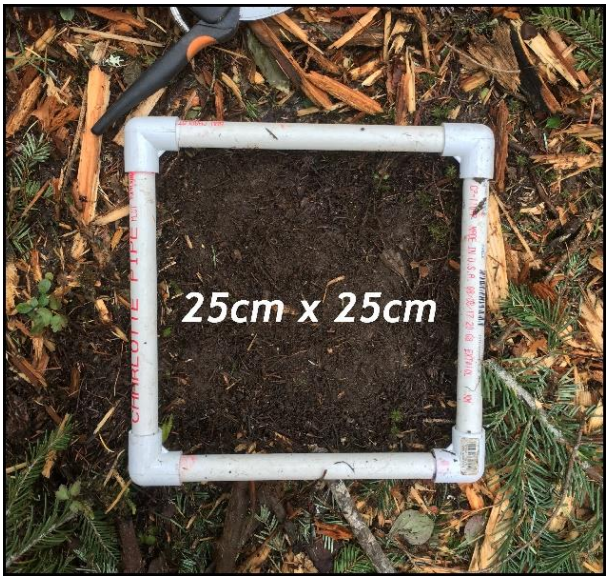

Figure 2.5. Fuel collection quadrat used in destructive fuel sampling.

It was assumed that when locating sample plots in the field, there may be instances where mastication, though planned, does not occur. This was a result of inaccessibility, due to the steep or very uneven terrain where the operator chose not to treat the area for safety reasons. In these instances, three supplemental sample points for each classification level of trees per hectare were randomly selected in each of the three stands. If an originally designated sample plot was found to be within an un-masticated area, a randomly selected supplemental sample plot of the same TPH class was selected for sampling instead. These supplemental plots were randomly generated from the remaining available pixels not included in the initial stratification prior to field sampling, using the same method used in the initial plot selection. Supplemental plots were used once in unit 117, four times in unit 120, and four times in unit 147. The final sampled plots across stands 117, 120, and 147 are shown in Figure 2.6.

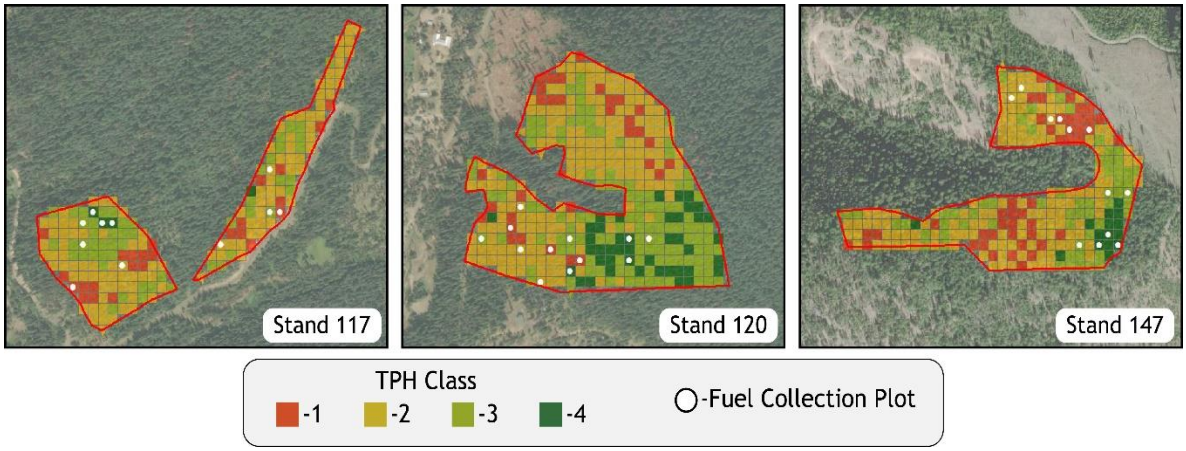

Figure 2.6. Field sampling plots within masticated stands 117, 120, and 147, selected based on stand density (TPH) prior to treatment.

2.3.4 Lab Measurements and Fuel Characterization

After field sampling was conducted, fuel collection bags were brought back to the lab to be processed by drying and sorting. A total of 133 quadrats of fuel was brought from the field for processing. If all plots had all quadrats collected, there would have been a total of 144. However, some quadrats were excluded from sampling because they were located on rock outcroppings, stumps, or other obstructions. One complete plot of quadrat fuel collections from stand 117, trees per hectare class 1, was misplaced during sampling, which constituted four of the eleven missing quadrat samples. Due to the omitted samples, stand 117 had two plots for trees per hectare class 1, resulting in 35 total plots rather than 36. Each collection sample was oven-dried at 105 degrees Celsius for 48 h, or until the sample weight stabilized, and was then weighted to the nearest gram. All fuels were then sorted, by quadrat, into five time-lag fuel classes: duff/litter and woody/masticated (1-h [<0.64 cm], 10-h [0.64–2.54 cm], 100-h [2.54–7.62 cm] and 1000-h [>7.62 cm]) [56] (Figure 2.7). Sorted fuels were then individually weighed to the nearest gram to determine the proportion of overall mass that each fuel class represented. These proportions for each quadrat were averaged with corresponding plot quadrats to determine the fuel composition proportions by mass for the entire plot. For each of the 35 sample plots, the fuel bed volume was calculated by multiplying the average of the fuel depths at the nine measured locations within each plot by the dimensions of the collection frame. We then determined the bulk density of the fuels in each plot by dividing the average oven-dried weight of the fuel classes in the four collection quadrats by the corresponding volume. Plot level values were calculated using the averages of each quadrat within the plot for fuel loading (Mg ha^{-1}) for the whole stand and by fuel class, fuel depth (cm), and bulk density (kg m^{-3}).

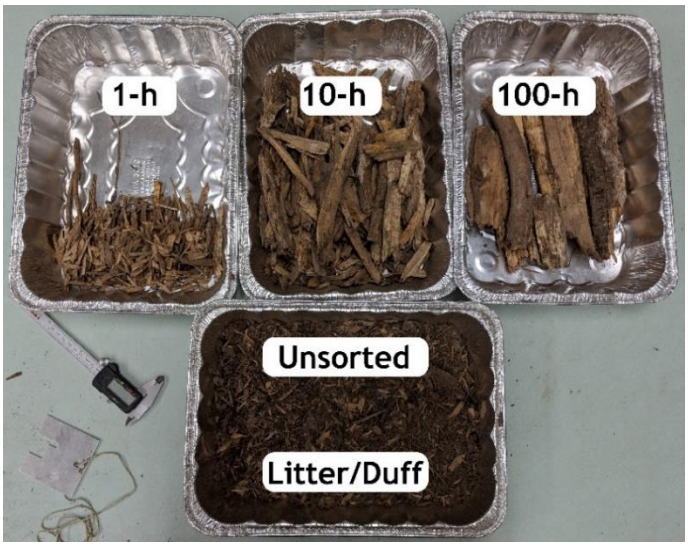

Figure 2.7. Sorting of dried surface fuels based on time-lag class (1-h, 10-h, 100-h, 1000-h, litter/duff).

To assess the correlation between pre-treatment lidar-derived forest metrics and post-treatment fuel conditions, all statistical analyses were performed using the R statistical programming environment. Pearson correlation coefficients were calculated to evaluate the strength of association between predictors. Additionally, linear mixed effects models were used to model the relationship between fuel loading following mastication treatments and the trees per hectare, stand density index, and basal area of plots prior to mastication, using the nlme R package [57]. The general equation for mixed effect models is described as:

$$y_i = X_i\beta + Z_i u_i + \varepsilon_i$$

$$u_i \sim N(0, D)$$

$$\varepsilon_i \sim N(0, R_i)$$

where β are fixed effects, u are random effects, X is the model matrix for fixed effects, Z is the model matrix for random effects, ε is the vector of errors, R is the variance-covariance matrix of within-individual measurements, and D is the variance-covariance matrix of random effects [58]. In linear mixed effects models evaluating predictors, stand, and TPH class were treated as random effects, with the TPH class nested within the stand. Random intercepts were used when fitting models. Due to the inconsistency of the mastication treatment in stand 147, two different mixed effects models were fit for each of the lidar predictors. One model contained all three stands, while the second model contained only stand 117 and 120. This was in order to avoid potential influential data artifacts associated with the treatment change in stand 147.

2.4 Results

Parameter estimates for the random forest models used in the pretreatment derivation of forest characteristics from lidar metrics for 20 × 20-m pixels are shown in Table 2.1. In this study, an acceptable maximum root-mean-square error (RMSE) of 50% of the prediction means was used based on values derived in previous studies [59], [60]. The RMSE was within the acceptable range for the density (TPH), basal area (m^2ha^{-1}), and stand density index models. For the random forest model predicting stand volume (m^3ha^{-1}), an RMSE of 166.93 was about 54% of the predicted mean and just outside of the desired range. Predicted volume was therefore excluded from use in subsequent analyses. Model accuracies for forest metrics were 71.5%, 77.4%, 74.3%, and 79% for trees per hectare, basal area, volume, and stand density index, respectively, which are comparable to those obtained by Falkowski et al. [61] and Hudak et al. [60]. These pretreatment maps of predicted stand characteristics provided the basis for study plot selection and the subsequent regression modeling of post-treatment fuel loading.

Table 2.1. Random forest model quality assessment for pre-treatment forest metrics.

Random Forest	Prediction Mean	RMSE	R-Squared	Accuracy (%)
Stand Density (TPH)	468.00	217.36	0.55	71.5
Basal Area (m^2ha^{-1})	30.56	12.95	0.63	77.4
Total Volume (m^3ha^{-1})	307.99	165.35	0.57	76.3
Stand Density Index (SDI)	299.17	110.296	0.45	79.0

Table 2.2 shows the summary data of the stands for the fuel collection as averages of the sampled plots and quadrats within each stand. Surface fuel loadings range from 9.3–83.4 Mg ha^{-1}, 1.8–34.5 Mg ha^{-1}, 5.4–80.5 Mg ha^{-1}, 0–48.1 Mg ha^{-1}, and 0–8.2 Mg ha^{-1} for litter/duff, to 1-h, 10-h, 100-h and 1000-h fuel classes, respectively, across all plots and stands. Fuel depths ranged from 6.4–26.3 cm and bulk densities ranged from 22.2 to 154.2 kg m^{-3}. Across all plots, there was a significant ($p = 0.029$) moderate positive (0.369) correlation between trees per hectare and fuel loading (Mg m^{-1}), found by performing a Pearson's correlation test. Additionally, there was a positive (0.3577) and significant ($p = 0.0349$) correlation between SDI and fuel loading. No significant relationship was found between pre-treatment TPH and bulk density of resulting fuels (kg m^{-3}); SDI and bulk density of resulting fuels; basal area (m^2h^{-1}) and loading or bulk density; nor between pre-treatment total volume (m^3ha^{-1}) and fuel loading or bulk density (Table 2.3). Based on the results of the correlation tests, the linear mixed effects model was fitted to evaluate the relationship of pre-treatment TPH and the resulting fuel loads as well as SDI and the resulting fuel loads.

Table 2.2. Stand-level summary data representing stand averages and standard errors for pre-treatment trees per hectare and post-treatment destructive plot-based surface fuel characteristics for stands 117, 120, and 147.

Stand	Pre-TPH Avg. (SE)	Fuel Loading (Mg ha^{-1}) Avg. (SE)						Fuel Depth (cm) Avg. (SE)	Bulk Density (kg m^{-3}) Avg. (SE)
		Litter/ Duff	1-h	10-h	100-h	1000-h	Total		
117	530	43.4	6.7	30.3	13.2	0.0	93.7	15.6	59.0
	(77)	(6.7)	(1.2)	(4.3)	(3.7)	(0.0)	(13.1)	(1.5)	(5.8)
120	515	31.9	5.5	25.3	13.4	0.7	76.8	16.1	48.2
	(77)	(3.3)	(1.0)	(3.2)	(2.6)	(0.7)	(8.8)	(1.2)	(4.4)
147	516	32.9	9.1	34.3	22.8	0.0	99.2	18.4	59.2
	(93)	(3.6)	(2.5)	(5.9)	(3.6)	(0.0)	(10.4)	(1.5)	(10.6)

Table 2.3. Pearson's correlation assessments for pre-treatment forest characteristics and surface fuel characteristics following mastication treatments, where T is the t-test statistic and DF is the degrees of freedom.

Correlation	T	DF	P-Value	Coefficient
Density (TPH)/Loading (Mg ha^{-1})	2.2812	33	0.0291	0.3691
Density (TPH)/Bulk Density (kg m^{-3})	1.566	33	0.1269	0.2630
Volume (m^3 ha^{-1})/Loading (Mg ha^{-1})	1.8018	33	0.0807	0.2993
Volume (m^3 ha^{-1})/Bulk Density (kg m^{-3})	1.1251	33	0.2687	0.1922
Basal Area (m^2 h^{-1})/Loading (Mg ha^{-1})	1.9676	33	0.0576	0.3240
Basal Area (m^2 h^{-1})/Bulk Density (kg m^{-3})	1.3492	33	0.1865	0.2286
Stand Density Index/Loading (Mg ha^{-1})	2.2004	33	0.0349	0.3577
Stand Density Index/Bulk Density (kg m^{-3})	1.8702	33	0.0704	0.3096

The linear mixed effects models predicting the total fuel loading of all time-lag classes from pre-treatment TPH showed no significant relationship between the two factors (test statistic = 0.05318, df = 22, p-value = 0.0527) when accounting for all three stands. In the reduced model, pre-treatment trees per hectare and fuel loading were significant (p-value = 0.0066) (Table 2.4). The linear mixed effects models predicting the total fuel loading of all time-lag classes from pre-treatment SDI showed significant relationships between the two factors for all three units (p = 0.0477) and when assessing stand 117 and 120 alone (p = 0.0337) (Table 2.4). Figure 2.8 shows the associated relationships between SDI and the resulting fuel load for all three units. The black line represents the regression line of the complete data set and the individual regression line for each stand.

Table 2.4. Mixed effects model summary assessing pre-treatment trees per hectare (TPH) and stand density index (SDI) impact on fuel loading (Mg ha−1) post-mastication. The influence of stand 147 on the overall significance of the factors is shown.

Stand 117, 120, 147				
Predictor	**Estimate**	**Std. Error**	**DF**	**P-Value**
TPH	0.05318	0.025974	22	0.0527
SDI	0.16736	0.079809	22	0.0477
Stand 117, 120				
Predictor	**Estimate**	**Std. Error**	**DF**	**P-Value**
TPH	0.09524	0.029924	14	0.0066
SDI	0.227069	0.09647	14	0.0337

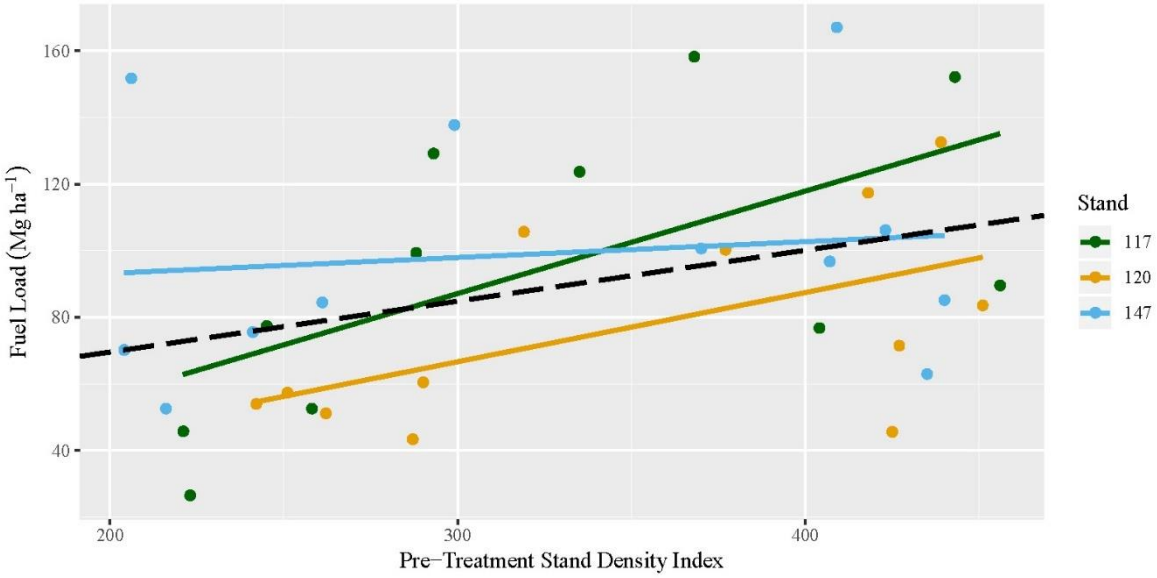

Figure 2.8. Surface fuel loading (Mg ha^{-1}) of all sampled plots by pre-treatment stand density index (SDI). The black dotted line represents the regression for all data, and the colored solid lines indicate the regression lines for each stand individually.

Additional linear mixed effects models were developed to further assess the impact of pre-treatment TPH and SDI on resulting fuels loads for each of the 5 time-lag fuel classes (litter/duff, 1-h, 10-h, 100-h, 1000-h). Only the litter/duff fuel class loading was found to be significantly correlated to pre-treatment trees per hectare for all three stands (Table 2.5). The litter/duff fuel class is generally independent of the mastication process, as most fuels in this class were present before treatment. However, when assessing stands 117 and 120, litter/duff ($p = 0.0242$), 1-h ($p = 0.0232$), and 100-h ($p = 0.0059$) were found to be significant. When assessing the relationship between SDI and the resulting fuel loading across all five time-lag cases, the model containing all three units showed that

both litter/duff (p = 0.0042) and 100-h (p = 0.0293) were significant, while the model describing units 117 and 120 showed that only 100-h (p = 0.0476) was significant. The data for the SDI model are shown in Figure 2.9.

Table 2.5. Mixed effects model summary assessing pre-treatment trees per hectare (TPH) and stand density index (SDI) impact on fuel loading (Mg ha−1) sorted by time-lag fuel class post-mastication. The influence of stand 147 on the overall significance of the predictors for each of the time-lag classes is shown.

Stand 117, 120, 147					
Fuel Class	**Predictor**	**Estimate**	**Std. Error**	**DF**	**P-Value**
Litter/Duff	TPH	0.0033284	0.0010120	22	0.0034
1-h	TPH	0.0000789	0.0003873	22	0.8405
10-h	TPH	0.0000719	0.0009999	22	0.9433
100-h	TPH	0.0015591	0.0008138	22	0.0685
1000-h	TPH	−0.0000106	0.0000901	22	0.9072
Litter/Duff	SDI	0.096484	0.030246	22	0.0042
1-h	SDI	0.001137	0.012228	22	0.9267
10-h	SDI	0.004637	0.031801	22	0.8854
100-h	SDI	0.0562922	0.024141	22	0.0293
1000-h	SDI	−0.0007695	0.002888	22	0.7924
Stand 117, 120					
Fuel Class	**Predictor**	**Estimate**	**Std. Error**	**DF**	**P-Value**
Litter/Duff	TPH	0.0038925	0.0015411	14	0.0242
1-h	TPH	0.0008194	0.0003215	14	0.0232
10-h	TPH	0.0021593	0.0010591	14	0.0608
100-h	TPH	0.0025606	0.0007890	14	0.0059
1000-h	TPH	−0.0000245	0.0001527	14	0.8747
Litter/Duff	SDI	0.095805	0.046646	14	0.0592
1-h	SDI	0.019364	0.010368	14	0.0829
10-h	SDI	0.058114	0.034173	14	0.1111
100-h	SDI	0.057603	0.026532	14	0.0476
1000-h	SDI	−0.002020	0.004787	14	0.6794

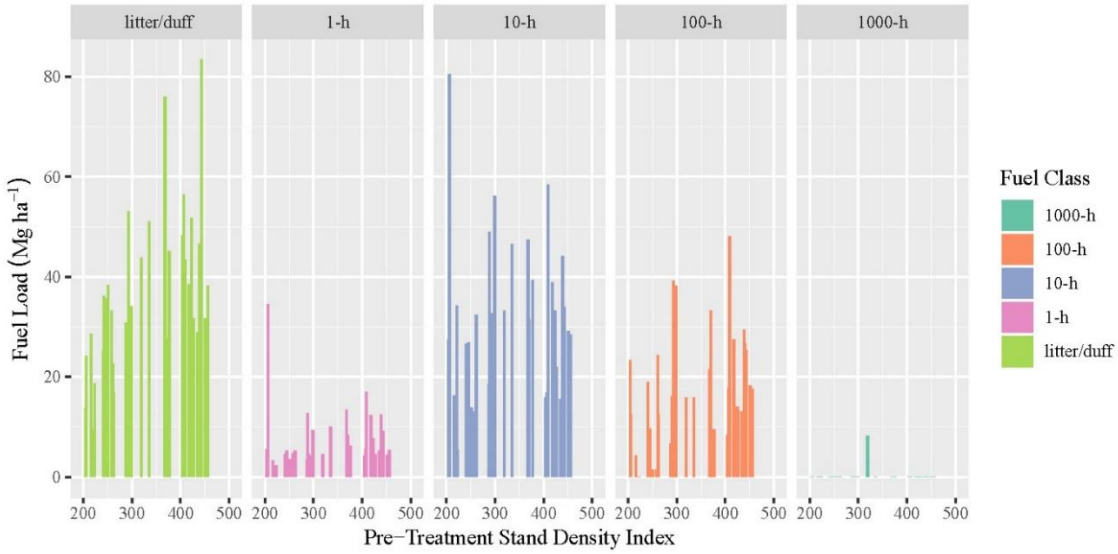

Figure 2.9. Surface fuel loading (Mg ha−1) distribution for all sample plots by pre-treatment stand density index (SDI) arranged by time-lag fuel class.

Our second research objective explored whether the in-plot distribution of masticated fuels among the five time-lag fuel classes was impacted by the stand density of the plot prior to treatment. Mixed effects models were developed to assess these questions, with results being found in Table 2.6. 10-h fuels in the sampled plots were the only fuel class found to change significantly as the pre-treatment TPH changed (test statistic = −0.01581, p = 0.0178, df = 22). SDI was shown to have a significant relationship with post-mastication fuel loading for both the 10-h (p = 0.0302) and 100-h (p = 0.0406) fuel classes (Table 2.6).

Table 2.6. Mixed effects model summary assessing pre-treatment stand density (TPH) and stand density index (SDI) impact on the percentage of total fuel load (Mg ha−1) by time-lag fuel class.

Stand Density (TPH)				
Fuel Class	**Estimate**	**Std. Error**	**DF**	**P-Value**
Litter/Duff	0.00560	0.009796	22	0.5736
1-h	−0.00190	0.0021351	22	0.3825
10-h	−0.01581	0.006169	22	0.0178
100-h	0.01161	0.006380	22	0.0823
1000-h	−0.0001	0.000850	22	0.9072
Stand Density Index (SDI)				
Fuel Class	**Estimate**	**Std. Error**	**DF**	**P-Value**
Litter/Duff	0.00766	0.03098	22	0.8069
1-h	−0.007688	0.006679	22	0.2620
10-h	−0.04619	0.019931	22	0.0302
100-h	0.042089	0.019346	22	0.0406
1000-h	−0.0007254	0.0027224	22	0.7924

The data distribution for the five time-lag classes as a percentage across the range of stand density indices and fuel loading are shown in Figure 2.10. Woody and mulched fuels (1-h, 10-h, 100-h, and 1000-h) were found to be between 30–85% of the overall fuel loads across all plots, which shows the variability found within the stands. 1-h, 10-h, 100-h, and 1000-h fuels contained 6–27%, 36–94%, 0–57%, and 0–13% of the woody and mulched fuels, respectively. On average, woody fuels made up about 58.2% of the overall surface fuel loading across all sites, with 1-h, 10-h, 100-h, and 1000-h fuel classes averaging 7.5%, 33.2%, 17.3%, and 0.2% of the loading, respectively.

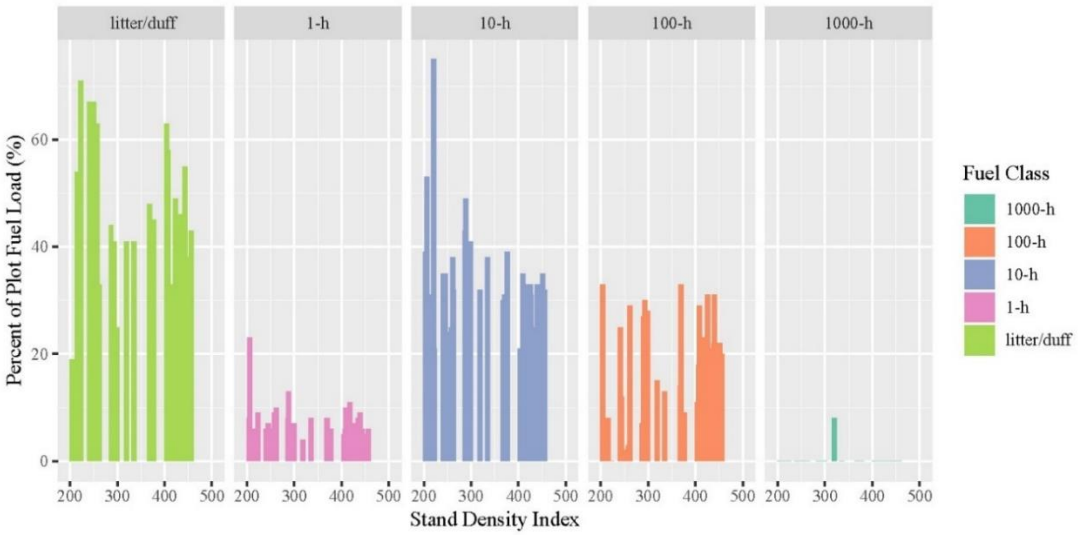

Figure 2.10. Percentage of total surface fuel load for all sample plots by pre-treatment stand density index (SDI) arranged by time-lag fuel class.

2.5 Discussion

Total surface fuel loadings varied widely across our study plots (26.4 to 158.2 Mg ha^{-1}), with woody/masticated surface fuels representing a similarly wide range (7.7 to 127.5 Mg ha^{-1}). Across all stands and plots, total surface fuel loading averaged 89.8 Mg ha^{-1}, and woody surface fuels averaged 53.9 Mg ha^{-1}. These total surface fuel loads were similar to those reported by Stephens and Moghaddas [16] in the Sierra Nevada Mountains (87.1 and 93.8 Mg ha^{-1}), Reiner et al. [18] in the Sierra Nevada (81.6 Mg ha^{-1}), Kane et al. [14] at study sites in Northern California and southwestern Oregon (83.6, 83.8 and 71.1 Mg ha^{-1}), and Hood and Wu [17] in the Northern Rockies (82.0–95.9 Mg ha^{-1}), but were higher than those reported by Brewer et al. [62] in mixed conifer Idaho stands (58.4 Mg ha^{-1}) and lower than those reported by Battaglia et al. [10] in mixed conifer stands in Colorado (110.4 Mg ha^{-1}). This finding was not surprising, as masticated fuel beds and characteristics have a

wide variability across sites and regions. The attempt to develop the surface fuel prediction model at a 20 x 20-m resolution in this study was meant to help address this site variability.

Based on results reported by previous mastication studies, the average total fuel depth of 16.7 cm recorded in the mixed conifer stands we studied was significantly higher than those in Battaglia et al. [10], but only slightly higher than those shown by Stephens and Moghaddas [16]: 14.6 and 14.7 cm. All fuel sampling in this study occurred within a month of mastication treatment, so fuels were still green at the time of collection and had not settled to the forest floor, whereas sampling of masticated fuels for other studies occurred 2–6 years post-mastication [10], [14]. These temporal changes in masticated fuel beds make the generalization of loadings difficult, especially across broad geographic extents. For example, a recently masticated stand may indicate greater fuel depths than a stand masticated several years ago, due to the decomposition and deterioration of fuel structural integrity. The additional compaction of fuel beds over time as they settle may affect subsequent fire behavior. Therefore, the development of the model estimating surface fuel characteristics directly after masticating would provide a consistent expectation of fuel loads, as was done in this study.

2.5.1. Relationship Between Pre-Treatment Stand Characteristics and Fuel Loading

Through the analysis performed across the three stands we studied—117, 120, and 147—no significant relationship was found between overall fuel loading following mastication and the pre-treatment tree per hectare we derived from lidar. However, SDI was found to be a significant predictor variable for post-mastication fuel loading when accounting for all management units and time-lag classes jointly. Initially, we expected to see an increase in the fuel loading as the pre-treatment TPH increased. It was believed that, given a consistent prescription implementation, greater TPH would result in more fuel, as a greater number of standing trees were mulched to meet treatment objectives. The contrary findings for absolute stand density may have resulted from the inconsistency in the initial treatment of stand 147, which was then corrected. When excluding stand 147, increasing pre-treatment TPH resulted in greater loading, as expected. However, even when including data from stand 147, the p-value of 0.0526 was just outside the level of significance needed to reject the null. The significance of both mixed effects models for SDI ($p = 0.0477$ and $p = 0.0337$) indicates fuel loading may be more accurately predicted using a metric that accounts for both tree size and number, as opposed to simply using trees per hectare where only the number of stems is accounted for.

Stand 147 was the first stand treated and was initially treated to prescription specifications. It was found that once treatment began, the original degree to which large downed woody debris was to be treated was operationally infeasible due to the increased treatment time. Further, stand 147 contained a small pocket of lodgepole pine killed by beetle, with a significant portion of downed trees

which were, under the original treatment specs, to be masticated heavily. This resulted in a larger amount of masticated fuels in plots with relatively low stand densities.

The decision to retain stand 147 in the analysis was made to maximize the data available for assessment and provide a realistic portrayal of the large variability of mastication treatments. As a relatively new treatment option being deployed over large areas, it is likely that similar inconsistency in operational treatments may occur during implementation and administration of mechanical fuel treatments, particularly as operators familiarize themselves with prescription requirements in new treatment areas. However, when the treatment prescription and execution was consistent for the entire stand, as seen in stands 117 and 120, a clear relationship between pre-treatment trees per hectare and fuel loading was seen. Given the potential for variability of mastication treatments and the heterogeneity of stand conditions in practice, the predictive success of SDI in a "real-world" management scenario is valuable for future modeling efforts.

Given the extent of our results, it remains unclear if a relationship exists between the fuel loading following mastication treatments and the pre-treatment stand density based solely on TPH or stand basal area, but SDI is a useful predictor. In mastication, the conservation of mass must be considered, as materials are not removed from the stand after treatment but rearranged in different physical forms. A larger masticated tree will understandably produce a larger amount of masticated material than a tree of smaller size. For example, two stands may both have similar numbers of trees per unit area, but one stand may have a larger average tree diameter than the other. If both stands are treated to the same prescription and reduced to a defined tree per unit area, it would be expected that the stand with the larger average stand diameter would produce heavier masticated fuel loadings. Accounting for both stem number per unit area and tree size in a single pre-treatment stand metric, SDI addresses this issue. Therefore, alternative approaches to modeling landscape scale fuel loading following mastication based on pre-treatment stand conditions that incorporate both stem numbers and size may offer improved prediction in future research and should be the focus of future study design and implementation.

When assessing the fuel loading for each time-lag class (litter/duff, 1-h, 10-h, 100-h, 1000-h), the litter duff class showed a significant relationship for the TPH and SDI models (Table 2.5). This may be a result of greater stand density, leading to higher amounts of organic material and litter on the forest floor. In all, minimal 1000-h fuels were collected at the plots, limiting the available data for the particular classes and making predictions difficult. This finding corroborates Kane et al.'s [11], who found that the plot-based method of surface fuel sampling does not assess a large enough area to

effectively capture the presence of 1000-h fuels as well as planar intersect methods. This is a result of 1000-h fuels generally occurring less frequently than other fuel classes in fuel beds.

2.5.2. Relationship between Pre-Treatment Stand Density and Fuel Class Distribution

As shown above (Table 2.6), only the 10-h fuels expressed as a percentage of the overall surface fuel loading were found to change as the TPH increased. It is unclear why the percentage of 10-h fuels would decrease with increasing TPH, but this may be a result of changes in treatment implementation. For example, the operator may spend less time masticating trees to maintain production in a denser stand, resulting in an increase in the proportion of larger fuel classes. It would be expected that, with one fuel class decreasing over increasing TPH, another fuel class would increase. This was seen in the SDI model, where the significant decrease in 10-h fuels (coefficient = −0.04616, p = 0.0302) was matched by a significant increase in 100-h fuels (coefficient = 0.042089, p = 0.0406). With increasing stand density, it is possible the operator attempted to maintain the desired operational production by decreasing the time spent masticating each tree. As a result, trees would be masticated less thoroughly, and there would be a larger percentage of larger fuel particles. The 10-h fuel class accounted for the highest fuel loads across all classes by a considerable amount in our study, which is consistent with other studies [10], [14]. Given the variability of the mastication as a whole, and the wide range of fuel loadings across 1-h, 10-h, 100-h, and 1000-h fuel classes, our results show that the distribution of surface fuels among time-lag fuel classes was not clearly modeled as a function of changes in TPH and SDI alone, apart from the 10-h and 100-h classes, in the case of this study.

2.5.3. Study Limitations and Future Work

Mastication is a highly variable operation impacted by many factors, and it is understood that there are some limitations to the scope of our research that should be addressed in future studies. One factor to consider in future applications of this methodology is the pixel size at which the lidar metrics were predicted. In the study development, it was believed that maximizing prediction resolution was the best option. Mastication, however, is a variable process, resulting in a scattered distribution of fuels on the forest floor. The directionality, travel distance, and particle size of comminuted materials may be affected by the type of mastication head (disk vs. drum), equipment type (all surface vehicle vs. excavator carrier), equipment horsepower, boom or attachment height, local topography within the stand, or other factors. While the sampling method developed by Hood and Wu [17] attempts to address the variability in stand and site conditions by sampling across multiple quadrats within the same plot, what was not accounted for in our study design was the possibility of fuels from adjoining pixels being distributed inter-pixel. During the observation of the treatment, fuels were clearly

distributed more irregularly and further than anticipated. The 20m × 20-m pixels used in the plot selection may have been too small to limit the influence of surrounding pixels in the resulting fuels found during sampling. For instance, a stand with a high stand density may have resulted in fuels initially in the stand as standing trees being distributed to an adjacent stand of a lower stand density, or to areas within the same stand that were not accounted for in our sampling design. During sampling, it would then appear that the pixel with the lower stand density was responsible for creating greater fuel loads than was possible. By decreasing the resolution and increasing the pixel size, this may be avoided.

In the fuel collection process, future studies should incorporate a hybrid, plot-based, and planar intersect method, as suggested by Kane et al. [14]. Doing so may help to ensure a more accurate representation of the fuel classes, as 1-h and 10-h fuels are more accurately represented in plot-based sampling [14], while planar intersect methods cover greater proportions of the overall masticated area, properly representing the 100-h and 1000-h fuels that may be missed in plot-based approaches [11]. Supplemental planar intersect sampling was not performed in this study due to the small 20 m × 20-m pixel size and the concern that sufficiently long intersect paths would extend too far to sample plot edges and be impacted by the distribution of fuels from adjacent pixels. Increasing the pixel size used in predicting the stand characteristics from the lidar, as described above, would enable an easier implementation of supplemental planar intersect sampling. Additionally, due to the variability of fuel distribution across the forest floor, plot-based sampling in future studies should use larger sampling quadrats than the 25 × 25-cm ones used in this study. Alternatively, a larger number of 25 × 25-cm sampling quadrats may also provide a greater representation of overall fuel variability within the sampling plot. The goal in using a smaller sampling quadrat in this study than those described in previous studies [17], [63] was to create an efficient and effective sampling procedure. However, larger quadrats will provide a greater representation of overall surface fuel loadings and should be studied.

2.6 Conclusions

The ability to predict surface fuel loads resulting quickly, efficiently, and effectively from mastication treatments is a valuable tool, as increased implementation of this management technique occurs. A variety of research and management questions regarding the longevity, fuel bed characteristics, and fire behavior within masticated fuels exist and will increase in relevance as lidar data become more widespread, along with the use of mastication to reduce fuels in stands where commercial thinning may be infeasible or more difficult to implement administratively. Existing

methods for predicting surface fuel loads rely on intensive, time-consuming sampling following treatment. While existing methods are effective for estimating fuel loading, methods based on remote sensing may help managers to proactively plan and predict post-treatment fire behavior over large areas to optimize treatments in ways that incorporate topography and stand adjacency.

The results from this study showed that pre-treatment stand density metrics that account only for tree number per unit area, such as TPH, were not good predictors of resulting surface fuel loads following mechanical fuel treatments with the sampling design and sample size we evaluated. TPH prior to treatment was not directly related to the distribution of fuel time-lag classes within the fuel bed, although the percentage of 10-h fuels could be predicted from pre-treatment conditions. However, stand density index, which accounts for both the relative stem number and DBH of the stand, effectively predicts post-treatment fuel loading across the whole study area. Further, SDI predicted that as the density of a stand increases, a greater percentage of the overall fuel load consisted of 100-h fuels, while 10-h fuels decreased in percentage, likely a result of operational adjustments. Future modeling efforts to predict post-mastication fuel loading should account for both the stem number and stem size, as stand density alone may not provide the necessary predictive ability. Attempting to predict resulting fuels from the number of trees per unit area alone does not account for variable volumes of materials in trees of different diameters. Stand density measures, such as SDI, provide greater insight into stand composition and overall stand biomass, which is significant when predicting fuel load volumes resulting from the physical conversion of standing biomass to surface-based mulched materials. Two stands with identical TPH may contain varying amounts of biomass as standing trees, whereas it is expected that two stands with identical SDI would have the same amount of overall biomass given similar forest types and species.

We believe that revisiting these methods, while taking into account the sampling considerations mentioned in the discussion, is an important undertaking and could lead to the increased implementation and effectiveness of mastication treatments. The rapid onset of lidar-derived models to map individual-tree locations and stem characteristics, coupled with onboard GNSS mapping of spatially, explicit, real-time equipment activities, offer the promise of improved high-resolution fuel bed prediction in the immediate future. Further expanding the scope of the field sampling to multiple, unique forest types, operators, and prescriptions would better capture the variability associated with the masticated surface fuel loads. Future work should address these factors more closely, though the determination of their impacts will likely require sampling at a higher intensity than that performed in this study, or with a sampling design that directly accounts for the spatial resolution at which comminuted material is scattered as a function of localized stand density,

treatment prescription, topography, equipment type and size, and the pattern of equipment movements.

2.7 Literature Cited

1. E. D. Reinhardt, R. E. Keane, D. E. Calkin, and J. D. Cohen, "Objectives and Considerations for Wildland Fuel Treatment in Forested Ecosystems of the Interior Western United States," *For. Ecol. Manag.*, vol. 256, pp. 1997–2006, 2008, doi: 10.1016/j.foreco.2008.09.016.

2. B. R. Hartsough *et al.*, "The Economics of Alternative Fuel Reduction Treatments in Western United States Dry Forests: Financial and Policy Implications from the National Fire and Fire Surrogate Study," *For. Policy Econ.*, vol. 10, pp. 344–354, 2008, doi: 10.1016/j.forpol.2008.02.001.

3. T. M. Oliveira, A. M. G. Barros, A. A. Ager, and P. M. Fernandes, "Assessing the Effect of a Fuel Break Network to Reduce Burnt Area and Wildfire Risk Transmission," *Int. J. Wildland Fire*, vol. 25, pp. 619–632, 2016, doi: 10.1071/WF15146.

4. F. J. Alcasena, A. A. Ager, M. Salis, M. A. Day, and C. Vega-Garcia, "Optimizing Prescribed Fire Allocation for Managing Fire Risk in Central Catalonia," *Sci. Total Environ.*, vol. 621, pp. 872–885, 2018, doi: 10.1016/j.scitotenv.2017.11.297.

5. J. K. Agee and C. N. Skinner, "Basic Principles of Forest Fuel Reduction Treatments," *For. Ecol. Manag.*, vol. 211, pp. 83–96, 2005, doi: 10.1016/j.foreco.2005.01.034.

6. S. L. Stephens *et al.*, "Fire Treatment Effects on Vegetation Structure, Fuels, and Potential Fire Severity in Western U.S. forests," *Ecol. Appl.*, vol. 19, no. 2, pp. 305–320, 2009.

7. J. K. Agee, "The Influence of Forest Structure on Fire Behavior," Redding, CA, USA, Jan. 1996, pp. 52–68.

8. S. L. Stephens, "Evaluation of the Effects of Silvicultural and Fuels Treatments on Potential Fire Behaviour in Sierra Nevada Mixed-conifer Forests," *For. Ecol. Manag.*, vol. 105, pp. 21–35, 1998.

9. R. J. Huggett Jr., K. L. Abt, and W. Shepperd, "Efficacy of Mechanical Fuel Treatments for Reducing Wildfire Hazard," *For. Policy Econ.*, vol. 10, pp. 408–414, 2008, doi: 10.1016/j.forpol.2008.03.003.

10. M. A. Battaglia, M. E. Rocca, C. C. Rhoades, and Michael G. Ryan, “Surface Fuel Loadings Within Mulching Treatments in Colorado Coniferous Forests,” *For. Ecol. Manag.*, vol. 260, pp. 1557–1566, 2010, doi: 10.1016/j.foreco.2010.08.004.

11. J. M. Kane, E. E. Knapp, and J. M. Varner, “Variability in Loading of Mechanically Masticated Fuel Beds in Northern California and Southwestern Oregon,” presented at the Fuels Management—How to Measure Success, Portland, OR, USA, Mar. 2006.

12. T. B. Jain *et al.*, “Restoration of Northern Rocky Mountain Moist Forests: Integrating Fuel Treatments from the Site to the Landscape,” presented at the 2007 National Silviculture Workshop, Portland, OR, USA, 2008.

13. T. Jain, P. Sikkink, R. Keefe, and J. Byrne, “To Masticate or Not: Useful Tips for Treating Forest, Woodland, and Shrubland Vegetation,” U.S. Department of Agriculture, Forest Service, Rocky Mountain Research Station, Fort Collins, CO, USA, General Technical Report RMRS-GTR-381, 2018.

14. J. M. Kane, J. M. Varner, and E. E. Knapp, “Novel Fuelbed Characteristics Associated with Mechanical Mastication Treatments in Northern California and Southwestern Oregon, USA,” *Int. J. Wildland Fire*, vol. 18, pp. 686–697, 2009, doi: 10.1071/WF08072.

15. J. K. Kreye *et al.*, “Fire Behavior in Masticated Fuels: A Review,” *For. Ecol. Manag.*, vol. 314, pp. 193–207, 2014, doi: 10.1016/j.foreco.2013.11.035.

16. S. L. Stephens and J. J. Moghaddas, “Fuel Treatment Effects on Snags and Coarse Woody Debris in a Sierra Nevada Mixed Conifer Forest,” *For. Ecol. Manag.*, vol. 214, pp. 53–64, 2005, doi: 10.1016/j.foreco.2005.03.055.

17. S. Hood and R. Wu, “Estimating Fuel Bed Loadings in Masticated Areas,” Portland, OR, USA, Mar. 2006, pp. 1–8.

18. A. L. Reiner, N. M. Vaillant, J. Fites-Kaufman, and S. N. Dailey, “Mastication and Prescribed Fire Impacts on Fuels in a 25-year Old Ponderosa Pine Plantation, Southern Sierra Nevada,” *For. Ecol. Manag.*, vol. 258, pp. 2365–2372, 2009, doi: 10.1016/j.foreco.2009.07.050.

19. L. A. Arroyo, C. Pascual, and J. A. Manzanera, “Fire Models and Methods to Map Fuel Types: The Role of Remote Sensing,” *For. Ecol. Manag.*, vol. 256, pp. 1239–1252, 2008, doi: 10.1016/j.foreco.2008.06.048.

20. R. E. Keane, R. Burgan, and J. van Wagtendonk, “Mapping Wildland Fuels for Fire Management Across Multiple Scales: Integrating Remote Sensing, GIS, and Biophysical Modeling,” *Int. J. Wildland Fire*, vol. 10, pp. 301–319, 2001, doi: 10.1071/WF01028.

21. M. G. Rollins, R. E. Keane, and R. A. Parsons, “Mapping Fuels and Fire Regimes Using Remote Sensing, Ecosystem Simulation, and Gradient Modeling,” *Ecol. Appl.*, vol. 14, no. 1, pp. 75–95, 2004.

22. M. J. Falkowski, P. E. Gessler, P. Morgan, A. T. Hudak, and A. M. S. Smith, “Characterizing and Mapping Forest Fire Fuels Using ASTER Imagery and Gradient Modeling,” *For. Ecol. Manag.*, vol. 217, pp. 129–146, 2005, doi: 10.1016/j.foreco.2005.06.013.

23. M. Maltamo, K. Eerikainen, J. Pitka¨nen, J. Hyyppa, and M. Vehmas, “Estimation of Timber Volume and Stem Density Based on Scanning Laser Altimetry and Expected Tree Size Distribution Functions,” *Remote Sens. Environ.*, vol. 90, pp. 319–330, 2004, doi: 10.1016/j.rse.2004.01.006.

24. H.-E. Andersen, R. J. McGaughey, and S. E. Reutebuch, “Estimating Forest Canopy Fuel Parameters Using LIDAR Data,” *Remote Sens. Environ.*, vol. 94, pp. 441–449, 2005, doi: 10.1016/j.rse.2004.10.013.

25. N. S. Skowronski, K. L. Clark, M. Duveneck, and J. Hom, “Three-dimensional Canopy Fuel Loading Predicted Using Upward and Downward Sensing LiDAR Systems,” *Remote Sens. Environ.*, vol. 115, pp. 703–714, 2011, doi: 10.1016/j.rse.2010.10.012.

26. T. L. Erdody and L. M. Moskal, “Fusion of LiDAR and Imagery for Estimating Forest Canopy Fuels,” *Remote Sens. Environ.*, vol. 114, pp. 725–737, 2010, doi: 10.1016/j.rse.2009.11.002.

27. Y. Chen, X. Zhu, M. Yebra, S. Harris, and N. Tapper, “Development of a Predictive Model for Estimating Forest Surface Fuel Load in Australian Eucalypt Forests with LiDAR Data,” *Environ. Model. Softw.*, vol. 97, pp. 61–71, 2017, doi: 10.1016/j.envsoft.2017.07.007.

28. M. K. Jakubowksi, Q. Guo, B. Collins, S. Stephens, and M. Kelly, “Predicting Surface Fuel Models and Fuel Metrics Using Lidar and CIR Imagery in a Dense, Mountainous Forest,” *Photogramm. Eng. Remote Sens.*, vol. 79, no. 1, pp. 37–49, 2013.

29. M. Mutlu, S. C. Popescu, C. Stripling, and T. Spencer, “Mapping Surface Fuel Models Using Lidar and Multispectral Data Fusion for Fire Behavior,” *Remote Sens. Environ.*, vol. 112, pp. 274–285, 2008, doi: 10.1016/j.rse.2007.05.005.

30. J. A. N. Van Aardt, M. Arthur, G. Sovkoplas, and T. L. Swetnam, “LiDAR-based Estimation of Forest Floor Fuel Loads Using a Novel Distributional Approach,” University of Tasmania, Australia, Oct. 2011, pp. 1–8.

31. M. Mutlu, S. C. Popescu, and K. Zhao, “Sensitivity Analysis of Fire Behavior Modeling with LIDAR-derived Surface Fuel Maps,” *For. Ecol. Manag.*, vol. 256, pp. 289–294, 2008, doi: 10.1016/j.foreco.2008.04.014.

32. H. A. Kramer, B. M. Collins, M. Kelly, and S. L. Stephens, “Quantifying Ladder Fuels: A New Approach Using LiDAR,” *Forests*, vol. 5, pp. 1432–1453, 2014, doi: 10.3390/f5061432.

33. N. Skowronski, K. Clark, R. Nelson, J. Hom, and M. Patterson, “Remotely Sensed Measurements of Forest Structure and Fuel Loads in the Pinelands of New Jersey,” *Remote Sens. Environ.*, vol. 108, pp. 123–129, 2007, doi: 10.1016/j.rse.2006.09.032.

34. M. García, D. Riaño, E. Chuvieco, J. Salas, and F. M. Danson, “Multispectral and LiDAR Data Fusion for Fuel Type Mapping Using Support Vector Machine and Decision Rules,” *Remote Sens. Environ.*, vol. 115, pp. 1369–1379, 2011, doi: 10.1016/j.rse.2011.01.017.

35. B. Koetz, F. Morsdorf, S. van der Linden, T. Curt, and B. Allgower, “Multi-source Land Cover Classification for Forest Fire Management Based on Imaging Spectrometry and LiDAR Data,” *For. Ecol. Manag.*, vol. 256, pp. 263–271, 2008, doi: 10.1016/j.foreco.2008.04.025.

36. O. F. Price and C. E. Gordon, “The Potential for LiDAR Technology to Map Fire Fuel Hazard Over Large Areas of Australian Forest,” *J. Environ. Manage.*, vol. 181, pp. 663–673, 2016, doi: 10.1016/j.jenvman.2016.08.042.

37. M. García *et al.*, “Extrapolating Forest Canopy Fuel Properties in the California Rim Fire by Combining Airborne LiDAR and Landsat OLI Data,” *Remote Sens.*, vol. 9, no. 394, pp. 1–19, 2017, doi: 10.3390/rs9040394.

38. Y. Chen, X. Zhu, M. Yebra, S. Harris, and N. Tapper, “Strata-based Forest Fuel Classification for Wild Fire Hazard Assessment Using Terrestrial LiDAR,” *J. Appl. Remote Sens.*, vol. 10, no. 4, 2016, doi: 10.1117/1.JRS.10.046025.

39. B. Vermey, “Nez Perce-Clearwater National Forest Red River Ranger District, Elk City, ID, USA,” 2017.

40. G. E. Dixon, *Essential FVS: A User's Guide to the Forest Vegetation Simulator*. Fort Collins, CO, USA: U.S. Department of Agriculture, Forest Service, Forest Management Service Center, 2002.

41. L. Breiman, "Random Forests," *Mach. Learn.*, vol. 45, pp. 5–32, 2001.

42. A. Liaw and M. Wiener, "Classification and Regression by randomForest," *R News*, vol. 2, no. 3, pp. 18–22, 2002.

43. R. M. Becker, R. F. Keefe, N. M. Anderson, and J. U. H. Eitel, "Use of Lidar-derived Landscape Parameters to Characterize Alternative Harvest System Options in the Inland Northwest," *Int. J. For. Eng.*, vol. 29, no. 3, pp. 179–191, 2018, doi: 10.1080/14942119.2018.1497255.

44. R Core Team, *R: A Language and Environment for Statistical Computing*. Vienna, Austria: R Foundation for Statistical Computing; R Core Team, 2020. Accessed: Feb. 12, 2020. [Online]. Available: https://www.R-project.org

45. Leo Breiman, "Manual on Setting Up, Using, and Understanding Random Forests v3.1," Statistics Department University of California Berkeley, CA, USA, 2002. Accessed: Feb. 13, 2020. [Online]. Available: https://www.stat.berkeley.edu/~breiman/RandomForests/cc_manual.htm

46. K. D. Brosofske, R. E. Froese, M. J. Falkowski, and A. Banskota, "A Review of Methods for Mapping and Prediction of Inventory Attributes for Operational Forest Management," *For. Sci.*, vol. 60, no. 4, pp. 733–756, 2014, doi: 10.5849/forsci.12-134.

47. S. Cinaroglu, "Comparison of Performance of Decision Tree Algorithms and Random Forest: An Application on OECD Countries Health Expenditures," *Int. J. Comput. Appl.*, vol. 138, no. 1, pp. 37–41, 2016.

48. M. Belgiu and L. Dragut, "Random Forest in Remote Sensing: A Review of Applications and Future Directions," *ISPRS J. Photogramm. Remote Sens.*, vol. 114, pp. 24–31, 2016, doi: 10.1016/j.isprsjprs.2016.01.011.

49. J. S. Evans and M. A. Murphy, *rfUtilities: Random Forests Model Selection and Performance Evaluation*. Accessed: May 15, 2017. [Online]. Available: http://rdocumentation.org/packages/rfUtilities/versions/2.0-1.html.

50. R. J. McGaughey, *FUSION/LDV: Software for LiDAR Data Analysis and Visualization*. University of Washington: Seattle,WA, USA: USDA Forest Service, Pacific Northwest Research Station, 2017. Accessed: Jun. 15, 2017. [Online]. Available: http://forsys.sefs.uw.edu/fusion/fusionlatest.html

51. L. H. Reineke, "Perfecting a Stand-density Index for Even-aged Forests," *J. Agric. Res.*, vol. 46, no. 7, pp. 627–638, 1933.

52. C. W. Woodall, P. D. Miles, and J. S. Vissage, "Determining Maximum Stand Density Index in Mixed Species Stands for Strategic-scale Stocking Assessments," *For. Ecol. Manag.*, vol. 216, pp. 367–377, 2005, doi: 10.1016/j.foreco.2005.05.050.

53. J. D. Shaw, "Reineke's Stand Density Index: Where are we and where do we go from here?," Fort Worth, TX, USA, Oct. 2005, pp. 1–13.

54. M. J. Ducey and R. A. Knapp, "A Stand Density Index for Complex Mixed Species Forests in the Northeastern United States," *For. Ecol. Manag.*, vol. 260, no. 9, pp. 1613–1622, 2010, doi: 10.1016/j.foreco.2010.08.014.

55. C. L. VanderSchaaf, "Reineke's Stand Density Index: A Quantitative and Non-unitless Measure of Stand Density," Hot Springs, AK, USA, Nov. 2008, vol. 2013, pp. 577–579.

56. J. K. Brown, "Handbook for Inventorying Downed Woody Material," USDA Forest Service, Ogden, Utah, General Technical Report INT-16, 1974.

57. J. Pinheiro and D. Bates, *nlme: Linear and Nonlinear Mixed Effects Models*. R Core Team, 2020. [Online]. Available: https://CRAN.R-project.org/package=nlme.

58. N. M. Laird and J. H. Ware, "Random-effects Models for Longitudinal Data," *Biometrics*, vol. 38, pp. 963–974, 1982.

59. P. A. Fekety, M. J. Falkowski, A. T. Hudak, T. B. Jain, and J. S. Evans, "Transferability of Lidar-derived Basal Area and Stem Density Models within a Northern Idaho Ecoregion," *Can. J. Remote Sens.*, vol. 44, no. 2, pp. 131–143, 2018, doi: 10.1080/07038992.2018.1461557.

60. A. T. Hudak *et al.*, "Mapping Forest Structure and Composition from Low-density LiDAR for Informed Forest, Fuel, and Fire Management at Englin Air Force Base, Florida, USA," *Can. J. Remote Sens.*, vol. 42, pp. 411–427, 2016.

61. M. J. Falkowski, A. T. Hudak, N. L. Crookston, P. E. Gessler, E. H. Uebler, and A. M. S. Smith, “Landscape-scale Parameterization of a Tree-level Forest Growth Model: A K-nearest Neighbor Imputation Approach Incorporating LiDAR Data,” *Can. J. For. Res.*, vol. 40, pp. 184–199, 2010, doi: 10.5589/m08-055.

62. N. W. Brewer *et al.*, “Fuel Moisture Influences on Fire-altered Carbon in Masticated Fuels: An Experimental Study,” *J. Geophys. Res. Biogeosciences*, vol. 118, pp. 30–40, 2013, doi: 10.1029/2012JG002079.

63. Z. D. Lyon, P. Morgan, C. S. Stevens-Rumann, A. M. Sparks, R. F. Keefe, and A. M. S. Smith, “Fire Behaviour in Masticated Forest Fuels: Lab and Prescribed Fire Experiments,” *Int. J. Wildland Fire*, 2018, doi: 10.1071/WF17145.

Chapter 3: Development of Activity Recognition Models for Mechanical Fuel Treatments Using Consumer-grade GNSS-RF Devices and Lidar

Published In:

Becker, R.M, Keefe, R.F. Development of activity recognition models for mechanical fuel treatments using consumer-grade GNSS-RF devices and lidar. *Forestry*. **2022**, DOI:10.1093/forestry/cpab058 (In Press).

3.1 Abstract

Mobile technologies are rapidly advancing the field of forest operations and providing opportunities to quantify management tasks in new ways through increased digitalization. For instance, devices equipped with global navigation satellite system and radio frequency transmission (GNSS-RF) enable real-time data collection and sharing of positional data in remote, off-the-grid environments where cellular and internet availability are otherwise inaccessible. In this study, consumer-grade GNSS-RF data were evaluated to determine their effectiveness in developing activity recognition models for excavator-based mastication operations. The ability to automate the classification of cycle elements for operations is valuable for quickly and efficiently quantifying production rates for research and industry applications. The GNSS-RF-based activity recognition model developed successfully classified productive elements versus delay with over 95% accuracy. Individual cycle elements were classified with an overall model accuracy of 73.6%, with individual element classification accuracy ranging from 51.3% for walk/reposition to 95.6% for mastication elements. Reineke's stand density index (SDI), basal area (m^2ha^{-1}) of treated areas, and the duration of cycle elements impacted the classification accuracy of the activity recognition model. Impacts of forest stand characteristics on the production rate of mastication treatments were also assessed. Production rates ($ha \cdot hr^{-1}$) for mastication treatments were affected by the basal area of treated areas. However, the degree to which this would impact operations in practice is minimal. Determining the proper application and capabilities of mobile technologies and remote sensing for quantifying forest operations is valuable in continuing the innovation and advancement of forest digitalization.

3.2 Introduction

Innovative methods for production analysis of forest stand treatments provide an alternative to conventional time-and-motion study methods used in forest operations. Time and motion studies provide important information that contractors and managers can use to quantify factors affecting production rates and treatment costs associated with timber harvesting, thinning, or fuel reduction

operations (McDonald and Fulton, 2005; George et al., 2021). Historically, these studies have been conducted using manual recording methods, with in-person observation and timing. These methods are costly, time-intensive, and expose observers to safety hazards. They are also prone to measurement error (Olsen and Kellogg, 1983; Strandgard and Mitchell, 2015). Direct observation of equipment by observers may bias results by influencing operator performance and decision making (Nuutinen et al., 2008). Automated methods to estimate treatment production rates and costs may help to improve forest operations, particularly as industry seeks to advance automation and digitalization.

Time and motion studies support improved efficiency and reduce operational delays through the definition, observation, analysis and quantification of individual work elements within productive cycles for equipment and work tasks (Miyata, 1980; Kellogg et al., 1996; Klepac and Rummer, 2002; Wang et al., 2003; Wang et al., 2004; Acuna and Kellogg, 2009; Acuna et al., 2011; Alam et al., 2013; Strandgard et al., 2014; Talbot et al., 2014; Borz et al., 2018). Using regression, relationships between productive cycles and stand and site characteristics are used to develop predictive production models for equipment (Kellogg et al., 1996; Huyler and LeDoux, 1997; Wang et al., 2004; Adebayo et al., 2007; Acuna and Kellogg, 2009; Acuna et al., 2011; Bell et al., 2017). Global navigation satellite system (GNSS) enabled devices have been used to characterize productive work cycle elements and perform production analysis (McDonald, 1999; McDonald et al., 2000; Taylor et al., 2001; Veal et al., 2001; McDonald and Fulton, 2005; de Hoop and Dupré, 2006; Gallo et al., 2013; Hejazian et al., 2013; Keefe et al., 2014; Strandgard and Mitchell, 2015; Olivera et al., 2016) and to assess ground disturbance (McMahon, 1997; McDonald et al., 1998; Carter et al., 2000; McDonald et al., 2002) of forestry equipment. This has been done, in part, through the development of activity recognition models, which use movements of machines across time and space captured by GNSS transponders to develop relationships with productive cycle elements (Becker et al., 2017). Once developed and validated, these models can replace traditional field observation techniques to predict production rates of forest machines and can also be used for a variety of safety applications. Additionally, global navigation satellite system with radio frequency (GNSS-RF) can be used to facilitate data sharing and transfer between devices in areas that lack cellular and internet connectivity (Keefe et al., 2014). With this system, data is transferred between GNSS transponders via radio frequency which serves as a cost-effective alternative to satellite data transfer. This system has been effectively used to characterize the swing movements of forestry machines with high accuracy (Becker et al., 2017) and logging safety applications (Grayson et al., 2016; Wempe and Keefe, 2017; Zimbelman et al., 2017; Newman et al., 2018; Wempe et al., 2019).

Many new forest machines are outfitted with integrated data collection systems that monitor and record machine production, logistics and diagnostics. Unfortunately, these are often proprietary, manufacturer-specific systems on recently built machines which limits the sharing and integration of data on specific job sites where the manufacturer, model, and vintage of machines working commonly vary. Previous studies have evaluated automated time study systems for forestry machines using data collected from the machine onboard computers using controlled-area network (CAN) hardware as the interface for a variety of sensors (Wang et al., 2003; Palander et al., 2013). Some of these early studies lacked real-time positional data, which provides valuable information for evaluating production and jobsite hazards. As methods for sharing mobile data at remote jobsites becomes more common, options for real-time analyses of ground workers and equipment for production analysis and improved situational awareness with machines is becoming increasingly possible. Consumer-available GNSS-RF devices or other Internet-of-Things (IoT) methods for location-sharing and data collection enable activity recognition methods for machines and personnel that are tailored to machine type (feller-buncher, skidder, processor) or work performed (tree planting, felling, bucking, etc.) and independent of machine specifications. This generalized approach to providing real-time analysis of forest operations enables universal data collection and sharing for forest machines and work tasks, something previously unavailable in operational forestry.

In a preliminary study, Becker et al. (2017) used this methodology in a controlled experiment to determine the effectiveness of GNSS-RF for capturing the swing movements of forestry machinery. Equipment productive cycle elements were accurately classified in over 90% of cases, with data transmission frequency and swing radius of transponders having the greatest impact on classification accuracy. Despite their proven effectiveness in controlled studies, use of GNSS-RF devices for real-time activity recognition of forest equipment during active operations has received little attention. Accurate classification of cycle elements using GNSS-RF devices in active operations would support the widespread development of activity recognition model libraries and facilitate use of Artificial Intelligence in operational forestry. Further, improved analytics could be developed and made widely available using user-friendly, affordable, and transferrable devices. In addition to the value to contractors, automatic production sampling and processing enables the collection of large amounts of data more cost effectively than physical observation, giving researchers the ability to collect additional pertinent information about thinning, fuel reduction, or harvesting operations without the need for more personnel (Palander et al., 2013). To determine the efficacy of GNSS-RF devices as the foundational data collection method for a universal activity recognition library for forest operations, research is needed to assess the accuracy with which individual cycle elements can be characterized using this spatially explicit data.

Predicting and modeling management production rates for equipment in real-time using activity recognition is also valuable for management planning (Keefe et al., 2014). Production metrics predicted from activity recognition models, if accurate, can be coupled with stand and site characteristics to forecast fuel treatment costs at forest and landscape levels. Topography and stand characteristics, including stand density and volume, impact the production of industrial forest operations (Acuna and Kellogg, 2009; Alam et al., 2013; Hiesel and Benjamin, 2013). Quantifying the impact of local variability in landscape treatment planning is an important step in the development of estate-level treatment optimization. Advances in remote sensing have made it possible to perform landscape-scale predictions of stand and site characteristics quickly and accurately. Light detection and ranging (lidar), specifically, is used extensively to quantify forest structure, attributes and terrain morphology (Falkowski et al., 2005; Reutebuch et al., 2005; Akay et al., 2009; Falkowski et al., 2009; Hudak et al., 2012; Wulder et al., 2012; Man et al., 2014; Silva et al., 2017). Utilizing lidar-derived forest metrics coupled with positional data from GNSS-RF provides new opportunities to quantify the relationships between the production of mechanized operations and stand characteristics. For example, Becker et al. (2018) showed the significant potential for characterizing the appropriateness of sites for logging systems at the stand and landscape scales using lidar-derived forest and site metrics and equipment-specific operable thresholds. These relationships can be used to support the pre-planning and implementation of industrial timber harvests and fuel treatments.

With changes in seasonal weather patterns, forest health and forest composition, interest in mechanical fuels management treatments to address forests at high risk for severe wildfire has increased. Mastication is a mechanized fuel treatment that reduces the size of both standing and downed woody materials through grinding, shredding, chunking or mulching (Kane et al., 2006; Jain et al., 2008). While increasingly used, determining the efficacy of mastication fuel treatments at landscape scales is challenging (Huggett Jr. et al., 2008), due in part to the difficulty of accurately quantifying production rates and costs of these treatments. Development of tools allowing managers to accurately study and forecast treatment rates and associated costs could considerably improve preplanning of fuel treatments prior to implementation and help optimize treatment expenditures on federal, state, tribal, and private lands in the western United States.

In this study, the effectiveness of using consumer-grade GNSS-RF multi-transponder devices to classify work cycle activities during mechanical fuel treatments was evaluated, building on prior work reported in Becker et al. (2017). Consumer-grade devices were used as a surrogate for more advanced multi-transponder systems that may be integrated into machines in the future. Activity recognition modelling success was quantified to determine the impact work cycle and stand

characteristics had on classification success. Additionally, production rates were modeled as a function of lidar-derived forest metrics to determine if these metrics could be used as predictors of operational efficiency and cost. This research will determine the feasibility and effectiveness of GNSS-RF-based activity recognition modeling and will help inform future management decisions regarding landscape scale use of mastication treatments. These technologies may help advance precision forestry and increased digitalization in forest operations.

3.3 Methods and Materials

3.3.1 Study Site and Treatment Details

All study treatment areas are located within the Orogrande Timber Sale area, located 11 kilometers (7 miles) southwest of Elk City, Idaho in mixed conifer forest typical of the region. The study area is within the 18,450 hectare (45,600 acre) Crooked River lidar acquisition flown in 2012 with a pulse density return of ≥4 points per square meter. These data were used to develop landscape scale forest vegetation metrics to quantify production rates. The areas where mastication occurred were originally designated to be harvest units. However, transportation logistics and low appraised value led forest managers to use of mastication as an alternative method to reduce stand density. The masticated stands encompassed 50 hectares (124 acres) with two treatment prescriptions. For the purposes of this study, sampling and analysis was concentrated in 38 hectares (95 acres) contained within three units with prescribed post-treatment stand densities of 40-80 trees per hectare. The three units treated, units 117, 120, and 147, were 13 hectares (33 acres), 15 hectares (37 acres) and 10 hectares (25 acres), respectively. Trees less than 18 centimeters (7 inches) were targeted for removal, with treatment goals of increasing average crown base height, creating space to encourage growth and vigor of residual future merchantable trees, and changing the fuel distribution within the stands to reduce ladder fuels and crown fire potential. Further, all dead and down material up to 30 centimeters (12 inches) was masticated. A Takeuchi TB290 compact excavator with a Fecon Bull Hog mastication head completed the treatments. Observation, time sampling, and GNSS-RF data collection occurred for two days in each of the three stands, providing three replicate measurements in similar stand conditions.

3.3.2 Time and Motion Field Sampling – GNSS-RF Data Collection and Preparation

All GNSS-RF data collection of machine movements were conducted using Garmin Alpha GNSS transponders and a corresponding Garmin Alpha receiver. Two GNSS-RF transponders were placed on the machine boom above the masticator head and at the center of the machine cab to capture the movements of each throughout the workday (Figure 3.1). Transmission interval for the GNSS-RF

transponders was set to transmit data packets to the receiving unit at the maximum frequency one measurement every 2.5 seconds, in order to classify machine cycle elements with the highest possible resolution. Becker et al. (2017) found that the 2.5 second transmission interval provided the highest element classification accuracy when analyzing swing movements of log loaders when compared to 5.0 and 10.0 second transmission rates. Similarly, the transponder was placed as far out on the boom of the mastication machine as possible without risk of device damage. Devices located farthest from the cab achieve the highest classification accuracy (Becker et al., 2017).

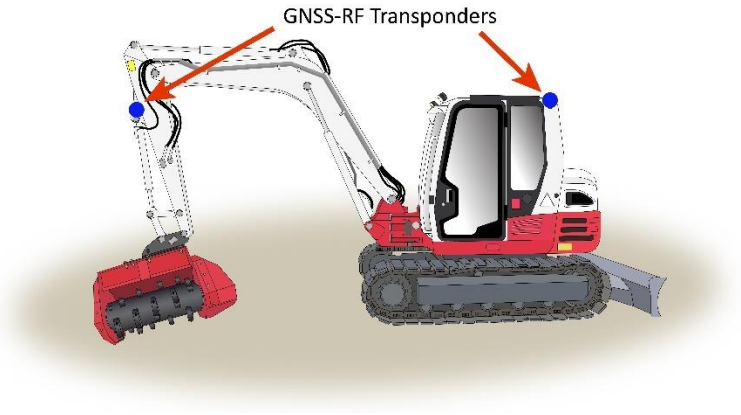

Figure 3.1. Takeuchi TB290 with the Fecon Bull Hog mastication head and the GNSS-RF multi-transponder device mounting locations.

When developing the activity profile for the mastication equipment, elemental cycle time observation data corresponding directly to the GNSS-RF data was recorded. A laptop computer synched with the nist.gov time server (*NIST Internet Time Servers*, 2017) was used to determine the start time of each productive cycle element to ensure manually recorded elements were synced with the time stamps derived from the GNSS-RF transponders and receiver. Two primary elements for the productive cycle of the mastication machine were chosen and defined: walk; and masticate (Table 3.1). Time and motion sampling was conducted for a minimum of four hours per day sampled.

Table 3.1. Cycle elements for mastication fuel treatments using a compact excavator-based masticator.

Element	Description
Walk/Reposition	Any lateral movement of the machine cab or boom without the mastication head treating standing or downed material. Begins as soon as swing or track movement starts and ends when standing or downed material mastication is contacted.
Masticate	The act of acquiring, clearing around and masticating target trees and downed woody debris and brush. Element begins once treatment of a target tree or downed material is initiated and ends at start of next element.
Delay	Periods where machine was inactive and stationary due for operational, mechanical, or personal factors.

Following field data collection, spatial data from the GNSS-RF transponders were merged by transponder location and date of treatment for each of the three stands sampled. This resulted in 6 days of spatially explicit data for the mastication process with two days at each of the three treatment stands. Observational data from the time and motion study was transcribed and then merged with the GNSS-RF data sets for analysis. The remaining analysis used a process similar to that used in Becker et al. (2017) (Figure 3.2).

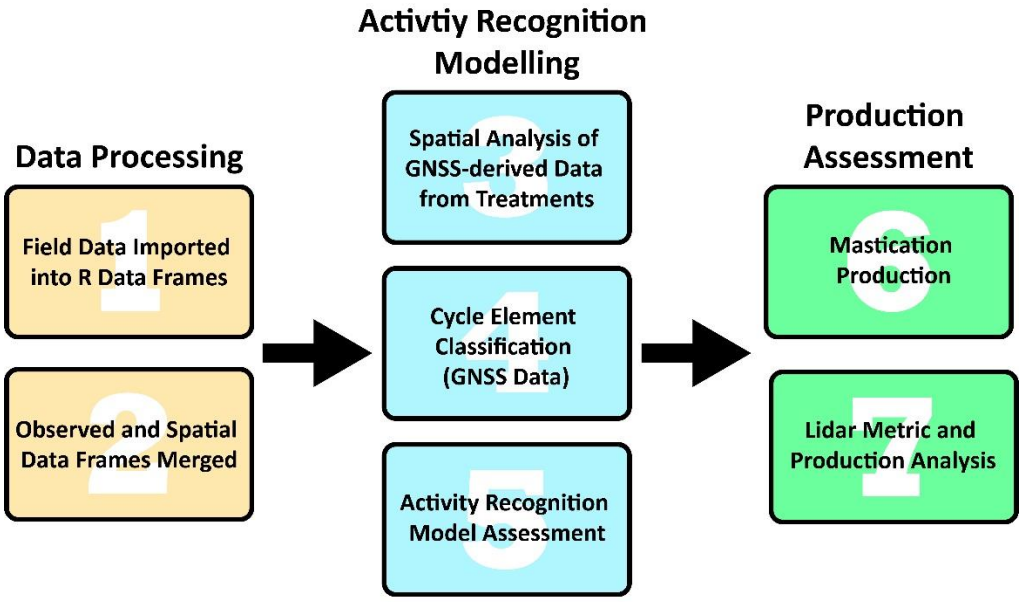

Figure 3.2. Flow diagram of the progression of analysis of the spatial and observed data.

3.3.3 GNSS-RF Activity Recognition Model Development

A script was written using the R statistical programming environment (R Core Team, 2020) that defined a rules-based, process modeling approach to productive cycle element classification based on machine movement and rotation in the coordinate space based on GNSS-RF derived locations from the boom and cab multi-transponders. The R script classifies data collected using the GNSS-RF transponders so that each row corresponds to a cycle element based on previously defined rules. The rules used to define the model accounted for the movements of the cab and boom mounted GNSS-RF devices independently and in relation to each other throughout the operation. These rules were developed based on observations of the equipment's movements while performing the cycle elements during field sampling. For example, prolonged durations where the GNSS-RF remained stationary would indicate delay where simultaneous movement of both devices would indicate the equipment was walking. Classification results were then compared to cycle elements observed during the time

and motion study. Evaluation of model performance was completed to determine how effectively and accurately spatial data from two GNSS-RF devices can classify mastication cycle elements. Following the development and processing of all time and motion observations using the activity recognition modelling scripts, the proportions of correctly classified elements within the extent of each treatment pixel were quantified by treatment unit and element. Correctly classified elements were compared to the total number of observed occurrences for each cycle element to calculate classification accuracy. Combined totals for all units were calculated as weighted averages due to varying occurrences of elements in each unit.

Delay-free production rates for the mastication treatments were determined as hectares treated per hour ($ha \cdot hr^{-1}$) for the three treatment units. Overall treatment extent was derived from the GNSS-RF transponder tracks, as it was assumed that all ground covered by the machine cab and boom was treated. This enabled treatment production rate to be estimated for the entirety of each treatment unit (117, 120, and 147) and for each individual forest metric prediction raster.

3.3.4 Lidar Processing and Mastication Production Rate Quantification

Characterizing relationships between stand characteristics and mastication treatment production rates required deriving the forest metrics of interest. In order to quickly and efficiently quantify forest metrics, random forest models (Breiman, 2001; Liaw and Wiener, 2002) were used to predict trees per hectare, stand net volume (m^3ha^{-1}), and basal area (m^2ha^{-1}) using lidar point cloud and inventory data from 91 forest inventory plots for the study area. These random forest models were developed using methods similar to those described in Becker et al. (2018) in the open source statistical analysis program, R (R Core Team, 2020), using the randomForests package (Liaw and Wiener, 2002). Random forests ensemble learning algorithms are commonly used because they provide excellent performance, high speed processing, the ability to reduce bias and correlation amongst trees and they also reduce overfitting compared to other classification and regression trees (CART) models (Brosofske et al., 2014; Belgiu and Dragut, 2016). This makes them a widely used machine learning solution (Breiman, 2002; Brosofske et al., 2014; Belgiu and Dragut, 2016; Cinaroglu, 2016). These random forest models were then used to develop 20 meter x 20 meter raster layers with predicted forest metrics for the entire Crooked River lidar acquisition extent, and more specifically the three stands studied in the Orogrande Timber Sale area.

3.3.5 Statistical Analysis – Forest Metrics Impacts on Production Rates and Activity Recognition

Linear mixed effects regression models were used to model the relationship between mastication treatment production rate ($ha \cdot hr^{-1}$) and lidar-predicted trees per hectare, stand density index, basal

area and total cubic foot volume of treatment plots using the nlme package (Pinheiro and Bates, 2020) in R. The general equation for mixed effect models is described as:

$$y_i = X_i\beta + Z_i u_i + \varepsilon_i \quad (1)$$

$$u_i \sim N(0, D), \quad \varepsilon_i \sim N(0, R_i), \quad (2)$$

where β are fixed effects, u are random effects, X is the model matrix for fixed effects, Z is the model matrix for random effects, ε is the vector of errors, R is the variance-covariance matrix of within-individual measurements and D is the variance-covariance matrix of random effects (Laird and Ware, 1982). Treatment unit was treated as random effect and random intercepts were used when fitting models.

Further, mixed effects logistic regression models were used to determine if the same forest metrics impacted the odds of correct classification of cycle elements from the activity recognition model using the R lme4 package (Bates et al., 2015). An additional model was included to determine if the duration of the element (seconds) impacted correct classification. A response variable of 1 indicated correct classification, 0 indicated incorrect classification, and treatment unit was once again treated as the random effect. The lidar-derived forest metrics and field observed element durations were used in this assessment.

3.3.6 Soil Disturbance Extent

GNSS-RF transponder tracks were used to determine the proportion of land area within treatment units impacted by the machine in comparison to the overall area treated. Undisturbed ground, in the context of our analysis, was any ground that the machine did not traverse with the tracks. The GNSS-RF track data for the machine cab was merged to create a record of the machine's position throughout the duration of the treatments in the three stands. It was assumed, due to the placement of the transponder, that the cab GNSS-RF transponder accurately represented the path covered by the machine tracks. An additional assumption made in the analysis was that the footprint of the machine encompassed both the ground surface in direct contact with the machine tracks and all area directly beneath the machine between the tracks. The machine's footprint on the ground surface is known to be 6.3 square meters. Therefore, a buffer was placed along the entirety of the cab path for the three stands, resulting in a total area of disturbance ground surface for the treatment in square hectares. The proportion of disturbed ground area was determined by dividing the estimated ground disturbance area by total stand area treated.

3.4 Results

3.4.1 Random Forest Models for Forest Stand Characteristics

The random forest model parameter estimates used to predict 20 x 20-meter treatment unit characteristics from lidar are shown in Table 3.2. Based on findings from prior studies and their conclusions regarding model validity, random forest models where the root mean square error (RMSE) exceeded 50% of the prediction mean for forest metrics were excluded from later analysis in this study (Hudak et al., 2016; Fekety et al., 2018). The random forest models for stem density (TPH), basal area (m^2ha^{-1}) and stand density index models resulted in RMSEs of 46%, 42%, and 38% of the prediction means respectively and therefore met the desired accuracies. For the random forest model predicting stand volume (m^3ha^{-1}), an RMSE of 166.93 was 54% of the predicted mean and was therefore excluded from use in subsequent analysis. Random forest accuracies of 71.5%, 77.4%, 74.3%, and 79.0% for trees per hectare, basal area per hectare, volume per hectare and stand density index respectively, were comparable to those achieved by Falkowski et al. (2010) and Hudak et al. (2016). Predicted stand characteristics provided the basis for regression modeling of mastication treatment production rate.

Table 3.2. Random forest model quality assessment.

Random Forest	Prediction Mean	RMSE	R-squared	Accuracy (%)
Stand Density (TPH)	468.00	217.36	0.55	71.5
Basal Area (m^2ha^{-1})	30.56	12.95	0.63	77.4
Total Volume (m^3ha^{-1})	307.99	165.35	0.57	76.3
Stand Density Index (SDI)	299.17	110.296	0.45	79.0

3.4.2 Stand Production Rate Summaries

Lidar-derived forest metric summaries and treatment production rate summaries including unit slope, area treated, and utilization rates for the three treatment units and the averages across all treated areas are shown in Table 3.3. Across all units the average trees per hectare was 564, with unit 120 containing the highest stand density at 665 trees·ha^{-1}. Average stand density index across all units was 385 and the average basal area was 39 m^2ha^{-1}. A total of approximately 4.6 hectares was treated during sampling with an average production rate of 0.163 h·hr^{-1} across all units. The values given for each of the forest metrics were the averages calculated within the extent of the area treated during time and motion sampling and not the average of the entire unit. Mastication accounted for 74.8%, 81.9% and 65.2% of the overall sampled time for unit 117, 120, and 147, respectively. The remaining

sampling time in the three units was split between walking and repositioning at 15.7%, 13.7% and 9.5%; and delay at 9.5%, 4.4% and 25.3% for unit 117, 120, and 147, respectively.

Table 3.3. Forest metric and mechanical fuel treatment production summary for the sampled portions of the treatment units.

	Unit			
	117	**120**	**147**	**All**
Forest Metric Summaries				
TPH (trees·ha^{-1})	489	665	409	564
SDI	329	405	288	358
BA (m^{2}ha^{-1})	33	49	28	39
Volume (m^{3}ha^{-1})	319	499	293	400
Standing Biomass (ton·ha^{-1})	238.61	373.25	219.16	299.20
Production Rate Summaries				
Avg. Slope (%)	24.0	25.0	27.0	25.3
Treated Area (ha)	1.532	2.330	0.712	4.574
Production Rate (ha·hr^{-1})	0.161	0.203	0.125	0.163
Utilization Rate (%)	90.5	95.6	74.7	87.3
Disturbed Area (ha)	0.506	0.576	0.269	1.351
Disturbed Area (%)	33	25	38	30

3.4.3 Activity Recognition Model

Modelling results from the activity recognition model can be found in Table 3.4. Across all units, masticate, walk/reposition, and delay were correctly classified 95.6%, 51.3%, and 80.4% of the time, respectively. Combined classification accuracy of all cycle elements across all units was 73.6%. The confusion matrix shown in Table 3.5 shows the results from the activity recognition modelling indicating the occurrences of true positives, false positives, true negatives, and false negatives for classification across all three treatment units.

Table 3.4. Percentage of correctly classified mechanical fuel treatment cycle elements within management units.

Unit	**Mastication**	**Walk/Reposition**	**Delay**	**All Elements**
117	97.6	55.9	73.3	76.8
120	96.3	52.1	71.4	74.2
147	90.8	41.4	87.5	67.0
All Units	**95.6**	**51.3**	**80.4**	**73.6**

Table 3.5. Confusion Matrix representing the results of the activity recognition model for units 117, 120, and 147.

		Actual		
		Delay	Masticate	Walk/ Reposition
	Delay	37	47	112
Prediction	Masticate	9	1684	740
	Walk/Reposition	0	30	895

In all, 3349 productive cycle elements composed of masticate and walk/reposition actions and 37 delay elements were correctly classified. With 3,554 overall elements sampled, this resulted in an overall classification accuracy of 95.3% for productive and delay elements. Attempting to differentiate the total productive time into individual elements exposed some potential limitations of using GNSS-RF data for production analysis in complex, active operations.

Compared to the 1684 successful mastication element classifications, the 77 false negatives resulted in a 95.6% overall classification success for mastication. There were 749 cases of false positive relating to the mastication element, with a majority (740) representing an actual walk and reposition element. This means the model overestimated mastication time. The walk and reposition element had the greatest number of false negative classifications across all three elements with a total of 852; 112 predicted as delay and 740 predicted as mastication. This was indicated by the poor individual classification success of the walk and reposition element of only 51% across all units.

3.4.4 Stand Metric Impacts on Production Rates

The results from linear mixed effects models predicting mastication production rate (ha hr^{-1}) from stand characteristics at the individual pixel level for the three treatment units are found in Table 3.6. There was no significant relationship between production rate and stand density index ($p=0.3040$, $R^2=0.225$) or trees per hectare ($p=0.8728$, $R^2=0.263$). However, basal area did significantly affect production rate ($p=0.0439$, $R^2=0.199$). Coefficients of determination (R^2) for these models represent the variance of the entire mixed model including fixed and random effects (Nakagawa and Schielzeth, 2013).

Results from the mixed effects logistic regression models used to quantify the relationship between stand metrics and classification accuracy of the recognition model are found in Table 3.7. All individual elements were assigned a specific stand metric pixel so all individual cycle elements, either correctly or incorrectly classified, were associated with the specific metrics. Of the stand metrics

assessed, all metrics other than trees per hectare (coefficient= -4.284e-05, odds ratio = 0.9996, p=0.0779) impacted classification accuracy. The relationship between correct element classification and stand density index (p=0.0189) showed every 1 unit increase in SDI resulted in a decrease in the log odds of correct classification of -1.518e-03, indicating a decrease in the model's ability to successfully classify cycle elements. This is supported by the odds ratio of 0.9984 which, with a value less than 1, indicates the same relationship. Similar significant relationships were found with basal area (coefficient=-2.559e-03, odds ratio = 0.9974, p = 0.0106). In the fourth model, the duration of element was found to have a strong significant relationship (p=<0.001) with every one- second increase in element duration increasing the odds of correct element classification 1.0946 times.

Table 3.6. Linear mixed effects regression results determining the relationship between mastication production rate ($ha \cdot hr^{-1}$) and forest metrics.

Dependent Variable	Independent Variable	Regression Coefficient	P-Value	R^2
Production Rate ($ha \cdot hr^{-1}$)	SDI	1.167e-04	0.3040	0.225
	TPH ($trees \cdot ha^{-1}$)	7.310e-06	0.8728	0.263
	BA ($m^2 ha^{-1}$)	3.495e-04	0.0439	0.199

Table 3.7. Mixed effects logistic regression models evaluating whether correct cycle element classification during activity recognition was impacted by changes in forest stand metrics and element duration.

Dependent Variable	Independent Variable	Regression Coefficient	Standard Error	Odds Ratio	P-Value
Correct Classification	SDI	-1.518e-03	6.46e-04	0.9984	0.0189
	TPH ($trees \cdot ha^{-1}$)	-4.284e-05	2.43e-04	0.9996	0.0779
	BA ($m^2 ha^{-1}$)	-2.559e-03	1.00e-03	0.9974	0.0106
	Element Dur. (sec)	9.043e02	4.99e-03	1.0946	<0.001

3.5 Discussion

3.5.1 GNSS-RF Activity Recognition Effectiveness and Influence of Forest Metrics

We successfully predicted the productive cycle elements of mastication treatments using spatially explicit data derived from two unique GNSS-RF devices during active mastication operations. These devices provided a simple and transferrable option for collecting and sharing location data of the mastication equipment, as the two devices could easily be swapped between equipment as needed. It was possible to determine the extent of the equipment's movements and quantify the area of the unit that was treated based on the movement of the boom transponder and the area impacted by the machine tracks based on the progression of the transponder on the machine cab. Further, these GNSS-

RF devices made it possible to differentiate between extended periods of delay and productive work elements when neither of the transponders were in motion.

While the applied sampling rate and transponder location data used in this study enabled successful classification of individual cycle elements over 90% of the time for all elements in Becker et al. (2017), the decreased total classification accuracy of 73.6% in this study may be a result of multiple factors. The GNSS-RF devices used in this study record coordinates snapped to an approximate 1.5 meter x 1.5 meter grid, which limits the precision of the recorded positions on the ground. While not a concern during study design and sampling, mastication necessitated slight and controlled equipment movements and slow progression through the treatment units. The equipment rarely made large, exaggerated swing movements with the boom fully extended. This challenge was compounded further due to the smaller size of the equipment used during the mastication treatments. The equipment used in the initial study maintained a consistent boom transponder distance from the cab of 9.5 meters, while the maximum possible distance between the cab and boom transponders used during mastication was approximately 7 meters. It was possible for the boom transponder to be as close as approximately 2 meters to the cab device when the boom was reaching into the canopy of the tree or swinging to avoid residual stems during walking and repositioning. The boom was also rarely at full extension during mastication due to the instability this would cause associated with the weight of the mastication head. Because the activity recognition model relied on movements of the GNSS-RF transponders to predict the cycle elements, the minimal equipment movements during or between elements limited the element characterization accuracy.

The GNSS-RF devices used a sampling rate of 2.5 seconds which alternated transponder position recording every 2 and 3 seconds for a sample every 2.5 seconds on average. Across all cycle elements, the average element duration was 37.7 seconds equating to approximately 15 positions recorded per element. However, there were 299 individual element observations with a duration less than 4 seconds where a maximum of 2 positions was possible. Of the 3,554 total elements observed, 753, over 20%, had a maximum representative sample of 3 positions. Unlike equipment like rubber-tired skidders for which cycle elements consistently last prolonged periods of time, masticators transitioned between elements rapidly and irregularly to improve stem access and avoid obstacles in the dense stands. This made capturing significant positional data per element using the 2.5 sampling rate challenging. The strong relation between odds of correct element classification and element duration (Table 3.7) suggests longer element durations were more accurately predicted because larger samples of positional data representing them were available during modelling. Therefore, by increasing the sampling rate and providing more representative data points per element, model classification accuracy may increase as well for elements with short durations.

Multipath error from forest canopies and vegetation can degrade accuracy and precision of GNSS signals (Sigrist et al., 1999; Taylor et al., 2001; Veal et al., 2001; Bolstad et al., 2005; Hasegawa and Yoshimura, 2007; Devlin and McDonnell, 2009; Strandgard and Mitchell, 2015; Zimbelman and Keefe, 2018). While we did not examine whether the canopy cover attenuated the overall GNSS signal, we assessed the degree to which varying forest metrics impacted the accuracy of the GNSS-based activity recognition using mixed-effects logistic regression models (Table 3.7). While the results indicated increases in SDI and basal area reduced correct element characterization from the model, the practical impact does not appear to be of concern for activity recognition. For instance, with an odds ratio of 0.9984, an increase in the SDI of 100 would mean the elements overall would be 0.16 times less likely to be correctly predicted.

To improve future element characterization using GNSS-RF-based approaches, methods for differential GNSS correction should be used to improve GNSS-RF accuracy and precision. Devices capable of faster sampling rates may also improve prediction accuracy. Further, integrating supplemental inertial measurement units (IMUs) that include accelerometer and gyroscope measurements into activity recognition models could provide additional resolution relating to intricate machine movements and may capture details missed by the coarser spatial data derived from GNSS-RF transponders alone (Palander et al., 2013). The data recorded using IMU sensors are independent of satellite visibility and therefore are not impacted by dense forest canopies and multipath error. IMUs integrated into mobile technologies have been used successfully in human activity recognition for fitness tracking, healthcare, smart environments, commerce, and more recently for forest operations applications (Khusainov et al., 2013; Bayat et al., 2014; Attal et al., 2015; Shoaib et al., 2015; Gjoreski et al., 2016; Keefe et al., 2019; Lima et al., 2019; Zimbelman and Keefe, 2021). These data could be used to supplement GNSS-RF location measurements that are unable to capture motions such as track slew while the boom and cab remain stationary. Supplementing GNSS-RF with IMU sensor measurements would provide additional information valuable for individual cycle element classification and has not been explored widely in activity recognition modeling for natural resource management applications.

3.5.1 Effect of Stand Characteristics on Mastication Production Rates and Site Impact

Production rates for each treatment unit were determined by averaging the unique production rate of each lidar prediction pixel. The within-pixel production rate represented the amount of area covered by the GNSS-RF transponder within each lidar pixel in hectares divided by the total time the transponder was within the extent of that pixel. Similarly, the stand metric summaries in Table 3.3 were those from within the area observed during time and motion sampling. It should be noted that the treatment unit means for the entire treatment units (Becker and Keefe, 2020) differed from the

areas where sampling and treatment observations occurred for this study because only a portion of the units were sampled during mastication. For example, the means for trees per hectare for the treatment units in their entirety were 530, 515 and 516 for units 117, 120 and 147 respectively, while the mean tree per hectare for the areas observed during mastication were 489, 665, and 409 (Table 3.3).

As expected, there was an increase in treatment production rates within the units as the utilization rate increased (Table 3.3). More time spent masticating or moving within the stand versus being delayed would lead to faster progression and treatment of the unit resulting in higher production rates. Despite having the highest production rate of 0.203 $ha \cdot hr^{-1}$, unit 120 contained the lowest percentage of treated area impacted by the machine at 25%, while unit 117 and 147 contained higher percentages of site impact at 33% and 38% respectively (Table 3.3). This may be attributed to the machine needing to navigate more deadfall, stumps or coarse woody debris decreasing terrain trafficability in units 117 and 147 than in unit 120. A previous mountain pine beetle (*Dendroctonus ponderosae Hopkins*) infestation in the lodgepole pine (*Pinus contorta var. latifolia Engelm.*) stands caused mortality and deadfall in portions of all treatment units. Figure 3.3 provides a visual representation of the composition of the areas masticated during the time and motion sampling. While all stands were impacted by beetle-kill, unit 147 was the most heavily impacted, followed by unit 117. The intensity of downfall in unit 120 was lower than both 117 and 147. This likely contributed to less time spent navigating around dead and downed trees in unit 120, and ultimately higher production rates and a lower percentage of impacted ground during treatment.

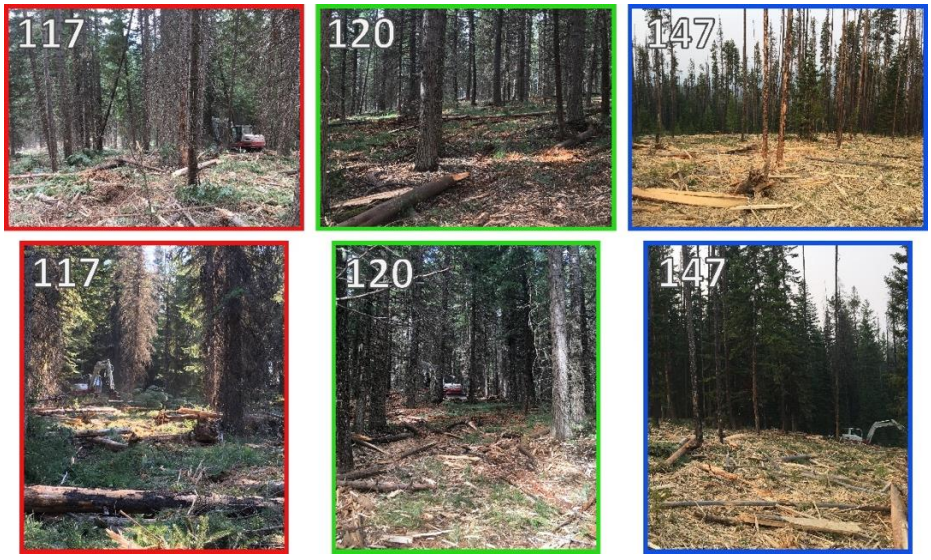

Figure 3.3. Forest structure and treatment implementation across the three mastication units.

Mechanical strain placed on the mastication head while masticating downed trees in unit 147 may have led to higher treatment delays and subsequently the lowest utilization rate of all units at 65%. The size and quantity of the downed material treated in unit 147 caused the equipment to overheat during mastication and required the operator to pause treatment while the hydraulic and mechanical systems cooled. This time compounded throughout the workday. Though not quantified, the findings of this study suggest deadfall and coarse woody debris played a significant role in the production rate and treatment of these mastication units. Unfortunately, due to operational constraints, deadfall was not quantified during sampling. Future research should include sampling procedures that quantify and map these materials to determine their impact on the production rate of small, tracked equipment similar to the masticator used in this study.

While representing the highest production possessing the highest rate at 0.203 $ha \cdot hr^{-1}$, unit 120 also contained the highest values for all stand metrics. Conversely, unit 147 represented the lowest value for all metrics and the lowest production rate at 0.125 $ha \cdot hr^{-1}$. This was seemingly supported by the linear mixed effects analysis, in which a significant relationship between production rate and basal area was found. However, despite being statistically significant, the overall impact of these variables on production rate is operationally insignificant. A 1 unit increase in basal area per hectare would result in an increase in production rate of 0.0003495 $ha \cdot hr^{-1}$. For instance, to double the production rate originally determined for unit 147, the existing basal area would need to more than quadruple. This result is also contrary to the general expectation that increases in basal area would lead to reduced area treated per hour due to larger amounts of biomass per hectare requiring treatment to achieve the desired prescription. Additional factors including slope, site topography, and soil type may have influenced production rates. While not addressed in this study, future work should include these site factors into the analysis.

Despite the challenges associated with the classification of individual cycle elements with high accuracy, GNSS-RF transponders were shown to provide a consumer-available solution for activity recognition for mastication treatments that effectively classified the difference between delay and productive elements over 95% of the time. Similar challenges with element level classification in GNSS-based models was found in operational settings (Wang et al., 2003; McDonald and Fulton, 2005; de Hoop and Dupré, 2006; Strandgard and Mitchell, 2015). While the preliminary study using GNSS-RF for element classification by Becker et al. (2017) justified further research consideration, this study exposed more challenges and limitations associated with operational implementation of consumer-grade GNSS-RF for individual element-level activity recognition. However, in remote, off-the-grid environments, RF enabled components still provide reliable and real-time data collection and

sharing capabilities which should not be overlooked. Recent improvements to GNSS accuracy using real-time correction (RTK) methods, sampling rate, and the integration of inertial measurement units (IMUs) in some available tools address previous limitations identified in this study and these devices should be reconsidered for use in real-time element level activity recognition modelling.

With advances in the accuracy and prediction capabilities of remotely sensed data, future modelling of production rates should incorporate individual tree detection and delineation metrics derived from lidar. Individual tree segmentation enables the estimation of tree metrics including diameter, height, and volume (Yu et al., 2010; Silva et al., 2016), which have been shown to influence the production rates of harvest operations (Kluender et al., 1998; Magagnotti et al., 2013; Parajuli et al., 2020). Each individual tree has a known location and given accurate machine location information, these two sets of coordinates may be matched to predict tree-level production metrics based on individual tree characteristics. GNSS devices have been shown to accurately record tree positions during harvest in previous studies, which is a promising result in the push to further advance precision forestry and management intensity (Kaartinen et al., 2015; Hauglin et al., 2017; Noordermeer et al., 2021). This would enable treatment production rate to be quantified at the individual tree level and regression models could be developed to predict operational productivity at the same scale. Tree-level production rate estimates resolve issues associated with the inability to sample for the entirety of an operation or to model unexpected or unsampled stand variables such as deadfall that can arise using area-based estimation approaches. These models could then be applied to any area where individual tree detection and delineation are available. This research opportunity should be pursued and provides opportunity to advance precision forestry and operations logistics.

3.6 Conclusion

The GNSS-RF based activity recognition model developed in this study successfully classified productive elements versus delay with over 95% accuracy. The three cycle elements defined were correctly classified 73.5% of the time which is a promising result for activity recognition using consumer-available GNSS-RF devices. The duration of the elements was the largest factor impacting cycle element classification success, with increases in element duration leading to increases in model performance. Increases in SDI and basal area per hectare were found to decrease the classification success of the activity recognition model though the impact on activity recognition was insignificant. When analyzing production rates of the mastication treatments, increases in basal area were shown to increase the production rate. However, this weak relationship is unlikely to be operationally significant.

Continued advances in remote sensing, mobile and GNSS-capable technologies is encouraging a paradigm shift from a stand level, area-based management to a precision forestry and individual tree-centric approach to forest management and operational digitalization. Applying these resources into the planning, implementation and assessment of forest management practices will enable the innovation, growth, and improvements necessary to address current and future challenges of sustainable forest management. Developing consumer-accessible and flexible technological solutions, like the one assessed in this study, may increase the application and utilization of these resources, and provide greater opportunity for contractors, researchers, and land managers to advance their fields and ensure their continued and increased effectiveness.

3.7 Literature Cited

Acuna, M., Skinnell, J., Evanson, T., and Mitchell, R. 2011 Bunching with a self-levelling feller-buncher on steep terrain for efficient yarder extraction. *Croat. J. For. Eng*. **32**, 521–531.

Acuna, M.A. and Kellogg, L.D. 2009 Evaluation of alternative cut-to-length harvesting technology for native forest thinning in Australia. *Int. J. For. Eng*. **20**, 17–25. doi:10.1080/14942119.2009.10702579

Adebayo, A., Han, H., and Johnson, L. 2007 Productivity and cost of cut-to-length and whole-tree harvesting in a mixed-conifer stand. *For. Prod. J.* **57**, 59–69.

Akay, A.E., Oğuz, H., Karas, I.R., and Aruga, K. 2009 Using lidar technology in forestry activities. *Environ. Monit. Assess.* **151**, 117–125. doi:10.1007/s10661-008-0254-1

Alam, M., Acuna, M., and Brown, M. 2013 Self-levelling feller-buncher productivity based on lidar-derived slope. *Croat. J. For. Eng*. **34**, 273–281.

Attal, F., Mohammed, S., Dedabrishvili, M., Chamroukhi, F., Oukhellou, L., and Amirat, Y. 2015 Physical human activity recognition using wearable sensors. *Sensors* **15**, 31314–31338. doi:10.3390/s151229858

Bates, D., Machler, M., Bolker, B., and Walker, S. 2015 Fitting linear mixed-effects models using lme4. *J. Stat. Softw*. **67**, 1–48. doi:10.18637/jss.v067.i01

Bayat, A., Pomplun, M., and Tran, D.A. 2014 A study on human activity recognition using accelerometer data from smartphones. *Procedia Comput. Sci*. **34**, 450–457.

Becker, R.M., and Keefe, R.F. 2020 Prediction of fuel loading following mastication treatments in forest stands in north Idaho, USA. *Sustainability* **12**, 1–20. doi:10.3390/su12177025

Becker, R.M., Keefe, R.F., and Anderson, N.M. 2017 Use of real-time GNSS-RF data to characterize the swing movements of forestry equipment. *Forests* **8**, 1–15. doi:10.3390/f8020044

Becker, R.M., Keefe, R.F., Anderson, N.M., and Eitel, J.U.H. 2018 Use of Lidar-derived landscape parameters to characterize alternative harvest system options in the Inland Northwest. *Int. J. For. Eng*. **29**, 179–191. doi:10.1080/14942119.2018.1497255

Belgiu, M., and Dragut, L. 2016 Random forest in remote sensing: A review of applications and future directions. *ISPRS J. Photogramm. Remote Sens*. **114**, 24–31. doi:10.1016/j.isprsjprs.2016.01.011

Bell, C.K., Keefe, R.F., and Fried, J.S. 2017 Validation of the OpCost logging cost model using contractor surveys. *Int. J. For. Eng*. **28**, 73–84. doi:10.1080/14942119.2017.1313488

Bolstad, P., Jenks, A., Berkin, J., and Horne, K. 2005 A Comparison of autonomous, WAAS, real-time, and post-processed global positioning systems (GPS) accuracies in northern forests. *North. J. Appl. For*. **22**, 5–11.

Borz, S.A., Talagai, N., Cheta, M., Gavilanes-Montoya, A.V., and Castillo-Vizuete, D.D. 2018 Automating data collection in motor-manual time and motion studies implemented in a willow short rotation coppice. *Bioresources* **13**, 3236–3249.

Breiman, L. 2001 Random Forests. *Mach. Learn*. **45**, 5–32.

Breiman, L. 2002 Manual on setting up, using, and understanding random forests v3.1. Statistics Department University of California Berkeley, CA, USA.

Brosofske, K.D., Froese, R.E., Falkowski, M.J., and Banskota, A. 2014 A review of methods for mapping and prediction of inventory attributes for operational forest management. *For. Sci*. **60**, 733–756. doi:10.5849/forsci.12-134

Carter, E.A., McDonald, T.P., and Torbert, J.L. 2000 Harvest traffic monitoring and soil physical response in a pine plantation. In *Proceedings of the 5th International Conference on Precision Agriculture and Other Resource Management*, Minneapolis, MN, USA, pp. 1–10.

Cinaroglu, S. 2016 Comparison of performance of decision tree algorithms and random forest: An application on OECD countries health expenditures. *Int. J. Comput. Appl*. **138**, 37–41.

de Hoop, C.F., and Dupré, R.H. 2006 Using GPS to document skidder motions- a comparison with manual data collection, In *Proceedings of the Council on Forest Engineering (COFE) - Working Globally – Sharing Forest Engineering Challenges and Technologies Around the World*, Coeur d'Alene, ID, USA, pp. 1–11.

Devlin, G.J., and McDonnell, K. 2009 Performance accuracy of real-time GPS asset tracking systems for timber haulage trucks travelling on both internal forest road and public road networks. *Int. J. For. Eng.* **20**, 45–49. doi:10.1080/14942119.2009.10702575

Evans, J.S., and Murphy, M.A. 2018 rfUtilities. R package version 2.1-3. https://cran.r-project.org/package=rfUtilities.

Falkowski, M.J., Evans, J.S., Martinuzzi, S., Gessler, P.E., and Hudak, A.T. 2009 Characterizing forest succession with lidar data: An evaluation for the Inland Northwest, USA. *Remote Sens. Environ.* **113**, 946–956. doi:10.1016/j.rse.2009.01.003

Falkowski, M.J., Gessler, P.E., Morgan, P., Hudak, A.T., and Smith, A.M.S. 2005 Characterizing and mapping forest fire fuels using ASTER imagery and gradient modeling. *For. Ecol. Manag.* **217**, 129–146. doi:10.1016/j.foreco.2005.06.013

Falkowski, M.J., Hudak, A.T., Crookston, N.L., Gessler, P.E., Uebler, E.H., and Smith, A.M.S. 2010 Landscape-scale parameterization of a tree-level forest growth model: A k-nearest neighbor imputation approach incorporating lidar data. *Can. J. For. Res.* **40**, 184–199. doi:10.5589/m08-055

Fekety, P.A., Falkowski, M.J., Hudak, A.T., Jain, T.B., and Evans, J.S. 2018 Transferability of lidar-derived basal area and stem density models within a northern Idaho ecoregion. *Can. J. Remote Sens.* **44**, 131–143. doi:10.1080/07038992.2018.1461557

Gallo, R., Grigolato, S., Cavalli, R., and Mazzetto, F. 2013 GNSS-based operational monitoring devices for forest logging operation chains. *J. Agric. Eng.* **44**, 140–145. doi:10.4081/jae.2013.s2.e27

George, A.K., Kizha, A.R., and Kenefic, L. 2021 Timber harvesting on fragile ground and impacts of uncertainties in the operational costs. *Int. J. For. Eng.*, 1-10. doi: 10.1080/14942119.2022.1988432

Gjoreski, M., Gjoreski, H., Luštrek, M., and Gams, M. 2016 How accurately can your wrist device recognize daily activities and detect falls? *Sensors* **16**, 1–21. doi:10.3390/s16060800

Grayson, L.M., Keefe, R.F., Tinkham, W.T., Eitel, J.U.H., Saralecos, J.D., Smith, A.M.S., and Zimbelman, E.G. 2016 Accuracy of WAAS-enabled GPS-RF warning signals when crossing a terrestrial geofence. *Sensors* **16**, 1–8. doi:10.3390/s16060912

Hasegawa, H., and Yoshimura, T. 2007 Estimation of GPS positional accuracy under different forest conditions using signal interruption probability. *J. For. Res*. **12**, 1–7. doi:10.1007/s10310-006-0245-4

Hauglin, M., Hansen, E.H., Naesset, E., Busterud, B.E., Gjevestad, J.G.O., and Gobakken, T. 2017 Accurate single-tree positions from a harvester: A test of two global satellite based positioning systems. *Scand. J. For. Res*. **8**, 774–781.

Hejazian, M., Hosseini, S., Lotfalian, M., and Ahmadikoolaei, P. 2013 Possibility of global positioning system (GPS) application for time studies in forest machinery. *Eur. J. Exp. Biol*. **3**, 93–98.

Hiesel, P., and Benjamin, J.G. 2013 Applicability of international harvesting equipment productivity studies in Maine, USA: A literature review. *Forests* **4**, 898–921. doi:10.3390/f4040898

Hudak, A.T., Bright, B.C., Pokswinski, S.M., Loudermilk, E.L., O'Brian, J.J., Hornsby, B.S., Klauberg, C., and Silva, C.A. 2016 Mapping forest structure and composition from low-density lidar for informed forest, fuel, and fire management at Englin Air Force Base, Florida, USA. *Can. J. Remote Sens*. **42**, 411–427.

Hudak, A.T., Strand, E.K., Vierling, L.A., Byrne, J.C., Eitel, J.U.H., Martinuzzi, S., and Falkowski, M.J. 2012 Quantifying aboveground forest carbon pools and fluxes from repeat lidar surveys. *Remote Sens. Environ*. **123**, 25–40. doi:10.1016/j.rse.2012.02.023

Huggett Jr., R.J., Abt, K.L., and Shepperd, W. 2008 Efficacy of mechanical fuel treatments for reducing wildfire hazard. *For. Policy Econ*. **10**, 408–414. doi:10.1016/j.forpol.2008.03.003

Huyler, N.K., and LeDoux, C.B. 1997 Yarding Cost for the Koller K300 cable yarder: Results from field trials and simulations. *North. J. Appl. For*. **13**, 5–9.

Jain, T.B., Graham, R.T., Sandquist, J., Butler, M., Brockus, K., Frigard, D., Cobb, D., Sup-Han, H., Halbrook, J., Denner, R., and Evans, J.S. 2008 Restoration of Northern Rocky Mountain moist forests: Integrating fuel treatments from the site to the landscape, In *Proceedings of the 2007 National Silviculture Workshop, Gen Tech Rep. PNW-GTR-733*, U.S. Department of Agriculture, Forest Service, Pacific Northwest Research Station, Portland, OR, USA.

Kaartinen, H., Hyyppä, J., Vastaranta, M., Kukko, A., Jaakkola, A., Yu, X., Pyörälä, J., Liang, X., Liu, J., Wang, Y., Kaijaluoto, R., Melkas, T., Holopainen, M., and Hyyppä, H. 2015. Accuracy of kinematic positioning using global satellite navigation systems under forest canopies. *Forests* **6**, 3218–3236. doi:10.3390/f6093218

Kane, J.M., Knapp, E.E., and Varner, J.M. 2006 Variability in loading of mechanically masticated fuel beds in northern California and southwestern Oregon. *In Proceedings of Fuels Management—How to Measure Success*, U.S. Department of Agriculture, Forest Service, Rocky Mountain Research Station, Portland, OR, USA, pp. 341-350.

Keefe, R.F., Eitel, J.U.H., Smith, A.M.S., Tinkham, W.T. 2014 Applications of multi transmitter GPS-VHF in forest operations. In *Proceedings of the 47th International Symposium on Forestry Mechanization and 5th International Forest Engineering Conference*, Gerardmer, France, 3 p.

Keefe, R.F., Zimbelman, E.G., and Wempe, A.M. 2019 Use of smartphone sensors to quantify the productive cycle elements of hand fallers on industrial cable logging operations. *Int. J. For. Eng*. **30**(2), 1–12. doi:10.1080/14942119.2019.1572489

Kellogg, L.D., Milota, G.V., and Miller Jr., M. 1996 A comparison of skyline harvesting costs for alternative commercial thinning prescriptions. *J. For. Eng*. **7**(3), 7–23. doi:10.1080/08435243.1996.10702687

Khusainov, R., Azzi, D., Achumba, I.E., and Bersch, S.D. 2013. Real-time human ambulation, activity, and physiological monitoring: Taxonomy of issues, techniques, applications, challenges and limitations. *Sensors* **13**, 12852–12902. doi:10.3390/s131012852

Klepac, J., and Rummer, B. 2002 Evaluation of a shovel logging system in the Gulf Coastal Plain, In *Proceedings of the Council on Forest Engineering (COFE) Conference - A Global Perspective*, Aubrun, AL, USA, pp. 1–5.

Kluender, R., Lortz, D., McCoy, W., Stokes, B., and Klepac, J. 1998 Removal intensity and tree size effects on harvesting cost and profitability. *For. Prod. J*. **48**, 54–59.

Laird, N.M., and Ware, J.H. 1982 Random-effects models for longitudinal data. *Biometrics* **38**, 963–974.

Liaw, A., and Wiener, M. 2002 Classification and regression by randomForest. *R News* **2**, 18–22.

Lima, W.S., Souto, E., El-Khatib, K., Jalali, R., and Gama, J. 2019 Human activity recognition using inertial sensors in a smartphone: An overview. *Sensors* **19**, 1–29. doi:10.3390/s19143213

Magagnotti, N., Kanzian, C., Schulmeyer, F., and Spinelli, R. 2013 A new guide for work studies in forestry. *Int. J. For. Eng*. **24**, 249–253. doi:10.1080/14942119.2013.856613

Man, Q., Dong, P., Guo, H., Liu, G., and Shi, R. 2014 Light detection and ranging and hyperspectral data for estimation of forest biomass: A review. *J. Appl. Remote Sens*. **8**, 1–22. doi:10.1117/1.JRS.8.081598

McDonald, T. 1999 Time study of harvesting equipment using GPS-derived positional data. *GIS Technical Papers*, Edinburgh University, Edinburgh, Scotland, 8 p.

McDonald, T.E., Carter, E., Taylor, S., and Torbert, J. 1998 Traffic patterns and site disturbance, In *Proceedings of the 21st Annual Council on Forest Engineering (COFE) - Harvesting Logistics: From Woods to Markets*. Portland, OR, USA, 5 p.

McDonald, T.P., Carter, E.A., and Taylor, S.E. 2002 Using the global positioning system to map disturbance patterns of forest harvesting machinery. *Can. J. For. Res*. **32**, 310–319. https://doi.org/10.1139/X01-189

McDonald, T.P., Fulton, J.P., 2005. Automated Time Study of Skidders Using Global Positioning System Data. Comput. Electron. Agric. 48, 19–37. doi:10.1016/j.compag.2005.01.004

McDonald, T.P., Taylor, SE., and Rummer, R.B. 2000 Deriving forest harvesting machine productivity from positional data. In *Proceedings of the 2000 ASAE Annual International Meeting*, Milwaukee, Wisconsin, USA, pp. 1–8.

McMahon, S.D. 1997 Unearthing soil compaction. *GPS World* 8, 40–45.

Miyata, E.S. 1980 Determining fixed and operating costs of logging equipment (General Technical Report No. NC-55). USDA-Forest Service, North Central Forest Experiment Station, St. Paul, Minnesota.

Nakagawa, S., and Schielzeth, H. 2013 A general and simple method for obtaining R2 from generalized linear mixed-effects models. *Methods Ecol. Evol*. **4**, 133–142. doi:10.1111/j.2041-210x.2012.00261.x

Newman, S.M., Keefe, R.F., Brooks, R.H., Ahonen, E.Q., and Wempe, A.M. 2018 Human factors affecting logging injury incidents in Idaho and the potential for real time location-sharing technology to improve safety. *Safety* **4**, 1–28. doi:10.3390/safety4040043

NIST Internet Time Servers, 2017 https://tf.nist.gov/tf-cgi/servers.cgi.

Noordermeer, L., Sørngård, E., Astrup, R., Næsset, E., and Gobakken, T. 2021 Coupling a differential global navigation satellite system to a cut-to-length harvester operating system enables precise positioning of harvested trees. *Int. J. For. Eng.* **32**(2), 1–9. doi:10.1080/14942119.2021.1899686

Nuutinen, Y., Väätäinen, K., Heinonen, J., Asikainen, A., and Röser, D. 2008 The accuracy of manually recorded time study data for harvester operation shown via simulator screen. *Silva Fenn*. **42**, 63–72.

Olivera, A., Visser, R., Acuna, M., and Morgenroth, J. 2016 Automatic GNSS-enabled harvester data collection as a tool to evaluate factors affecting harvester productivity in a eucalyptus spp. harvesting operation in Uruguay. *Int. J. For. Eng*. **27**, 15–28. doi:10.1080/14942119.2015.1099775

Olsen, E.D., and Kellogg, L.L. 1983 Comparion of time-study techniques for evaluating logging production. *Trans. Am. Soc. Agric. Eng*. **1672**, 1665–1668.

Palander, T., Nuutinen, Y., Kariniemi, A., and Vaatainen, K. 2013 Automatic time study method for recording work phase times of timber harvesting. *For. Sci*. **59**, 472–483.

Parajuli, M., Hiesl, P., Smidt, M., and Mitchell, D. 2020 Factors influencing productivity and cost in the whole-tree harvesting system (No. LGP 1079). Clemson University Extension.

Pinheiro, J., and Bates, D. 2020 nlme: linear and nonlinear mixed effects models. R Core Team.

R Core Team 2020 R: A language and environment for statistical computing. R Foundation for Statistical Computing; R Core Team, Vienna, Austria.

Reutebuch, S.E., Andersen, H.E., and McGaughey, R.J. 2005 Light detection and ranging (lidar): An emerging tool for multiple resource inventory. *J. For*. **September**, 286–292.

Shoaib, M., Bosch, S., Incel, O.D., Scholten, H., and Havinga, P.J.M. 2015 A survey of online activity recognition using mobile phones. *Sensors* **15**, 2059–2085. doi:10.3390/s150102059

Sigrist, P., Coppin, P., and Hermy, M. 1999 Impact of forest canopy on quality and accuracy of GPS measurements. *Int. J. Remote Sens*. **20**, 3595–3610.

Silva, C.A., Hudak, A.T., Vierling, L.A., Loudermilk, E.L., O'Brien, J.J., Hiers, J.K., Jack, S.B., Gonzalez-Benecke, C., Lee, H., Falkowski, M.J., and Khosravipour, A. 2016 Imputation of individual longleaf pine (Pinus palustris Mill.) tree attributes from field and lidar data. *Can. J. Remote Sens*. **42**, 554–573. doi:10.1080/07038992.2016.1196582

Silva, C.A., Klauberg, C., Hudak, A.T., Vierling, L.A., Jaafar, W.S.M., Mohan, M., Garcia, M., Ferraz, A., Cardil, A., and Saatchi, S. 2017 Predicting stem total and assortment volumes in an industrial Pinus taeda L. forest plantation using airborne laser scanning data and random forest. *Forests* **8**, 1–17. doi:10.3390/f8070254

Strandgard, M., Alam, M., and Mitchell, R. 2014 Impact of slope on productivity of a self-levelling processor. *Croat. J. For. Eng*. **35**, 193–200.

Strandgard, M., and Mitchell, R. 2015 Automated time study of forwarders using GPS and a vibration sensor. *Croat. J. For. Eng*. **36**, 175–184.

Talbot, B., Aalmo, G.O., and Stampfer, K. 2014 Productivity analysis of an un-guyed integrated yarder-processor with running skyline. *Croat. J. For. Eng*. **35**, 201–210.

Taylor, S.E., McDonald, T.P., Veal, M.W., and Grift, T.E. 2001 Using GPS to evaluate productivity and performance of forest machine systems. In *Proceedings of the First International Precision Forestry Symposium*, Seattle, WA, USA, pp. 1–20.

Veal, M.W., Taylor, S.E., McDonald, T.P., McLemore, D.K., and Dunn, M.R. 2001 Accuracy of tracking forest machines with GPS. *Trans. Am. Soc. Agric. Eng*. **44**, 1903–1911.

Wang, J., Long, C., McNeel, J., Baumgras, J. 2004 Productivity and cost of manual felling and cable skidding in central Appalachian hardwood forests. *For. Prod. J.* **54**, 45–51.

Wang, J., McNeel, J., and Baumgras, J. 2003 A computer-based time study system for timber harvesting operations. *For. Prod. J*. **53**, 47–53.

Wempe, A.M., and Keefe, R.F. 2017 Characterizing rigging crew proximity to hazards on cable logging operations using GNSS-RF: Effect of GNSS positioning error on worker safety status. *Forests* **8**, 1–17. doi:10.3390/f8100357

Wempe, A.M., Keefe, R.F., Newman, S.M., and Paveglio, T.B. 2019 Intent to adopt location sharing for logging safety applications. *Safety* **5**, 1–22. doi:10.3390/safety5010007

Wulder, M.A., White, J.C., Nelson, R.F., Næsset, E., Ørka, H.O., Coops, N.C., Hilker, T., Bater, C.W., and Gobakken, T. 2012 Lidar sampling for large-area forest characterization: A review. *Remote Sens. Environ*. **121**, 196–209. doi:10.1016/j.rse.2012.02.001

Yu, X., Hyyppä, J., Holopainen, M., and Vastaranta, M. 2010 Comparison of area-based and individual tree-based methods for predicting plot-level forest attributes. *Remote Sens*. **2**, 1481–1495. doi:10.3390/rs2061481

Zimbelman, E.G., and Keefe, R.F. 2021 Development and validation of smartwatch-based activity recognition models for rigging crew workers on cable logging operations. *PLoS ONE* **16**, 1–25. doi:10.1371/journal. pone.0250624

Zimbelman, E.G., and Keefe, R.F. 2018 Real-time positioning in logging: Effects of forest stand characteristics, topography, and line-of-sight obstructions on GNSS-RF transponder accuracy and radio signal propagation. *PLoS ONE* **13**, 1–17. doi:10.1371/journal. pone.0191017

Zimbelman, E.G., Keefe, R.F., Strand, E.K., Kolden, C.A., and Wempe, A.M. 2017 Hazards in motion: Development of mobile geofences for use in logging safety. *Sensors* **17**, 1–16. doi:10.3390/s17040822

Chapter 4: A Novel Smartphone-based Activity Recognition Modeling Method for Tracked Equipment in Forest Operations.

Submitted to:

Becker, R.M, Keefe, R.F. A novel smartphone-based activity recognition modeling method for tracked equipment in forest operations. *PLOS ONE*. **2022** (In Review).

4.1 Abstract

Activity recognition modelling using smartphone Inertial Measurement Units (IMUs) is an underutilized resource defining and assessing work efficiency for a wide range of natural resource management tasks. This study focused on the initial development and validation of a smartphone-based activity recognition system for excavator-based mastication equipment working in Ponderosa pine (Pinus ponderosa) plantations in North Idaho. During mastication treatments, sensor data from smartphone-based gyroscopes, accelerometers, and sound pressure meters (decibel meters) were collected at three sampling frequencies (10, 20, and 50 hertz (Hz)). These data were then separated into 9 time domain features using 4 sliding window widths (1, 5, 7.5 and 10 seconds) and two window overlaps (50% and 90%). Random forest machine learning algorithms were trained and evaluated for 40 combinations of model parameters to determine the best combination of parameters assessed. 5 work elements (masticate, clear, move, travel, and delay) were classified with the performance metrics for individual elements of the best model (50 Hz, 10 second window, 90% window overlap) falling within the following ranges: area under the curve (AUC) (95.01% - 99.90%); sensitivity (74.90% - 95.58%); specificity (90.83% - 99.93%); precision (81.12% - 98.27%); F1-score (81.87% - 96.91%); balanced accuracy (87.41% - 97.70%). Smartphone sensors effectively characterized individual work elements of mechanical fuel treatments. This study is the first example of developing a smartphone-based activity recognition solution for ground-based forest equipment. The continued development and dissemination of smartphone-based activity recognition models may assist land managers and operators with ubiquitous, manufacturer-independent systems for continuous and automated time study and production analysis for mechanized forest operations.

4.2 Introduction

Time and motion studies are used widely in forest operations and provide insight for improving efficiency and reducing delays in forest operations through the observation, analysis, and quantification of productive cycles and work elements [1–11]. Traditionally, harvest cycle times and

individual elements are estimated using stopwatches, video recorders and handheld data loggers [12]. These studies are often labor intensive and cost prohibitive due to the manual, observational sampling they require. The application of production functions and treatment cost simulation models developed from time and motion studies with associated machine rate estimates is often limited in scope due these constraints [13,14]. The methods by which productive work is defined in forestry and natural resource management are rapidly evolving, where traditional sampling techniques are increasingly replaced by less labor-intensive methods resulting from advances in real-time spatial data collection, activity recognition, remote sensing, and wearable and mobile technologies [15].

In forest operations, global navigation satellite systems (GNSS) have been successfully used in various forestry applications to automate the sampling of machinery, aid in production analysis, monitor the movements of ground workers and assess machinery and ground-worker interactions for both safety and production purposes in lieu of or in support of traditional time and motion methods [16,17]. GNSS-supported approaches for production analysis have been developed for timber harvesting equipment including skidders [18–22], forwarders [14], and cable logging carriages [23]. Use of GNSS in forest operations research works particularly well for equipment such as forwarders and skidders due to the large distances they cover and the relationship of their movements, speed and location with their productive activities [14]. In most harvester studies, Standard for Forest Data (StandForD) and CAN bus data have been used in combination with GNSS devices to perform production analysis [12,24–26]. Further, Carter et al. successfully used GNSS to monitor traffic intensity and soil impacts resulting from timber harvesting [27].

One limitation of many basic GNSS devices is the inability to share and process data in real-time independently of additional hardware, limiting their usefulness for production analysis where immediate feedback and processing may be desired. GNSS-RF uses radio frequency to transmit and share data in real-time independent of cellular and satellite infrastructures, enabling data sharing in remote work environments and off-the-grid scenarios. The use of these technologies for improving safety and situational awareness in forest management and logging scenarios has received significant interest [28–31]. Further, real-time communication between multiple GNSS-RF devices has successfully been used to assess independently moving components of a single machine to characterize productive work elements [32]. Unfortunately, quantifying GNSS-RF-derived productive cycles classification of component work elements has been shown in certain instances to be limited by the spatial resolution and accuracy at which data can be recorded [32]. GNSS accuracy degradation due to multipath error from dense forest canopies or topography further limits the extent

spatially explicit data can be used for production analysis in forest operations [14,16,19,33]. This may prohibit the exclusive use of GNSS-based devices for data collection and production representation where high-accuracy position, navigation, and timing (PNT) data are required to ensure worker safety and effective work assessment [34]. In response, additional data inputs may be necessary to increase the robustness of production models and ensure their improved accuracy and utility across varying sites and applications. Sensor-based data, including those derived from triaxial accelerometers and gyroscopes, provide a rich, high resolution, and highly descriptive data source for characterizing equipment activities. Wearable and mobile devices, including smartphones and smartwatches, are regularly equipped with inertial measurement units (IMUs), GNSS chipsets, and other sensors providing valuable information regarding the environment in which the device is located [35,36]. Inertial measurement units (IMU) contain both a triaxial accelerometer and gyroscope and enables the measurement of acceleration and angular velocity along three orthogonal axes and are regularly used in activity recognition modelling [37].

Activity recognition refers to the prediction of an individual's actions based on sensor-derived data capturing their movements or other biophysical characteristics and was first deployed in the lifecare and wellness industries in the 1980's [38]. The ubiquity of smartphones and smartwatches has led to rapid expansion in their use for human activity recognition modeling techniques characterizing physical activities. Data collected from smart device-based accelerometers, gyroscopes and sound pressure meters have been widely used successfully in various human activity recognition applications [35,36,39,40]. This includes uses in healthcare, behavior modelling, commerce, traffic condition monitoring, transportation identification, intelligent environments, fall detection, and to assess the wellness and fitness of athletes [36,40–48]. Zhang et al. [49] and Akhavian and Behzadan [50] studied the use of smartphones for activity recognition and classification in the construction industry, showing the ability of smartphones to detect and define various human-performed work activities. While sensor-based activity recognition has proven effective, model development and evaluation in the natural resource management field provides new opportunities to quantify and log both human and equipment-based work activities simultaneously within a common framework. Research on the development of mobile, consumer accessible activity recognition solutions based on smartphones and smartwatches is lacking.

Previous work in activity recognition modelling using accelerometers, GNSS devices, and gyroscopes in natural resource industries has examined applications for motor-manual felling, motor-manual willow coppice operations, bandsaw mills, and carriages in cable logging operations [11,51–

54]. Pierzchala et al. [55] used a combination of smartphone derived IMU and GNSS data, video recording and real-time data transfer using tethered onboard computers and a wireless local area network (WLAN) to perform automatic work phase recognition and subsequent quantification for a cable logging carriage with activity segmentation success of 78%. Keefe et al. [39] was the first successful use of stand-alone smartphone-based data collection for the development of human activity recognition models in forestry by assessing manual fallers in industrial forest operations. Using a single smartphone secured to the belt of a timber faller, the activity recognition model characterized manual felling work elements and delay with accuracies between 65.9% and 99.6%. More recently, smartwatch sensors were successfully used to develop activity recognition models for rigging crew workers setting and disconnecting log chokers on active cable logging operations [56]. These new smart device-based activity recognition applications show promise for further integration into the forest industries, and there is a significant need for continued development of models for real-time production analysis and logistics. For new automated technologies to be used for time study research purposes, McDonald and Fulton [20] suggested several requirements need to be met: 1.) It must be unobtrusive, simple, and easy to implement; 2.) It must be applicable for a wide range of machinery and site conditions without need for major reconfiguring; 3.) It must be durable and robust; and 4.) It must produce data of comparable accuracies to that collected by a skilled field crew. Smartphones and smartwatches have been shown to provide a technological solution capable of addressing and fulfilling these evaluation metrics.

There is no currently published research on the development of stand-alone smartphone-based activity recognition models for predicting work cycle elements and production rates of forestry equipment. Smartphones are an attractive choice for activity recognition model development due to their ubiquity, unobtrusiveness, ease of use, portability, high storage capacity, powerful computing, powerful embedded sensors, low energy consumption, extensive developer support and programmable capabilities [57–59]. Production and logistic monitoring systems for collecting and processing data regarding machine and operator condition and performance are now integrated into new forest equipment from the manufacturer and exist for harvesters, forwarders, and other equipment [24,25,55]. However, in most instances in the United States, these are typically machine specific, proprietary hardware and software systems that are limited to a single machine, application, and manufacturer. Mobile activity recognition tools using smartphone-based IMUs present a standalone, mobile solution enabling integration, utilization, and customization for a wide range of mechanized equipment and work activities through a single device, similar to fitness tracking applications. Forest equipment movements entail unique, but significant, actions including lateral

movements, swings, hydraulic boom manipulation and hydraulic cutting or processing head operations. The distinct work elements and the cycles they comprise may enable the development of activity recognition-based applications based on equipment movements within their environments.

Accurately capturing, recording, and characterizing the elements of equipment is key to successful activity recognition development and opens the door to correlating equipment productivity analysis to environmental and site characteristics. However, the production and costs of mechanized felling, skidding and processing equipment are directly impacted by forest stand metrics (tree size, stand density, undergrowth) and geophysical attributes (slope, rocks, debris, soils) [6,8,60]. Representing geographic and forest characteristics and their resulting impacts on equipment trafficability, tractability and production is also important for developing accurate, reliable, and robust activity recognition models for automating work activity characterization.

Remotely sensed data may be used support activity recognition model development by providing descriptive information related to site and stand conditions within the work environment. Light detection and ranging (lidar) is widely used across land management disciplines including forest, range, and fire management for quantifying vertical forest structure, succession and other forest attributes and terrain morphology [61–69]. Accurate inventories of existing geophysical and ecological conditions across various temporal and spatial scales from lidar has great economic and ecological implications for land management agencies and forest industries [70]. In forest operations, lidar has been used to locate skid roads, log landings [64], detect disturbance related to harvest [71–73], quantify harvesting productivity [8], delineate harvest units and cable corridors [74,75] and perform harvest system classification [76]. Additionally, Maltamo et al. (2019) assessed the accuracy of stand stem distributions derived using single-tree data from a harvester with an integrated positioning system and lidar metrics [77].

Area-based and individual tree-based approaches for deriving forest information from lidar data have both been widely studied and compared [78–82]. With improvements in lidar technologies and increased pulse densities, individual tree-based methods for analysis of lidar have increased rapidly [83]. Pulse densities of 5-10 per square meter enable the efficient detection and segmentation of individual trees, and many current lidar acquisitions are easily within or exceed this pulse density [78]. Single tree detection and delineation is not becoming a common tool for forestry applications including individual tree demography, growth modelling, wildlife habitat classification, ecosystem modelling, fire behavior modelling, growth and yield modelling, and precise biomass measurements for inventory and operational applications [84–86]. Individual tree metrics including height, diameter

at breast height (DBH), canopy base height, crown condition, crown area, biomass, stem volume and species can be derived from segmented tree data [63,70,78,87]. However, to effectively use these high-resolution, remotely sensed data for forest operations application, it is necessary to accurately position equipment in the forests during operations. Lidar-derived products, when properly processed, have high geographic precision and accuracy, while positional data derived from GNSS-based devices can return high positional error. The inaccurate positioning of equipment in relation to remotely sensed products may lead to invalid assumptions regarding relationship between these two data types and ultimately limit the utility of these powerful data. The efficacy of integrating these two data sources for work and management assessment needs to be examined.

The combined use of smart devices and lidar-derived products for data collection and interpretation will progress precision forestry and its applications in forest operations. Precision forestry, which commonly utilizes remotely sensed data sources and analysis, is the forest management technique emphasizing data-intensive and innovative practices, technologies, and processes to increase productivity, reduce costs, reduce negative site impacts resulting from management, and increase overall forest management success [88,89]. These concepts are used in many applications including forest inventory and forest planning and have many opportunities for advancing industrial forest operations, as described above, while also allowing forest management planning and implementation at microsite levels [18]. Advances in precision forestry will provide greater insight into operational trends, processes, production, and machine interactions during logging operations for both production and safety analysis. In turn, this may lead to more sustainable, efficient, and safe forest operations. The expansion of smartphone and mobile-based internet of things (IoT) in forested environments through activity recognition will help evolve the definition, monitoring, and assessment of work in the woods.

This study focuses on the development and validation of a smartphone-based activity recognition modelling framework for forestry equipment. These initial efforts in developing equipment specific, smartphone-based activity recognition models will be conducted for an excavator-based masticator. Random forest machine learning algorithms will serve as the foundation for these activity recognition models and variable model parameters (sliding window, window overlap, and sampling rate) will be examined to determine their impact on model performance. Additionally, this study will evaluate the efficacy of matching equipment locations derived from consumer-grade GNSS-RF devices to lidar-derived individual tree locations to identify treated stem

locations. Success in identifying treated stems would enable the quantification of relationships between individual tree characteristics and productive cycle elements for mastication.

The development, validation and future dissemination of the smartphone-based activity recognition models will assist land managers and operators by providing a ubiquitous system for continuous and unattended time study and analysis of mastication fuel treatments. Additionally, successful integration of lidar-derived single tree inventories and location-enabled activity recognition may enable the enhanced evaluation of forest and operational factors affecting production and costs in real-time while simultaneously providing data which can be used in planning and implementation of future forest operations and management. Identifying masticated trees within a stem map also allows for accurate predictions of residual stand stocking and conditions which is valuable for long-term management and planning.

4.3 Methods

4.3.1 Study Site

Three replicated stands on the University of Idaho Experimental Forest (UIEF) were sampled as part of a larger fuels management operation with treatment units located in three of the main UIEF management units: Flat Creek; West Hatter; and East Hatter. The UIEF is located approximately 20 kilometers northeast of Moscow, Idaho in the Palouse Range. All sampled stands were approximately 25-year-old ponderosa pine (*Pinus ponderosa*) plantations established following a clearcut timber harvest and subsequent prescribed burn. The primary treatment objective was the reduction of stand density to a tree spacing of 5 x 5 meters using mastication. This pre-commercial treatment focused on reduction of stand density, treatment of western pine beetle damage, and hazardous fuels reduction for the residual stand.

4.3.2 Mastication Sampling and Field Procedures

A time and motion study was performed within the three stands to facilitate the observation of mastication work cycles with corresponding and simultaneously collected smartphone sensor data. Treatments were with a tracked excavator (Kobelco ED150) running a hydraulic disk mastication head (Promac Brush Cutter). Due to hazardous conditions for observers during mastication and the density of the stands, traditional time and motion observational sampling was supplemented with video recording captured by two Garmin Dash Cam 45 devices placed within the cab of the machine. These devices provided time-stamped video and audio recordings, enabling productive work cycle

classification while increasing observer safety and reducing sampling errors associated with poor visibility, observer inattentiveness, or element misclassification. GNSS-RF multi-transponder devices with sampling intervals of 2.5 seconds were secured outside the cab of the equipment to record equipment movements and treatment progression throughout sampling. Data recorded from these devices was shared in real-time via radio transmission to a handheld receiver.

Google Pixel smartphones were used to collect the sensor data necessary for activity recognition modelling. These devices were placed within the cab of the machine oriented with the rear of the phones facing the front windshield. The AndroSensor application [90] was used to record the IMU and other smartphone sensor measurements. Within the AndroSensor application, the data sampling rate was set to three frequencies on the phones used: 10, 20, and 50 hertz (Hz). The 10, 20, and 50 Hz sampling rates recorded information every 0.1, 0.05, and 0.02 seconds respectively. Placement of all devices on the equipment used in field sampling is shown in Figure 4.1.

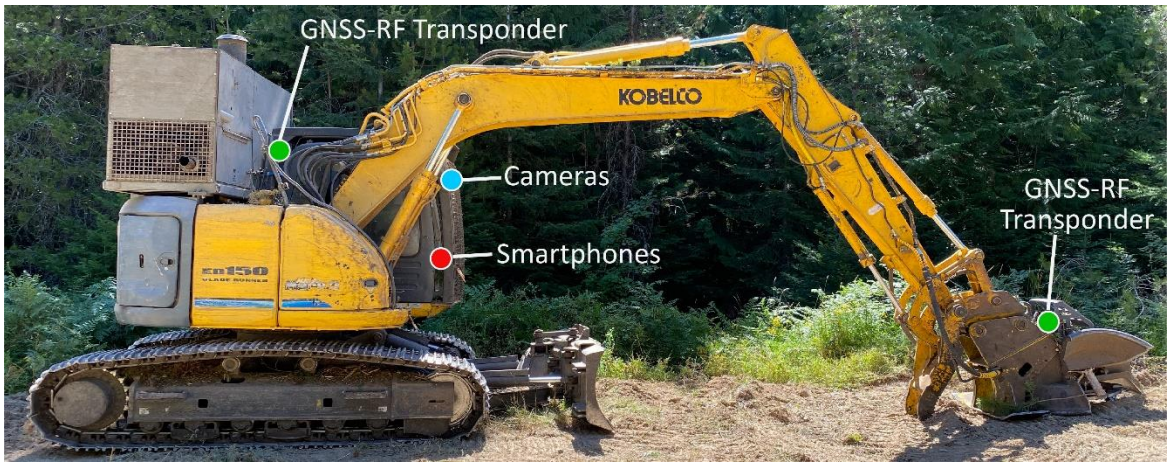

Figure 4.1. Smartphone, camera, and GNSS-RF transponder device locations on the masticator

In human activity recognition, sampling frequencies vary greatly from 1 Hz [91] to 200 Hz [92,93]. 50 Hz is used widely for capturing dynamic activities [57,94], though 20 Hz has been shown to provide acceptable recognition accuracy while also preserving smartphone battery life [36,44,45,95]. While decreasing sampling rate can increase the battery life of devices, reducing frequencies too drastically can limit the potential for achieving accurate activity recognition [91]. Collecting data at a high sampling rate (50 Hz) enables the data to be downsampled to lower frequencies allowing for additional analysis [59,96,97]. Therefore, the 50 Hz sensor data was downsampled to 20 Hz and 10 Hz to determine if downsampled data returned similar activity recognition classification results as natively sampled signals of the same frequencies.

Sensor data for acceleration, linear acceleration, orientation, and sound level was measured during field sampling using the Google Pixel. The IMU in the smartphone is a combination accelerometer and gyroscope that detects triaxial acceleration measurements in the x, y and z directions in meters per second squared (m s^{-2}), triaxial linear acceleration measurements in the x, y and z directions in meters per second squared (m s^{-2}), and triaxial orientation or tilt using the gyroscope in radians per second (rad s^{-1}). Sound pressure levels were measured in decibels (dB) using an integrated sensor. Each recorded data point is assigned a date and time stamp recording the year, month and day and the associated hour, minute, second and millisecond (Y-M-D h:m:s:SSS).

Productive work cycles and cycle elements were defined using the audio and video recordings obtained from the dash cameras used during sampling and were subsequently merged with smartphone-derived sensor data. Cycle elements for the masticator are described in Table 4.1 below.

Table 4.1. Cycle elements used for the mastication time and motion sampling.

Element	Description
Move	Starts when machine begins track or boom movement to successive masticating or clearing element and ends once head contacts material
Masticate	Starts when mulching head contacts standing tree and ends when tree bole is fully masticated.
Clearing	Starts when machine initiates mulching or moving downed trees, shrubs, etc. and ends when machine starts subsequent element
Travel	Prolonged machine walking within previously masticated area from one mastication location to the next
Delay	Any interruption to the productive cycle that falls outside previously described elements

4.3.3 Activity Recognition Modelling and Assessment

4.3.3.1 Smartphone-derived Sensor Data Processing

Activity recognition modelling using Random Forests and other shallow learning algorithms primarily consist of four main phases: data collection; segmentation; feature extraction and selection; and classification [36,58,98]. Once data is collected, extracted from the smartphones, and work elements for the entirety of the data set are manually added to the data based on corresponding time stamps, data was imported into the R statistical programming environment where all remaining analysis and modelling occurred [99]. The segmentation phase of activity recognition entailed dividing the full data set into smaller time segments to simplify data retrieval and consisted of two steps; signal preprocessing and windowing [36,58]. The Google Pixel accelerometer and gyroscope

recorded raw data across three axes (x,y,z) enabling the detection of orientation changes. To reduce the impact of influence on activity recognition performance, the vector magnitudes of the three-axis sensors were calculated using equation 1 [98,100,101]. This resulted in single orientation independent measures for acceleration, linear acceleration, and orientation/tilt.

$$a = \sqrt{ax^2 + ay^2 + az^2} \quad (1)$$

In activity recognition, sliding windows are often used to segment data into set time series where defined time domain features are calculated [36,37,42,44,45,94,102]. Studies have examined and compared model accuracies using multiple window sizes ranging from 1 to 13 seconds [39,42,44,56,91,94,102–109]. Activity recognition accuracy is greatly influenced by window size, with windows that are too short not covering the extent of the activity being classified and windows that are too long overlapping multiple unrelated activities [45]. Based on past research and our study objectives, four different windows (1, 5, 7.5 and 10 seconds) were assessed in an attempt to balance the ability of short windows to recognize simple activities and the ability of longer windows to capture less repetitive activities effectively [36,39,110]. The assigned window size is passed through the entire data set incrementally, with either overlapping or non-overlapping windows [111]. The strength of the impact that window size has on classification is dependent on how much subsequent windows overlap [45]. While overlap enables the classification of activities in smaller time intervals than the window, it does require greater computational capacity than non-overlapping windows [103]. 50% window overlap is commonly used in activity recognition modelling [37,42,50,94,109,110], though other window overlaps, including 90%, have been used successfully [39,56,104,108]. Both 50% and 90% overlapping windows were selected for this study.

Within each sliding window, time domain features were derived using mathematical and statistical techniques [112]. The nine time domain features calculated included mean, maximum, minimum, kurtosis, variance, standard deviation, skewness, root mean square (RMS) and signal vector magnitude, comparable with those used in Zhang et al. [49], Keefe et al. [39], Shoaib et al. [110], and Zimbelman & Keefe [56]. Mean is a versatile metric for various types of sensors for discriminating between rest and activity in multi-activity recognition and assists in preprocessing data by removing random spikes and noise [45,112]. Similarly, RMS, signal vector magnitude and standard deviation are all effective statistics for activity classification and distinguishing between periods of rest and activity [45]. Skewness is used to measure “the degree of asymmetry of a probability density curve compared to the average” [49]. The overall purpose of sampling and data

collection of various sensors is not to restore the raw signals of activities, but to detect different activities according to their statistical properties through use of the aforementioned time domain features [91]. That is why selection of appropriate time domain features for activity recognition is important.

4.3.3.2 Random Forest

Following windowing, data was separated into training and testing sets with a 70/30 split, respectively, to provide an unseen partition of data for final model assessment. Stratified random sampling was applied to each cycle element class to preserve element distribution ratios between testing and training data. Random forest (RF) was selected to develop machine learning algorithms for the productive cycle element classification. RF is an ensemble classifier that produces multiple decision trees using bagging and randomly selected subsets of training samples and variables to provide a majority vote from which a prediction is made [113–117]. Excellent classification results, speed of processing, and the ability to reduce bias, correlation, and overfitting compared to other classification and regression trees (CART) models make RF one of the most widely used machine learning methods available [117–120]. In activity recognition modelling, random forest has been widely tested with high levels of resulting classification success [39,42,46,49,56,101,102,104,107]. Performance was found to exceed 90% in instances when using multiple smartphone-based sensors and RF classifiers [35,49].

Forty unique RF algorithms were developed to account for all combinations of sampling rate (10 Hz, 20 Hz, 50 Hz, 10 Hz downsampled, 20 Hz downsampled), window overlap (50% and 90%), and sliding window length (1 second, 5 seconds, 7.5 seconds, 10 seconds). The workflow for all data processing and model development is found in Figure 4.2. The R package *caret* (version 6.0-88) was used for all random forest training and development [121]. Hyperparameters, specifically *mtry* and *ntree*, are adjustable components of random forest which can increase the performance of algorithms when properly tuned. The *mtry* parameter determines the number of variables split at each node of the decision trees and *ntree* is the number of trees used in the forest [117]. Repeated k-fold cross validation with 10 folds and 3 repeats was used on training datasets to train and validate *mtry* and *ntree* values for the machine learning algorithms. *Mtry* values (1-25) and *ntree* values (1-550) were assessed during this process. The final selected value for *mtry* was chosen based on the maximum accuracy achieved. For *ntree*, it is understood that prediction accuracy increases at a decreasing rate as trees are added and larger values for *ntree* increase computational demands [113]. To balance processing time and model performance, *ntree* was selected by determining the point at which out of

box error (OOB) and accuracy (%) of the model stabilized [122]. These hyperparameter values were then applied to the final training of the random forest algorithms which were then used to predict the test data.

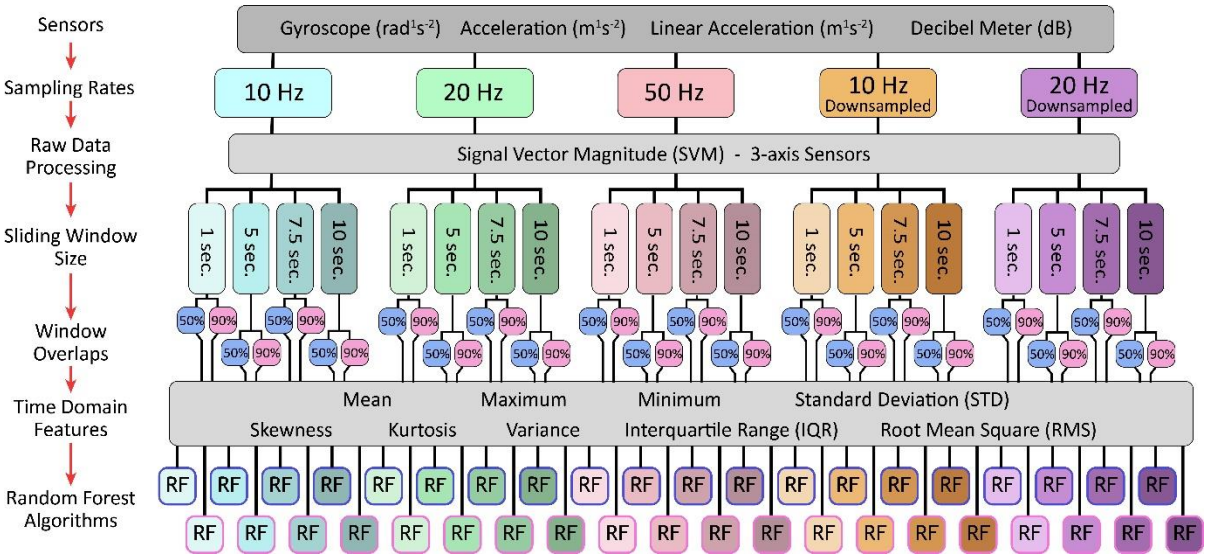

Figure 4.2. Activity recognition modelling data inputs and workflow.

The multiclass area under the curve (AUC) of the receiver characteristic operator (ROC) was used to evaluate the individual element characterization and overall activity recognition algorithm performance using the *multiclass.roc* function of the R *pROC* package (version 1.17.0.1) [123]. This measure of performance is commonly used for binary and multiclass classification algorithms [124–127] and performs well when working with imbalanced datasets [56,125,128–130]. The AUC for ROC represents the probability of a classifier ranking a randomly drawn positive before a randomly drawn negative [131]. In general, AUC provides an aggregate measure of classifier performance across all thresholds. This value falls between 0 and 1, with higher values indicating better performance [132]. AUC's between 0.5 and 0.7 are considered low accuracy; 0.7 and 0.9 are moderate accuracy; and accuracy is considered high when AUC exceeds 0.9 [124]. These values were converted to percentages. The AUC of all 40 trained random forest models were compared to determine which combination of window size, window overlap, and sampling frequency returned the highest AUC. The highest value indicated the best performing model overall.

Final model performance was also assessed using the *confusionMatrix* function in the *caret* package [121]. Five metrics quantifying the classification success of the activity recognition models per cycle element were provided by this function: sensitivity, specificity, precision, F1, and balanced

accuracy. These accuracy metrics were used to determine the impact of sliding window, window overlap, and sampling frequency on activity recognition performance. Sensitivity, also referred to as recall, is the true positive rate and represents the percentage of instances where an element was correctly classified [125]. This metric is calculated by dividing the number of true positives by the sum of the true positives and false negatives. Specificity is the true negative rate and is the percentage of negative instances correctly classified [125]. To calculate specificity, the number of true negatives is divided by the sum of the true negatives and false positives. Precision is used to capture the percentage of classified elements that represent an actual occurrence of that element and is calculated by dividing the number of true positives by the sum of the true positives and false positives [125]. In a basic sense, precision represents how sure one can be of their true positives, while sensitivity represents how sure one can be that no positive classifications are missed for a particular class. F1-score, or F-measure, combines the sensitivity and precision into a single performance metric and represents the harmonic mean of these two metrics [132–134]. This is the most common performance metric used in unbalanced classification problems [135–137]. The value of the F1-score ranges from 0 to 1, with values close to one indicating high classification performance [132], though they can easily be converted to a percentage scale and were in this study. Finally, the balanced accuracy was found for each model which combines the sensitivity and specificity metrics to find their average and works well with balanced and imbalanced data [132]. The equations for F1-score and balanced accuracy are found in equations 2 and 3 where F1 is the F1-score, and BA is the balanced accuracy.

$$F1 = 2 * \frac{Precision * Sensitivty}{Precision + Sensitivity} \quad (2)$$

$$BA = \frac{1}{2}\left(Sensitivity + Specificity\right) \quad (3)$$

4.3.4 Lidar Point Cloud Processing Procedures

Airborne laser scanning (ALS) is a commonly used lidar acquisition method for natural resource applications and derived products include terrain elevation, vegetation heights, stand volume, tree density, and tree species identification [67,68]. The ALS data used in this study were collected using an Optech Galaxy Prime Lidar system mounted on a fixed-wing aircraft. This was part of a 9,363 km^2 (3,615 $mile^2$), multi-agency, state-wide, lidar acquisition performed by Atlantic LLC in October 2019. Nominal point spacing of 0.33 meters and an average nominal pulse density of

9.11 pulses m^{-2} was achieved. Individual tree detection and segmentation derived from the lidar point cloud was performed by Northwest Management Incorporated (NMI) using a proprietary software and processing workflow associated with NMI's ForestView™ software [138]. This point-based lidar processing resulted in a full coverage stem map for the four main University of Idaho Experimental Forest (UIEF) management units. In addition to individual stem coordinates, each segmentation provides species, height (m), crown height (m), diameter (cm), crown diameter (m), and gross volume (MBF). It should be noted the 9.11 pulses m^{-2} point cloud density used to develop the individual stem map using NMI's ForestView™ software was a trial using lower resolution pulse densities. Standard applications of this software use point densities of 16-20 pulses m^{-2} on average but were unavailable for the study area at the time of sampling.

4.3.5 Cycle Element and Individual Stem Location Matching

Quantifying intensive equipment production that accounts for individual tree characteristics requires matching individual mastication events and tree locations. The machine's location for each mastication element was determined by aligning the time series data for the GNSS-RF transponders and observed time and motion data. Once the equipment location for each mastication element was determined, it was then necessary to locate feasibly treated stems within the treatment zone of the masticator at that point in time. The equipment used had a maximum boom reach of approximately 9 meters. A circular buffer of 7 meters placed around the cab's locations for each mastication element enabled the filtering of trees to include only those within the equipment's reach. 7 meters was used because the mastication of standing trees does not enable the full boom extension, thus limiting the overall reach of the machine.

Potential target trees were further filtered by accounting for the orientation of the machine cab within the stand in relation to the stems within the treatment zone. The cab and boom GNSS-RF devices enabled the derivation of the cab's orientation as an azimuth. The azimuths between the cab of the equipment and each target tree within the associated buffer was then quantified. Cab-to-boom and cab-to-tree azimuths were compared, and it was assumed cab-to-tree azimuths within +/- 10 degrees of cab-to-boom within the treatment zone indicated a feasibly masticated tree. All spatial analysis was performed using the sf packages in R [139]. A visual representation of the process used for identifying potentially treated trees using the stem map and GNSS-RF positions is shown in Figure 4.3.

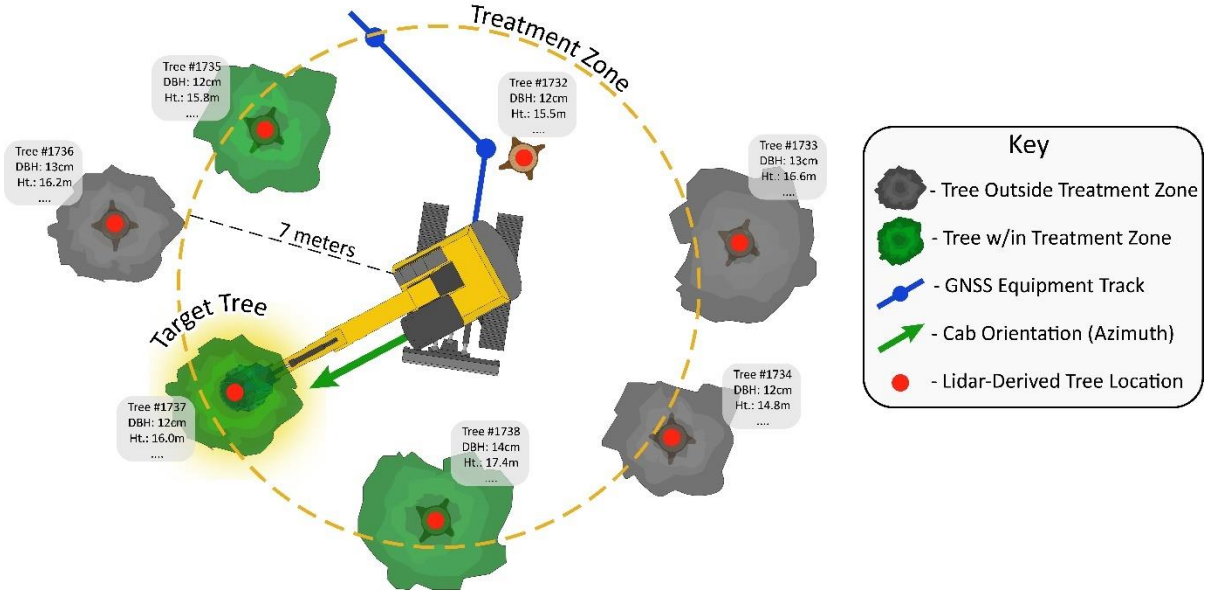

Figure 4.3. Identifying target trees. Process for identifying potential targeted trees for mastication using GNSS-RF-based equipment locations, equipment orientation, equipment to tree orientation, and individual tree locations.

4.4 Results

4.4.1 Work Sampling and Cycle Analysis

Summarized results from the mastication work sampling data are found in Table 4.2. A total of 88,829 seconds (~24.67 hours) of mechanical fuel treatments were observed across the three treatment units, with units 1, 2, and 3 accounting for approximately 41%, 29%, and 30% of the sampling time, respectively. The equipment performed the *move* element most often during work sampling, accounting for 32.2% of the overall sampling time, which corresponds directly with the most individual occurrences of a single element, 1,348. *Delay* and *travel* occurred significantly fewer times than the other elements, accounted for the smallest percentages of total duration of sampled time, but also had the highest mean element duration, largest range of element durations, and the largest standard deviations in element durations. The *delay* element had the largest coefficient of variation (223.8%) indicating a large variation of values around the mean. This is, in part, a direct result of the large range of observed element durations with a total of 2,244 seconds (37.4 minutes) separating the longest and shortest elements. Total sampling duration for the *clear*, *masticate* and *move* elements were relatively equal and accounted for 26.0, 28.7 and 32.2% of the total work sampling time respectively.

Table 4.2. Work sampling summary statistics for mastication equipment by element for the full field sampling period.

Element	n	Total Duration (s)	Total Duration (%)	Mean (s)	Range (s)	SD (s)	CV (%)
Clear	932	23132	26.0	25.7	2.0 – 202.0	24.6	95.7
Delay	53	8417	9.5	211.5	14.0 – 2258.0	473.4	223.8
Masticate	921	25499	28.7	23.7	2.0 – 139.0	18.6	78.3
Move	1348	28626	32.2	20.2	2.0 – 207.0	17.7	87.7
Travel	33	3155	3.6	96.6	10.0 – 298.0	55.8	59.8
Total	**3287**	**88829**	**100.0**	**27.0**	**2.0 – 2258.0**	**56.1**	**207.7**

4.4.2 Random Forest and Activity Recognition

Following the repeated 10-fold cross validation training and evaluation for the machine learning algorithms, 40 final random forest algorithms were assessed for the varying combinations of data sampling rate (Hz), sliding window size (seconds), and sliding window overlap (%). An *ntree* value of 150 was used for all random forests, with model training indicating a stabilization of error and accuracy at this number. This was found across all models, with training results for the 50% and 90% window overlap models for 50 Hz sampling rate and 10 second sliding window algorithms shown in Figure 4.4. While larger *ntree* values provided slight increases in model performance, the added benefits were outweighed by the significant increases in processing time which poses concerns with the feasibility of real-time model applications. Therefore, *ntree* values of 150 provided an acceptable balance between model performance and processing time.

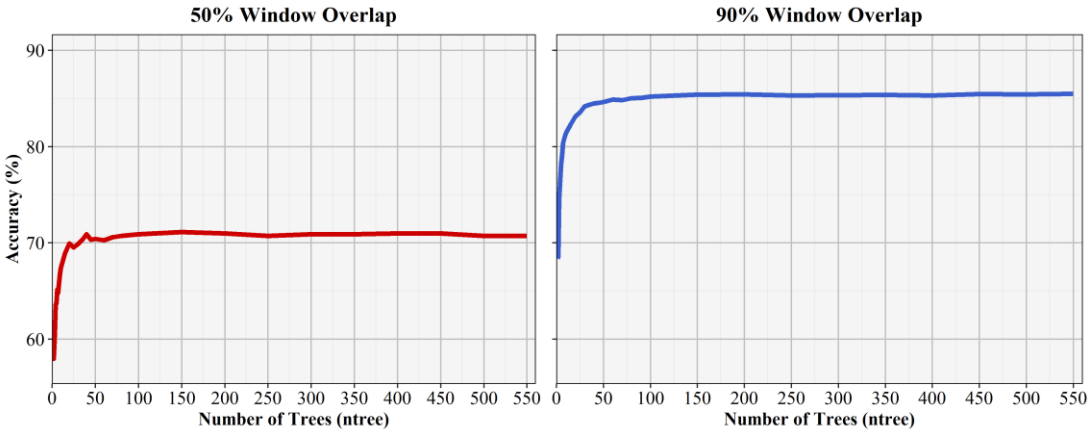

Figure 4.4. Repeated 10-fold cross validation ntree training results for the 50 Hz sampling rate and 10 second sliding window for both the 50 and 90% window overlaps.

Overall activity recognition performance was quantified using the area under the curve (AUC) with results for all models (5 sampling rates, 4 window sizes, 2 window overlaps) displayed in Figure 4.5. In every instance, models with 90% window overlaps significantly outperformed the models with identical sampling rates and window sizes but 50% window overlaps. Increasing sampling rate led to increases in AUC in most cases and similar trends were found when accounting for sliding window size. These trends were far more exaggerated in models with 50% sliding window overlaps. Final model selection was based on overall model AUC, with the best overall performance resulting from the 50 Hz sampling rate, 10 second sliding window, and 90% sliding window overlap combination with an AUC of 97.82%. AUC values for individual elements are found in Table 4.3.

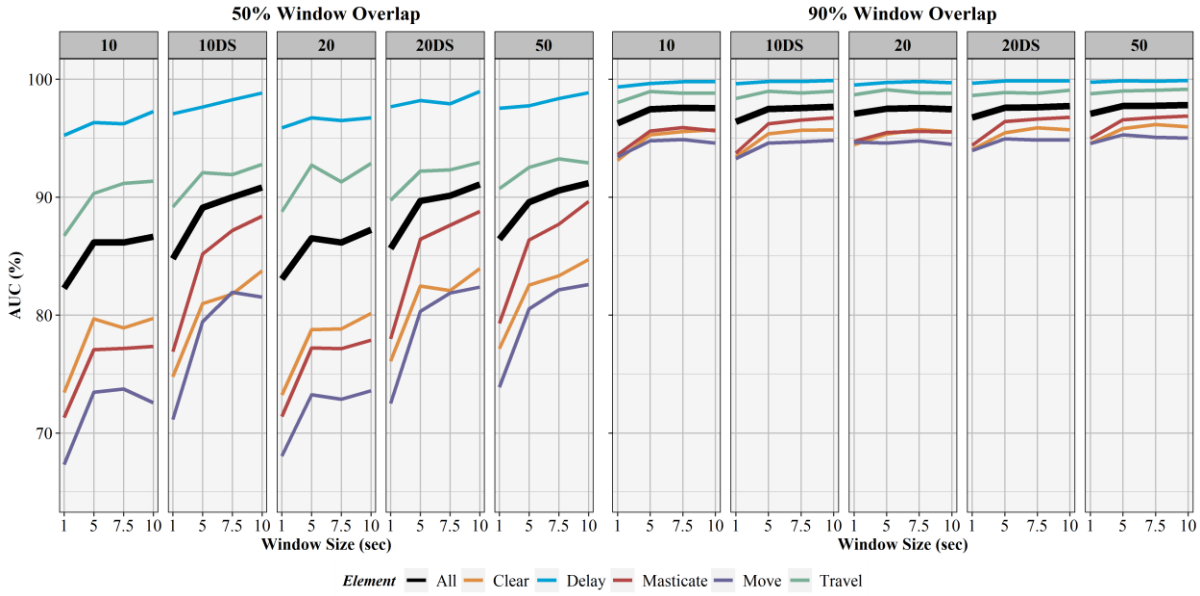

Figure 4.5. AUC results for activity recognition models. Comparison of activity recognition model area under the curve (AUC) percentages for 50% and 90% sliding window overlaps across the four sliding window lengths (1, 5, 7.5, 10 seconds) for each work element (clear, delay, masticate, move, travel) and for full models (All).

Table 4.3. Activity recognition performance metrics for the best performing classification model (50 Hz sampling rate, 10 second window, 90% widow overlap).

Element	AUC (%)	Sensitivity (%)	Specificity (%)	Precision (%)	F1-score (%)	Balanced Accuracy (%)
Clear	95.96	82.23	93.52	81.51	81.87	87.88
Delay	99.90	95.58	99.83	98.27	96.91	97.70
Masticate	96.88	86.01	94.49	86.12	86.06	90.25
Move	95.01	84.17	90.83	81.12	82.62	87.50
Travel	99.16	74.90	99.93	98.08	84.94	87.41

The influence of sampling rate, window overlap and window size on activity recognition sensitivity, specificity, precision, F1-score, and balanced accuracy are found in Figures 4.6, 4.7, 4.8, 4.9, and 4.10, respectively. Like AUC, window overlap had the greatest impact on model performance for all metrics, with 90% models performing better than 50% overlap models. Increases in sampling rate provided marginal increases in model performance, with 10 and 20 Hz data downsampled from the 50 Hz data performing better than the natively sampled 10 and 20 Hz data for classification. Positive trends between increasing model performance and increasing sliding window size were also seen, with 10 second windows returning the highest performance metrics in most instances. Select work elements in some models returned higher performance metrics at 7.5 second windows than 10 second windows, but this was not consistent for all elements in these classification algorithms. Performance metrics for the best performing activity recognition model (50 Hz sampling rate, 10 second sliding window, 90% sliding window overlap) are found in Table 4.3.

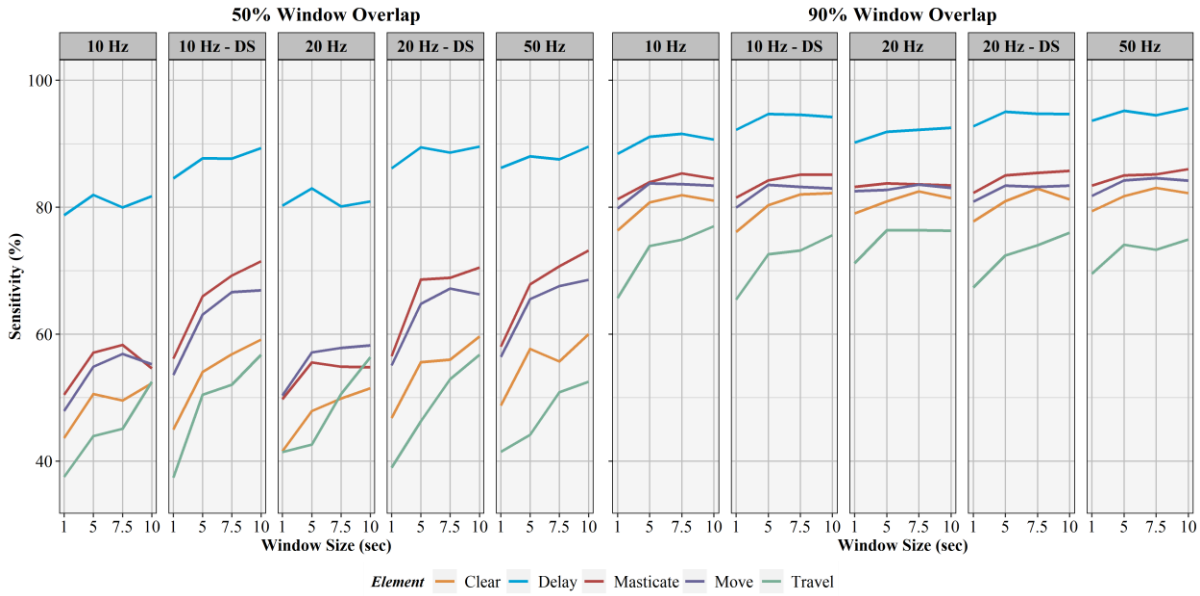

Figure 4.6. Sensitivity results for activity recognition models. Comparison of activity recognition model sensitivity percentages for 50% and 90% sliding window overlaps across the four sliding window lengths (1, 5, 7.5, 10 seconds) for each work element (clear, delay, masticate, move, travel).

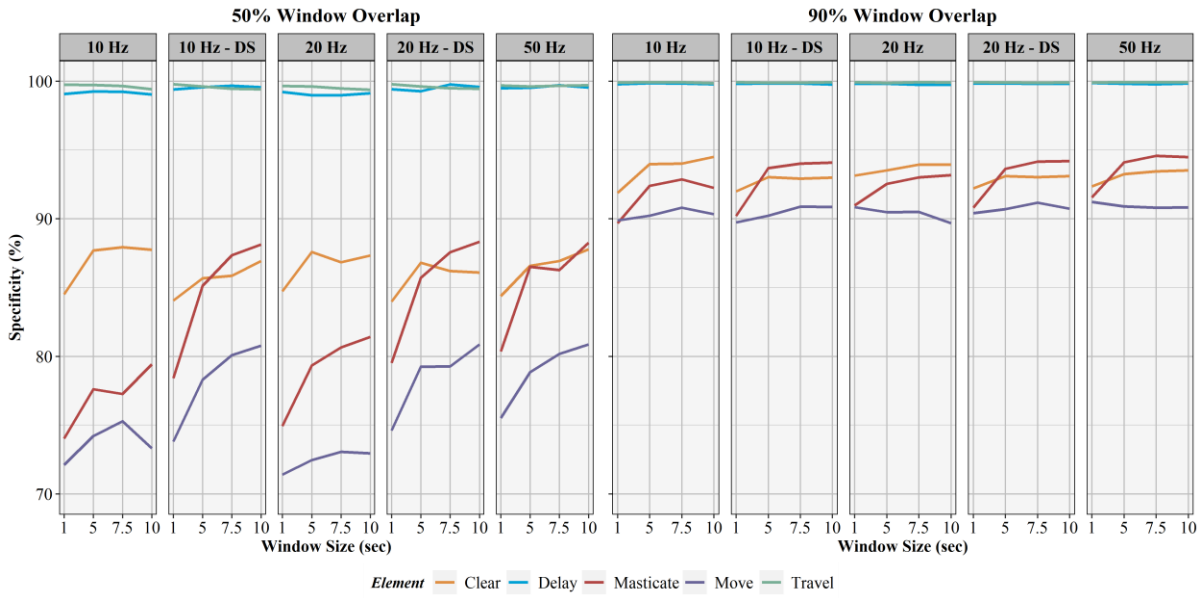

Figure 4.7. Specificity results for activity recognition models. Comparison of activity recognition model specificity percentages for 50% and 90% sliding window overlaps across the four sliding window lengths (1, 5, 7.5, 10 seconds) for each work element (clear, delay, masticate, move, travel).

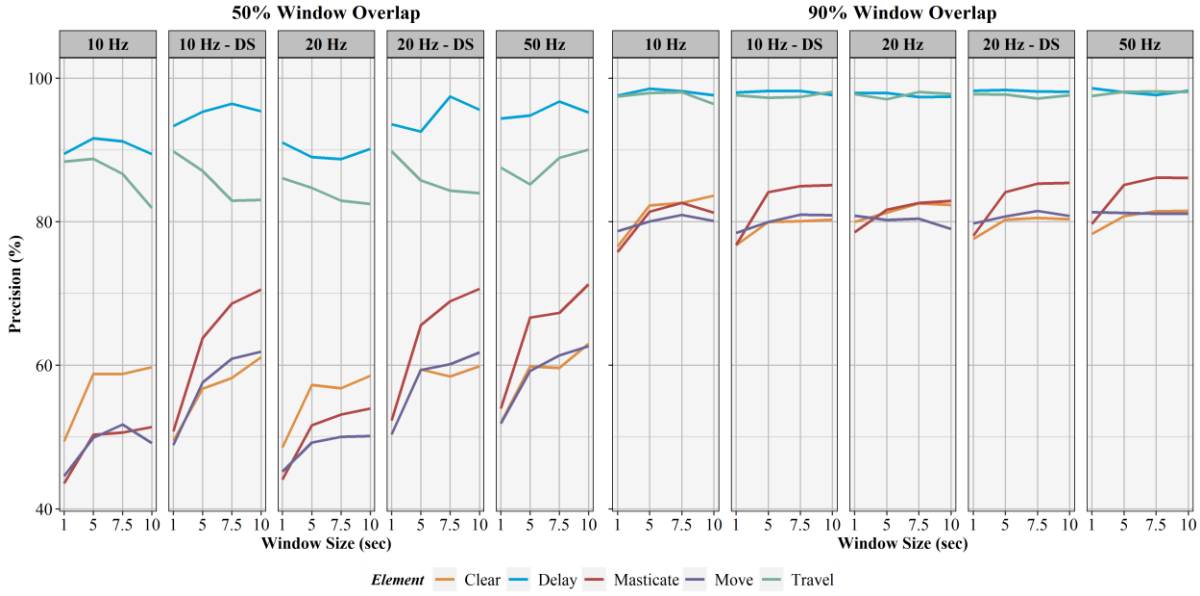

Figure 4.8. Precision results for activity recognition models. Comparison of activity recognition model precision percentages for 50% and 90% sliding window overlaps across the four sliding window lengths (1, 5, 7.5, 10 seconds) for each work element (clear, delay, masticate, move, travel).

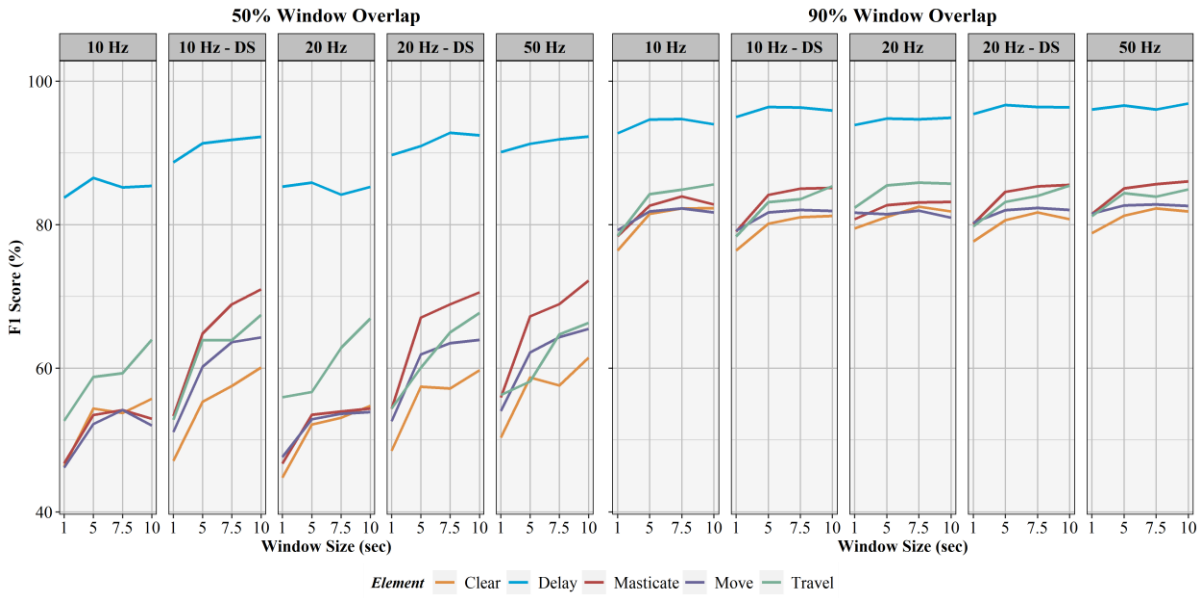

Figure 4.9. F1-score results for activity recognition models. Comparison of activity recognition model F1-score percentages for 50% and 90% sliding window overlaps across the four sliding window lengths (1, 5, 7.5, 10 seconds) for each work element (clear, delay, masticate, move, travel).

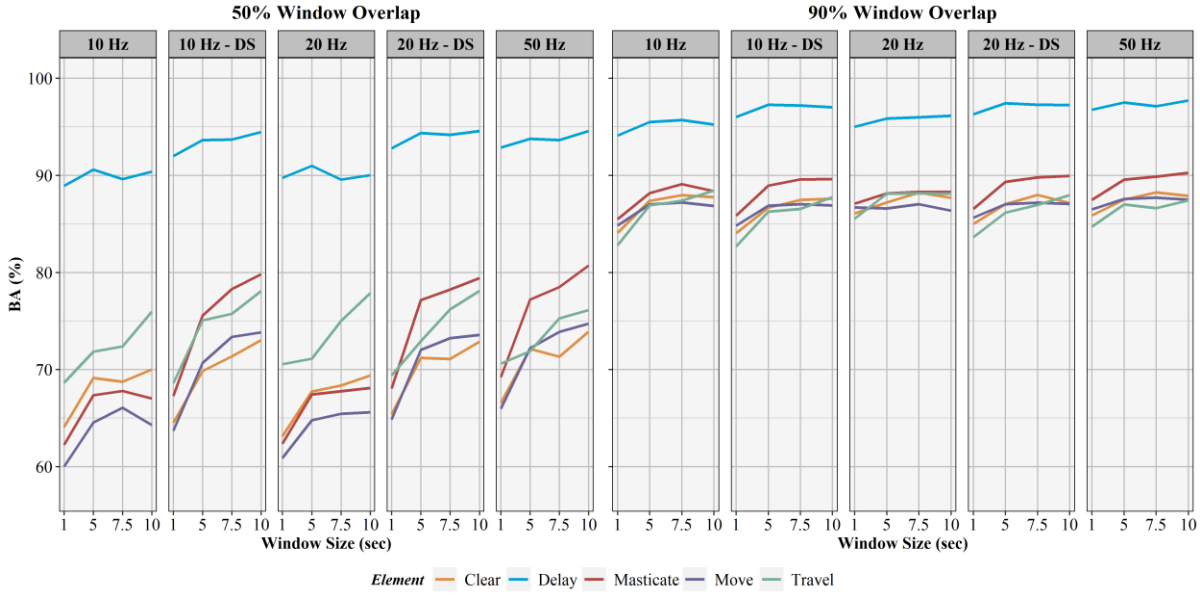

Figure 4.10. Balanced accuracy results for activity recognition models. Comparison of activity recognition model balanced accuracy percentages for 50% and 90% sliding window overlaps across the four sliding window lengths (1, 5, 7.5, 10 seconds) for each work element (clear, delay, masticate, move, travel).

The ranges of performance metrics used to assess the classification of the 5 work elements (*masticate*, *move*, *clear*, *delay*, *travel*) for the best model are as follows: AUC (95.01 - 99.90%); sensitivity (74.90 - 95.58%); specificity (90.83 - 99.93%); precision (81.12 - 98.27%); F1-score (81.87 - 96.91%); and balanced accuracy (87.41 - 97.70%). The *delay* element was correctly classified with the highest percentage of all elements and had sensitivity of 95.58%. *Travel* had the lowest sensitivity at 74.90%, but also achieved the highest specificity at 99.93%. The very high specificity means other work elements were rarely incorrectly classified as *travel*, though lower sensitivity shows actual *travel* events were incorrectly predicted as other elements relatively often, approximately 25% of the time. *Travel* element misclassification was most often associated with the *move* element, with 250 *travel* events incorrectly classified as *move* (Table 4.4). The *move* element had the lowest specificity at 90.83%, with 787 *clear*, 66 *delay*, 574 *masticate*, and 250 *travel* elements incorrectly classified as *move*. This shows the activity recognition model had the lowest ability to discern between false positives and true negatives with the *move* element.

The confusion matrix in Table 4.4 provides a detailed breakdown of activity recognition classification, with green shaded cells indicating correctly classified instances for each element. It is clear from the confusion matrix that the greatest misclassification occurred between the *move*, *masticate* and *clear* elements. The precision measures for all elements exceeded 80%, meaning over 80% of all elements predicted as a particular element were correctly classified. In all instances, the balanced accuracy exceeded 85%, showing the model's ability to account for both positive and negative classification outcomes for elements as an average of specificity and sensitivity. Areas under the curve (AUC) exceeding 95% for all elements shows excellent overall classification accuracy and activity recognition performance for this model. Each individual event shown in the confusion matrix represents a single 10 second window used for activity classification. As a result, models with smaller window sizes would contain larger numbers of instances within each cell because more windows were necessary to elapse the entire sampling period. The importance of the top-20 time domain features used in the final model are described by mean decrease in Gini and are found in Figure 4.11. Features from the gyroscope and sound derived features were consistently some of the most influential features in the models for all combinations of factors, consistent with the findings of Keefe et al. [39].

Table 4.4. Confusion matrix. Confusion matrix for the best performing activity recognition model (50 Hz sampling rate, 10 second window, 90% window overlap) indicating true positives (TP), true negatives (TN), false positives (FP), and false negatives (FN).

		Actual				
		Clear	**Delay**	**Masticate**	**Move**	**Travel**
Predicted	**Clear**	5692	26	486	726	53
	Delay	1	2333	7	29	4
	Masticate	440	13	6570	588	18
	Move	787	66	574	7207	250
	Travel	2	3	2	12	970

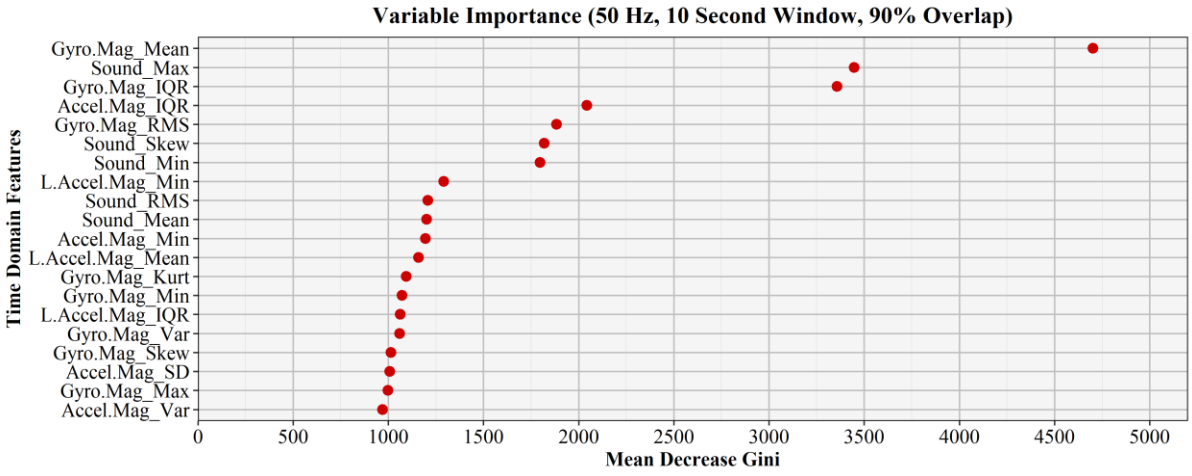

Figure 4.11. Time domain feature variable importance. Variable importance of the top 20 time domain features used during model development for the best performing activity recognition algorithm in terms of mean decrease in Gini.

4.4.3 Stem and Cycle Element Matching

A total of 11,758 individual trees were detected within the treatment units, though work sampling did not encompass the entirety of the planned treatment area due to time constraints (Table 4.5). Throughout the entirety of the work sampling period, 1,140 individual trees fell within the 7m buffer of the equipment cab during mastication elements. However, only 221 of these trees were within a range of azimuths from the cab to constitute a feasibly treated tree based on the GNSS-RF coordinates derived from the cab and boom transponders. In all, 921 mastication elements were observed during work sampling, though only 890 of these elements occurred with a lidar detected tree falling within the 7m cab buffer. 315 *masticate* elements could also be matched with an individual

tree based on machine orientation at the time of mastication. A larger number of *masticate* elements (315) were matched with an individual tree than there were feasible unique trees (221) because *masticate* elements were matched with the same unique tree on multiple occasions. It can be assumed that once a tree is masticated, it can no longer be masticated again. Therefore, a maximum of 24% of all *masticate* elements could be matched with a unique individual tree based on the data derived from the lidar-based individual tree locations and GNSS-RF-derived machine locations.

Table 4.5. Machine and individual stem location matching. This table displays the number of lidar-derived individual trees based on the ForestView™ software: within the overall treatment units; within the 7m treatment buffer of the machine cab during mastication elements; and within the cab buffer while corresponding with the machine orientation. The total number of mastication elements and the number of elements where an individual tree fell within the machine buffer and matched the machine orientation are also shown.

Lidar-derived Individual Trees			**Mastication Elements**		
Total	Buffer	Buffer + Azimuth	Total	Buffer	Buffer + Azimuth
11758	1140	221	921	890	315

4.5 Discussion

Class imbalance has been shown to impact and bias classification results, specifically towards the majority classes [140]. The most common sampling methods to fix imbalanced data are over and under sampling [141]. Over sampling approaches resolve data imbalance by duplicating cases of the minority class but at the expense of computational intensity required for machine learning, and increased risk of model overfitting [141–143]. This can lead to models that are very computationally demanding. Under sampling entails the reduction of majority classes to meet minority class sample sizes, but can lead to a loss of valuable data trends and information necessary for effective classification and was therefore not used in this study [136,142]. A third approach, synthetic minority oversampling technique (SMOTE), generates synthetic examples as opposed to data replication used in traditional oversampling methods, but are limited to binary classification models [142]. Ultimately, the data imbalanced did not appear to have significant impacts on activity recognition model performance, even in the *delay* and *travel* minority classes, as seen in the performance metrics found in Table 4.3. Therefore, sampling procedures to address class imbalance in the data were forgone. This decision was further supported by Kamei et al. who found sampling techniques provided no performance benefit for classification tree models which encompasses random forest algorithms [144] and Dittman et al. [145] who concluded sampling procedures are not always a necessary step for classification because random forest classifiers' robustness to imbalanced data.

While this imbalance likely contributed to the slightly lower sensitivity of the *travel* element, this was not a concern, as the F1-score and balanced accuracy remained relatively high at 84.94 and 87.41%, respectively. The *travel* element is operationally similar in function to the *move* element, apart from element duration. These similarities in the *move* and *travel* elements may account for the comparatively poor sensitivity of the *travel* element. Here, data imbalance may have favored the majority class (*move*) over the minority class (*travel)* during classification. During classification, *travel* was misclassified as *move* more than any other element. The confusion matrix (Table 4.4) showed actual *travel* elements misclassified as *move* 250 times, which account for approximately 20% of the actual *travel* element occurrences and 77% of the total *travel* element misclassifications. In future work, the *travel* and *move* elements could be combined into a single element to simplify the classification process given their operational similarities. Primary productive cycle elements: *masticate*, *clear*, and *move*, returned sensitivities exceeding 80% and balanced accuracies exceeding 85% showing the strength of the model in classifying these work elements (Table 4.3).

Despite being a minority class, *delay* returned the highest performance metrics for AUC, sensitivity, precision, F1-score and balanced accuracy among all work elements and the second highest specificity only behind the *travel* element. The machine was predominantly stationary during *delay* which simplified the classification of this element and attributed to the comparatively high performance metrics. The limited impact of data imbalance identified in this study may vary with other datasets and should be examined further in future studies. The sensitivity (74.90-95.58%), specificity (90.83-99.93%), precision (81.12-98.27%), F1-score (81.87-96.91%) and balanced accuracy (87.41-97.70%) for element classification of the best performing activity recognition model were similar to those in other studies using random forest algorithms, though all other studies focused on human activity recognition [40,46].

During modelling, all time domain features were retained for the four sensors. To improve processing time for future iterations, the number of time domain features could be reduced, only including the more influential variables. The limited presence of linear acceleration in the top tier of time domain feature importance suggests this sensor data may be excluded in future work without significant impacts to overall model performance to decrease overall processing complexity. The five time domain features with the lowest importance were all derived from linear acceleration. The high importance ranking of the sound pressure meter derived time domain features is consistent with the findings of Keefe et al. [39]. Sound is a valuable measure for activity recognition for equipment as

delay, lateral machine movements, clearing of light materials and the mastication of standing stems all expectedly produce distinct levels of sound and should be included in future modelling efforts.

Window overlap percentage was the largest factor associated with improved model performance for all combinations of sliding window length and sampling rate. The 50% window overlap was outperformed by the 90% window overlap by significant margins in all instances. This is consistent with findings from other studies [56,108]. For example, the 50 Hz, 10-second sliding window model returned an overall model accuracy of 68.81% for the 50% window overlap and 84.78% for the 90% window overlap. This trend was consistent for all other model combinations as well. One disadvantage of a greater window overlap is the added computational load of the model, with 90% overlap models taking longer to process than 50% overlap models. However, the increased performance metrics for activity recognition necessitates this computational cost to ensure effective and accurate models. Despite longer processing times, 90% window overlap can support real-time activity recognition by increasing the frequency by which predictions are made on the data and users receive activity characterizations [104].

Marginal improvements in performance metrics were obtained by moving between 1, 5, 7.5, and 10 second sliding windows for the 90% window overlap models. For example, the overall model AUC for 50 Hz, 90% window overlap models for the 1, 5, 7.5, and 10 second windows were 97.07, 97.73, 97.76, and 97.82, respectively (Figure 4.5). Window size impacted model performance more significantly for 50% overlap models than the 90% overlap models which is supported by Khusainov et al. [45]. Overall AUCs for 50 Hz, 50% window overlap models for 1, 5, 7.5, and 10 second windows were 86.43, 89.58, 90.57, and 91.19, respectively. While 1, 5, 7.5, and 10 second windows can be used with similar effectiveness when using 90% window overlaps, the increased processing time required by the shorter window sizes should also be considered. Shorter sliding windows require high computational overhead because the recognition algorithm is required to classify a larger number of windows over a set period of time than a larger window would require [111]. The 10 second window provides strong model performance while minimizing this computational cost which is an important consideration in real-time activity recognition. Increasing window length has also been shown to improve the performance of activity recognition models [39,104,110,137]. This is contrary to findings of Zimbelman and Keefe who found better model performance with shorter window sizes when modeling work activities for rigging-crew workers on cable logging operations [56]. These findings may differ for other forest equipment where work element duration may favor shorter

window lengths due to faster transitions between subsequent elements and the inability of longer window lengths to differentiate between short actions.

While limited, there were model performance improvements when comparing the 10 Hz and 20 Hz sampling rates to the 50 Hz rate. Highly active or “agitated” movements have been shown to be more accurately represented by higher sampling rates [36]. These improvements were more significant with the 50% window overlap models compared to the models with 90% overlap, similar to findings associate with sliding window length. When accounting for only the models using a 90% window overlap, all models regardless of sampling rate returned strong values for AUC exceeding 90%, indicating strong classification success. However, the strongest classification models resulted from the 50 Hz rates. The increased performance of downsampled 10 and 20 Hz models over natively sampled 10 and 20 Hz models was likely a direct result of these data being a subsample of the 50 Hz data. The performance trends in relation to cycle element, window overlap, and window size mimicked those seen with the 50 Hz models, albeit with slight performance reductions.

Reduced battery consumption associated with sampling at lower frequencies [44,95] was not found to be a necessary consideration in this study and computational resources needed for modelling were not impacted by sampling rate. During field sampling, all smartphones experienced similar battery draw when removed from auxiliary power, though longer periods of sampling and additional computational requirements associated with real-time activity recognition may show greater discrepancies. The use of equipment auxiliary electricity to power devices while sampling removes any concerns about sensor sampling frequency or other factors impacting battery life of devices during use. This is a distinguishing consideration when using smart devices for activity recognition on equipment versus human activity recognition where auxiliary power may be unavailable or cumbersome.

Integrating GNSS-RF derived machine positions and lidar-derived individual tree detection and segmentation to provide a simple approach for equipment positioning in addition to the smartphone activity recognition model was ultimately ineffective for our data. The ~25% success rate achieved matching mastication elements and individual stems is not operationally useful. This low percentage of matching limits confidence in the stems which were matched, and further work should explore more effective and accurate means for this process. While the exact reason for this poor performance is unclear, a combination of multiple factors may have led to the outcomes encountered. First, the accuracy of the tree detection and segmentation processes used in developing the singe tree stem map have not been assessed. The lidar used for segmentation is approximately half the pulse

density of lidar normally acquired to develop the ForestView™ single tree product and was being evaluated simultaneously in a separate study. It is possible that suppressed or intermediate trees were occluded or omitted during lidar-processing which would have reduced the number of detected stems, especially in areas of high stand density [146–149]. The mastication treatments primary focused on stand density reduction and stand improvement. Stems that were masticated were often smaller than those left in the residual stand. The use of terrestrial-based lidar may prove a more effective means of producing precise and accurate stems maps used for this application in future work. Mobile terrestrial laser scanning systems help reduce the problem of occlusion, omission and enable easier acquisition of multi-temporal lidar data sets [150,151].

Increasing the precision and accuracy of the GNSS positioning of the equipment during the operation is another area for improvement in future work. Improving the positioning of equipment relative to individual stems detected from lidar would likely increase the accuracy of detecting removed stems. It is well established that forest canopies impact the accuracy of GNSS devices. However, the increased availability of consumer technologies to improve the GNSS accuracy of mobile devices provide new opportunities to enhance real-time positioning and logistics in forested environments. External smartphone antennas, raw GNSS data collection, availability of consumer-grade devices with differential correction and improved dual-frequency GNSS chipsets available for the newest generations of smartphones provide new opportunities to greatly increase GNSS accuracy [152–158]. These technological advances may enable the exclusion of separate GNSS-RF devices from data collection and analysis, streamline activity recognition and positioning integration, and remove the potential for variability caused when fusing sensor data from multiple devices.

4.6 Conclusion

We have shown that models developed from the sensors on smart phones placed in machine cabs can recognize activities of mechanical fuel treatments in forested stands with balanced accuracies for elements between 87.41% and 97.70%. As the first known smartphone-based activity recognition study for mechanical forestry equipment, it was necessary to examine multiple factors impacting recognition accuracy and set the foundation for future equipment activity recognition modeling research. By demonstrating the application of this technology time studies and production analysis, we have advanced research supporting ubiquitous smartphone-based activity recognition solution for forestry equipment. This work can be improved by further refining field sampling procedures, model processing and integration of new mobile technologies to enable the collection of

sensor and accurate positional data from a single device. Additional field sampling with varying topographic and stand conditions, operators, and equipment types should also be completed to help quantify the extent to which these factors may impact activity recognition performance given the limited scope of conditions encountered in this study.

Activity recognition of forest equipment and common management practices using ubiquitous, consumer available devices is an important advancement in the field of precision forestry and forest operations management. By identifying effective sampling and modelling processes, future work can focus on refining and optimizing data processing and model development and continue advancing toward real-time data support in smartphone applications. As the era of forest digitalization and smart and precision operational forestry continues to advance, it is necessary land managers, operators, and researchers alike are equipped with the latest resources and technologies needed to successfully address the complex forest resource management challenges we face. Accurate and efficient assessment of equipment productivity and work practices through activity recognition is valuable for advancing safer, more cost effective, and sustainable operational forestry supply chains.

4.7 Literature Cited

1. Miyata ES. Determining fixed and operating costs of logging equipment. St. Paul, Minnesota: USDA-Forest Service, North Central Forest Experiment Station; 1980 p. 1–16. Report No.: NC-55.

2. Kellogg LD, Milota GV, Miller Jr. M. A comparison of skyline harvesting costs for alternative commercial thinning prescriptions. J For Eng. 1996;7–23.

3. Klepac J, Rummer B. Evaluation of a shovel logging system in the gulf coastal plain. In: A Global Perspective. COFE 2002: Proceedings of the Council on Forest Engineering; 2002 Jun 16-20; Aubrun, AL, USA; 2002. p. 1–5.

4. Wang J, McNeel J, Baumgras J. A computer-based time study system for timber harvesting operations. For Prod J. 2003;53(3):47–53.

5. Wang J, Long C, McNeel J, John Baumgras. Productivity and cost of manual felling and cable skidding in central Appalachian hardwood forests. For Prod J. 2004;54(12):45–51.

6. Acuna MA, Kellogg LD. Evaluation of alternative cut-to-length harvesting technology for native forest thinning in Australia. Int J For Eng. 2009;20(2):17–25.

7. Acuna M, Skinnell J, Evanson T, Mitchell R. Bunching with a self-levelling feller-buncher on steep terrain for efficient yarder extraction. Croat J For Eng. 2011;32(2):521–31.

8. Alam M, Acuna M, Brown M. Self-levelling feller-buncher productivity based on lidar-derived slope. Croat J For Eng. 2013;34(2):273–81.

9. Strandgard M, Alam M, Mitchell R. Impact of slope on productivity of a self-levelling processor. Croat J For Eng. 2014;35(2):193–200.

10. Talbot B, Aalmo GO, Stampfer K. productivity analysis of an un-guyed integrated yarder-processor with running skyline. Croat J For Eng. 2014;35(2):201–10.

11. Borz SA, Talagai N, Cheta M, Gavilanes Montoya AV, Castillo Vizuete DD. Automating data collection in motor-manual time and motion studies implemented in a willow short rotation coppice. Bioresources. 2018;13(2):3236–49.

12. Strandgard M, Walsh D, Mauricio Acuna. Estimating harvester productivity in pinus radiata plantations using stanford stem files. Scand J For Res. 2013;28(1):73–80.

13. Bell CK, Keefe RF, Fried JS. Validation of the OpCost logging cost model using contractor surveys. Int J For Eng. 2017;28(2):73–84.

14. Strandgard M, Mitchell R. Automated time study of forwarders using GPS and a vibration sensor. Croat J For Eng. 2015;36(2):175–84.

15. Keefe RF, M.Wempe A, Becker RM, Zimbelman EG, Nagler ES, Gilbert SL, et al. Positioning methods and the use of location and activity data in forests. Forests. 2019;10(458):1–46.

16. Taylor SE, McDonald TP, Veal MW, Grift TE. Using GPS to evaluate productivity and performance of forest machine systems. In: Proceedings of the First International Precision Forestry Symposium; 2001 June 17-20; Seattle, WA, USA; 2001. p. 1–20.

17. Keefe RF, Eitel JUH, Smith AMS, Wade T. Tinkham. Applications of multi transmitter GPS-VHF in forest operations. In: Proceedings of the 47th International Symposium on Forestry Mechanization and the 5th International Forest Engineering Conference; 2014 Jan; Gerardmer, France; 2014.

18. McDonald TP, Taylor SE, Rummer RB. Deriving forest harvesting machine productivity from positional data. In: 2000 ASAE Annual International Meeting; 2000 Jul 9-12; Milwaukee, Wisconsin, USA; 2000. p. 1–8.

19. Veal MW, Taylor SE, McDonald TP, McLemore DK, Dunn MR. Accuracy of tracking forest machines with GPS. Trans Am Soc Agric Eng. 2001;44:1903–11.

20. McDonald TP, Fulton JP. Automated time study of skidders using global positioning system data. Comput Electron Agric. 2005;48:19–37.

21. de Hoop CF, Dupré RH. Using GPS to document skidder motions- a comparison with manual data collection. In: Working Globally – Sharing Forest Engineering Challenges and Technologies Around the World. Coeur d'Alene, ID, USA; 2006. p. 1–11.

22. Hejazian M, Hosseini S, Lotfalian M, Ahmadikoolaei P. Possibility of global positioning system (GPS) application for time studies in forest machinery. Eur J Exp Biol. 2013;3(4):93–8.

23. Gallo R, Grigolato S, Cavalli R, Mazzetto F. GNSS-based operational monitoring devices for forest logging operation chains. J Agric Eng. 2013;44(2):140–5.

24. Palander T, Nuutinen Y, Kariniemi A, Vaatainen K. Automatic time study method for recording work phase times of timber harvesting. For Sci. 2013;59(4):472–83.

25. Olivera A, Visser R. Using the harvester on-board computer capability to move towards precision forestry. N Z J For. 2016;60(4):3–7.

26. Olivera A, Visser R, Acuna M, Morgenroth J. Automatic GNSS-enabled harvester data collection as a tool to evaluate factors affecting harvester productivity in a eucalyptus spp. harvesting operation in Uruguay. Int J For Eng. 2016;27(1):15–28.

27. Carter EA, McDonald TP, Torbert JL. Application of GPS technology to monitor traffic intensity and soil impacts in a forest harvest operation. In: Tenth Biennial Southern Silvicultural Research Conference; 1999 Feb 16-18; Shreveport, LA, USA; 1999. p. 609–13.

28. Grayson LM, Keefe RF, Tinkham WT, Eitel JUH, Saralecos JD, Smith AMS, et al. Accuracy of WAAS-enabled GPS-RF warning signals when crossing a terrestrial geofence. Sensors. 2016;16(912):1–8.

29. Wempe AM, Keefe RF. Characterizing rigging crew proximity to hazards on cable logging operations using GNSS-RF: effect of GNSS positioning error on worker safety status. Forests. 2017;8(357):1–17.

30. Zimbelman EG, Keefe RF, Strand EK, Kolden CA, Wempe AM. Hazards in motion: development of mobile geofences for use in logging safety. Sensors. 2017;17(882):1–16.

31. Newman SM, Keefe RF, Brooks RH, Ahonen EQ, Wempe AM. Human factors affecting logging injury incidents in Idaho and the potential for real time location-sharing technology to improve safety. Safety. 2018;4(4):1–28.

32. Becker RM, Keefe RF, Anderson NM. Use of real-time GNSS-RF data to characterize the swing movements of forestry equipment. Forests. 2017;8(44):1–15.

33. Zimbelman EG, Keefe RF. real-time positioning in logging: effects of forest stand characteristics, topography, and line-of-sight obstructions on GNSS-RF transponder accuracy and radio signal propagation. PLoS ONE. 2018;13(1):1–17.

34. Noordermeer L, Sørngård E, Astrup R, Næsset E, Gobakken T. Coupling a differential global navigation satellite system to a cut-to-length harvester operating system enables precise positioning of harvested trees. Int J For Eng. 2021;1–9.

35. Shoaib M, Bosch S, Incel OD, Scholten H, Havinga PJM. Fusion of smartphone motion sensors for physical activity recognition. Sensors. 2014;14:10146–76.

36. Lima WS, Souto E, El-Khatib K, Jalali R, Gama J. Human activity recognition using inertial sensors in a smartphone: an overview. Sensors. 2019;19(3213):1–29.

37. del Rosario MB, Redmond SJ, Lovell NH. Tracking the evolution of smartphone sensing for monitoring human movement. Sensors. 2015;15:18901–33.

38. Hur T, Bang J, Kim D, Banos O, Lee S. Smartphone location-independent physical activity recognition based on transportation natural vibration analysis. Sensors. 2017;17(931):1–21.

39. Keefe RF, Zimbelman EG, Wempe AM. Use of smartphone sensors to quantify the productive cycle elements of hand fallers on industrial cable logging operations. Int J For Eng. 2019;1–12.

40. Bayat A, Pomplun M, Tran DA. A study on human activity recognition using accelerometer data from smartphones. Procedia Comput Sci. 2014;34:450–7.

41. Reddy S, Mun M, Burke J, Estrin D, Hansen M. Using mobile phones to determine transportation modes. ACM Trans Sens Netw. 2010;6(2):1–27.

42. Casale P, Pujol O, Radeva P. Human activity recognition from accelerometer data using a wearable device. In: IbPRIA 2011; 2011. p. 289–96.

43. Chen L, Hoey J, Nugent CD, Cook DJ, Yu Z. Sensor-based activity recognition. IEEE Trans Syst Man Cybern. 2012;42(6):790–808.

44. Khan AM, Siddiqi MH, Lee S-W. Exploratory data analysis of acceleration signals to select light-weight and accurate features for real-time activity recognition on smartphones. Sensors. 2013;13:13099–122.

45. Khusainov R, Azzi D, Achumba IE, Bersch SD. Real-time human ambulation, activity, and physiological monitoring: taxonomy of issues, techniques, applications, challenges and limitations. Sensors. 2013;13:12852–902.

46. Attal F, Mohammed S, Dedabrishvili M, Chamroukhi F, Oukhellou L, Amirat Y. Physical human activity recognition using wearable sensors. Sensors. 2015;15:31314–38.

47. Shoaib M, Bosch S, Incel OD, Scholten H, Havinga PJM. A survey of online activity recognition using mobile phones. Sensors. 2015;15:2059–85.

48. Gjoreski M, Gjoreski H, Luštrek M, Gams M. How accurately can your wrist device recognize daily activities and detect falls? Sensors. 2016;16(800):1–21.

49. Zhang M, Chen S, Zhao X, Yang Z. Research on construction workers' activity recognition based on smartphone. Sensors. 2018;18(2667):1–18.

50. Akhavian R, Behzadan AH. Smartphone-based construction workers' activity recognition and classification. Autom Constr. 2016;71:198–209.

51. Gallo R, Visser R, Mazzetto F. Developing an automated monitoring system for cable yarding systems. Croat J For Eng. 2021;42(2):213–25.

52. Borz SA, Paun M. Integrating offline object tracking, signal processing, and artificial intelligence to classify relevant events in sawmilling operations. Forests. 2020;11(1333):1–19.

53. Cheţa M, Marcu MV, Iordache E, Borz SA. Testing the capability of low-cost tools and artificial intelligence techniques to automatically detect operations done by a small-sized manually driven bandsaw. Forests. 2020;11(739):1–13.

54. Cheta M, Marcu MV, Borz SA. Effect of training parameters on the ability of artificial neural networks to learn: a simulation on accelerometer data for task recognition in motor-manual felling and processing. Bull Transilv Univ Braşov. 2020;13(62):1–18.

55. Pierzchała M, Kvaal K, Stampfer K, Talbot B. automatic recognition of work phases in cable yarding supported by sensor fusion. Int J For Eng. 2018;29(1):12–20.

56. Zimbelman EG, Keefe RF. Development and validation of smartwatch-based activity recognition models for rigging crew workers on cable logging operations. PLoS ONE. 2021;16(5):1–25.

57. Fahim M, Fatima I, Lee S, Park Y-T. EFM: Evolutionary fuzzy model for dynamic activities recognition using a smartphone accelerometer. Appl Intell. 2013;39:475–88.

58. Incel OD, Kose M, Ersoy C. A review and taxonomy of activity recognition on mobile phones. BioNano Sci. 2013;3:145–71.

59. San-Segundo R, Blunck H, Moreno-Pimentel J, Stisen A, Gil-Martín M. Robust human activity recognition using smartwatches and smartphones. Eng Appl Artif Intell. 2018;72:190–202.

60. Hiesel P, Benjamin JG. Applicability of international harvesting equipment productivity studies in Maine, USA: a literature review. Forests. 2013;4:898–921.

61. Reutebuch SE, Andersen H-E, McGaughey RJ. Light detection and ranging (lidar): an emerging tool for multiple resource inventory. J For. 2005;September:286–92.

62. Falkowski MJ, Gessler PE, Morgan P, Hudak AT, Smith AMS. Characterizing and mapping forest fire fuels using ASTER imagery and gradient modeling. For Ecol Manag. 2005;217:129–46.

63. Falkowski MJ, Evans JS, Martinuzzi S, Gessler PE, Hudak AT. Characterizing forest succession with lidar data: an evaluation for the inland northwest, USA. Remote Sens Environ. 2009;113:946–56.

64. Akay AE, Oğuz H, Karas IR, Aruga K. Using lidar technology in forestry activities. Environ Monit Assess. 2009;151:117–25.

65. Hudak AT, Strand EK, Vierling LA, Byrne JC, Eitel JUH, Martinuzzi S, et al. Quantifying aboveground forest carbon pools and fluxes from repeat lidar surveys. Remote Sens Environ. 2012;123:25–40.

66. Wulder MA, White JC, Nelson RF, Næsset E, Ørka HO, Coops NC, et al. Lidar sampling for large-area forest characterization: a review. Remote Sens Environ. 2012;121:196–209.

67. Man Q, Dong P, Guo H, Liu G, Shi R. Light detection and ranging and hyperspectral data for estimation of forest biomass: a review. J Appl Remote Sens. 2014;8:1–22.

68. Silva CA, Klauberg C, Hudak AT, Vierling LA, Jaafar WSM, Mohan M, et al. Predicting stem total and assortment volumes in an industrial pinus taeda l. forest plantation using airborne laser scanning data and random forest. Forests. 2017;8(254):1–17.

69. Silva CA, Klauberg C, Hudak AT, Vierling LA, Fennema SJ, Corte APD. modeling and mapping basal area of pinus taeda l. plantation using airborne lidar data. Ann Braz Acad Sci. 2017;89(3):1895–905.

70. Falkowski MJ, Smith AMS, Gessler PE, Hudak AT, Vierling LA, Evans JS. the influence of conifer forest canopy cover on the accuracy of two individual tree measurement algorithms using lidar data. Can J Remote Sens. 2008;34:338–50.

71. d'Oliveira MVN, Reutebuch SE, McGaughey R j., Andersen H-E. Estimating forest biomass and identifying low-intensity logging areas using airborne scanning lidar in Antimary State Forest, Acre State, Western Brazilian Amazon. Remote Sens Environ. 2012;124:479–91.

72. Ellis P, Griscom B, Walker W, Gonçalves F, Tina Cormier. Mapping selective logging impacts in Borneo with GPS and airborne lidar. For Ecol Manag. 2016;365:184–96.

73. Slesak RA, Kaebisch T. Using lidar to assess impacts of forest harvest landings on vegetation height by harvest season and the potential for recovery over time. Can J For Res. 2016;46:869–75.

74. Heinimann HR, Breschan J. Pre-harvest assessment based on lidar data. Croat J For Eng. 2012;33(2):169–80.

75. Kato A, Schiess P. Lidar derived tree parameters for optimal cable logging system design. In: Proceedings of the International Mountain Logging and 13th Pacific Northwest Skyline Symposium; 2007 Apr; Corvallis, OR, USA; 2007. p. 173–9.

76. Becker RM, Keefe RF, Anderson NM, Eitel JUH. Use of lidar-derived landscape parameters to characterize alternative harvest system options in the inland northwest. Int J For Eng. 2018;29(3):179–91.

77. Maltamo M, Hauglin M, Næsset E, Gobakken T. Estimating stand level stem diameter distribution utilizing harvester data and airborne laser scanning. Silva Fenn. 2019;53(3):1–19.

78. Yu X, Hyyppä J, Holopainen M, Vastaranta M. Comparison of area-based and individual tree-based methods for predicting plot-level forest attributes. Remote Sens. 2010;2:1481–95.

79. Yao W, Krzystek P, Heurich M. Tree species classification and estimation of stem volume and dbh based on single tree extraction by exploiting airborne full-waveform lidar data. Remote Sens Environ. 2012;123:368–80.

80. Hyyppä J, Yu X, Hyyppä H, Vastaranta M, Holopainen M, Kukko A, et al. Advances in forest inventory using airborne laser scanning. Remote Sens. 2012;4:1190–207.

81. Melville G, Stone C, Turner R. Application of lidar data to maximise the efficiency of inventory plots in softwood plantations. N Z J For Sci. 2015;45(9):1–16.

82. Jeronimo SMA, Kane VR, Churchill DJ, McGaughey RJ, Franklin JF. Applying lidar individual tree detection to management of structurally diverse forest landscapes. J For. 2018;116(4):336–46.

83. Rahman MZA, Gorte BGH, Bucksch AK. A new method for individual tree measurement from airborne lidar. In: Proceedings of Silvilaser 2009; 2009 Oct 14-16; College Station, Texas, USA; 2009. p. 1–10.

84. Jakubowski MK, Li W, Guo Q, Kelly M. Delineating individual trees from lidar data: a comparison of vector- and raster-based segmentation approaches. Remote Sens. 2013;5:4163–86.

85. Kandare K, Ørka HO, Chan JC-W, Dalponte M. Effects of forest structure and airborne laser scanning point cloud density on 3d delineation of individual tree crowns. Eur J Remote Sens. 2016;49:337–59.

86. Luo L, Zhai Q, Su Y, Ma Q, Kelly M, Guo Q. Simple method for direct crown base height estimation of individual conifer trees using airborne lidar data. Opt Express. 2018;26(10):1–17.

87. Silva CA, Hudak AT, Vierling LA, Loudermilk EL, O'Brien JJ, Hiers JK, et al. Imputation of individual longleaf pine (pinus palustris mill.) tree attributes from field and lidar data. Can J Remote Sens. 2016;42(5):554–73.

88. Taylor S, Veal M, Grift T, McDonald T, Corley F. Precision forestry: operational tactics for today and tomorrow. In: Proceedings of the 25th Annual Meeting of the Council of Forest Engineers; 2002. Available from: www.eng.auburn.edu/files/file169.pdf

89. Kovacsova P, Antalova M. Precision forestry - definition and technologies. Sumar List. 2010;134(11):603–11.

90. Asim F. AndroSensor [Internet]. 2015 [cited 2018 Sep 15]. Available from: https://play.google.com/store/apps/details?id=com.fivasim.androsensor&hl=en&gl=US

91. Zheng L, Wu D, Ruan X, Weng S, Peng A, Tang B, et al. A novel energy-efficient approach for human activity recognition. Sensors. 2017;17(2064):1–21.

92. Ermes M, P¨arkk¨a J, M¨antyj¨arvi J, Ilkka Korhonen. Detection of daily activities and sports with wearable sensors in controlled and uncontrolled conditions. IEEE Trans Inf Technol Biomed. 2008;12(1):20–7.

93. Koping L, Shirahama K, Grzegorzek M. A general framework for sensor-based human activity recognition. Comput Biol Med. 2018;95:248–60.

94. Hassan MM, Uddin MdZ, Mohamed A, Almogren A. A robust human activity recognition system using smartphone sensors and deep learning. Future Gener Comput Syst. 2018;81:307–13.

95. Krause A, Ihmig M, Rankin E, Leong D, Gupta S, Siewiorek D, et al. Trading off prediction accuracy and power consumption for context-aware wearable computing. In: Proceedings of the 9th IEEE International Symposium on Wearable Computers; 2005. p. 1–7.

96. Maurer U, Smailagic A, Siewiorek DP, Deisher M. Activity recognition and monitoring using multiple sensors on different body positions. In: Proceedings of the International Workshop on Wearable and Implantable Body Sensor Networks; 2006. p. 1–4.

97. Siirtola P, Laurinen P, Roning J. Efficient accelerometer-based swimming exercise tracking. In: Proceedings of the 2011 IEEE Symposium on the Computational Intelligence and Data Mining; 2011 Apr 11-15; Paris, France; 2011. p. 1–6.

98. Siirtola P, Roning J. Ready-to-use activity recognition for smartphones. In: Proceedings of the 2013 IEEE Symposium on Computational Intelligence and Data Mining; 2013 Apr 16-19; Singapore; 2013. p. 1–6.

99. R Core Team. R: A Language and Environment for Statistical Computing [Internet]. Vienna, Austria: R Foundation for Statistical Computing; R Core Team; 2020 [cited 2020 Feb 12]. Available from: https://www.R-project.org

100. Bianchi F, Redmond SJ, Narayanan MR, Cerutti S, Lovell NH. Barometric pressure and triaxial accelerometry- based falls event detection. IEEE Trans Neural Syst Rehabil Eng. 2010;18(6):619–27.

101. Ellis K, Kerr J, Godbole S, Lanckriet G, Wing D, Marshall S. A random forest classifier for the prediction of energy expenditure and type of physical activity from wrist and hip accelerometers. Physiol Meas. 2014;35(11):2191–203.

102. Lara OD, Labrador MA. A mobile platform for real-time human activity recognition. In: Proceedings of the 6th IEEE International Workshop on Personalized Networks; 2012. p. 667–71.

103. Morales J, Akopian D. Physical activity recognition by smartphones, a survey. Biocybern Biomed Eng. 2017;37:388–400.

104. Mehrang S, Pietilä J, Korhonen I. An activity recognition framework deploying the random forest classifier and a single optical heart rate monitoring and triaxial accelerometer wrist-band. Sensors. 2018;18(613):1–13.

105. Sun L, Zhang D, Li B, Guo B, Li S. Activity recognition on an accelerometer embedded mobile phone with varying positions and orientations. In: Proceedings of the International Conference on Ubiquitous Intelligence and Computing; 2010. p. 548–62.

106. Trost SG, Zheng Y, Wong W-K. Machine learning for activity recognition: hip versus wrist data. Physiol Meas. 2014;35:2183–9.

107. Weiss GM, Timko JL, Gallagher CM, Yoneda K, Schreiber AJ. Smartwatch-based activity recognition: a machine learning approach. In: Proceedings of the 2016 IEEE-EMBS International Conference on Biomedical and Health Informatics; 2016 Feb 24-27; Las Vegas, Nevada; 2016. p. 426–9.

108. Achumba IE, Bersch S, Khusainov R, Azzi D, Kamalu U. On time series sensor data segmentation for fall and activity classification. In: Proceedings of the IEEE 14th International Conference on e-Health Networking, Applications and Services; 2012 Oct 10-13; Beijing, China; 2012. p. 427–30.

109. Wu W, Dasgupta S, Ramirez EE, Peterson C, Norman GJ. Classification accuracies of physical activities using smartphone motion sensors. J Med Internet Res. 2012;14(5):1–9.

110. Shoaib M, Bosch S, Incel OD, Scholten H, Havinga PJM. Complex human activity recognition using smartphone and wrist-worn motion sensors. Sensors. 2016;16(426):1–24.

111. Lara OD, Labrador MA. A survey on human activity recognition using wearable sensors. IEEE Commun Surv Tutor. 2013;15(3):1192–209.

112. Figo D, Diniz PC, Ferreira DR, Cardoso JMP. Preprocessing techniques for context recognition from accelerometer data. Pers Ubiquit Comput. 2010;14:645–62.

113. Breiman L. Random Forests. Mach Learn. 2001;45:5–32.

114. Liaw A, Wiener M. Classification and regression by randomForest. R News. 2002;2(3):18–22.

115. Strobl C, Boulesteix A-L, Kneib T, Augustin T, Zeileis A. Conditional variable importance for random forests. BMC Bioinformatics. 208AD;9(307):1–11.

116. Genuer R, Poggi J-M, Tuleau-Malot C. Variable selection using random forests. Pattern Recognit Lett. 2010;31(14):2225–36.

117. Belgiu M, Dragut L. Random forest in remote sensing: a review of applications and future directions. ISPRS J Photogramm Remote Sens. 2016;114:24–31.

118. Leo Breiman. Manual on setting up, using, and understanding random forests v3.1 [Internet]. Statistics Department University of California Berkeley, CA, USA; 2002 [cited 2020 Feb 13]. Available from: https://www.stat.berkeley.edu/~breiman/RandomForests/cc_manual.htm

119. Brosofske KD, Froese RE, Falkowski MJ, Banskota A. A review of methods for mapping and prediction of inventory attributes for operational forest management. For Sci. 2014;60(4):733–56.

120. Cinaroglu S. Comparison of performance of decision tree algorithms and random forest: an application on OECD countries health expenditures. Int J Comput Appl. 2016;138(1):37–41.

121. Kuhn M, Wing J, Weston S, Williams A, Keefer C, Engelhardt A, et al. caret: classification and regression training [Internet]. 2021 [cited 2020 Feb 13]. Available from: https://cran.r-project.org/web/packages/caret/index.html

122. Svetnik V, Liaw A, Tong C, Culberson JC, Sheridan RP, Feuston BP. Random forest: a classification and regression tool for compound classification and QSAR modeling. J Chem Inf Comput Sci. 2003;43(6):1947–58.

123. Robin X, Turck N, Hainard A, Tiberti N, Lisacek F, Sanchez J-C, et al. pROC: an open-source package for R and S+ to analyze and compare ROC curves. BMC Bioinformatics [Internet]. 2011;12(77). Available from: http://expasy.org/tools/pROC/

124. Streiner DL, Cairney J. What's under the roc? an introduction to receiver operating characteristics curves. Can J Psychiatry. 2007;52(2):121–8.

125. Sokolova M, Japkowicz N, Szpakowicz S. Beyond accuracy, F-score and ROC: a family of discriminant measures for performance evaluation. Lect Notes Comput Sci. 2006;

126. Hajian-Tilaki K. Receiver operating characteristic (ROC) curve analysis for medical diagnostic test evaluation. Casp Jounral Int Med. 2013;4(2):627–35.

127. Hand DJ, Till RJ. A simple generalisation of the area under the ROC curve for multiple class classification problems. Mach Learn. 2001;45:171–86.

128. Luque A, Carrasco A, Martín A, de las Heras A. The impact of class imbalance in classification performance metrics based on the binary confusion matrix. Pattern Recognit. 2019;91:216–31.

129. Boughorbel S, Jarray F, El-Anbari M. Optimal classifier for imbalanced data using matthews correlation coefficient metric. PLoS ONE. 2017;12(6):1–17.

130. Ling C, Li C. Data mining for direct marketing: problems and solutions. KDD. 1998;1–7.

131. Hanley JA, Barbara J. McNeil. The meaning and use of the area under a receiver operating characteristic (ROC) curve. Radiology. 1982;143(1):29–36.

132. Tharwat A. Classification assessment methods. Appl Comput Inform. 2021;17(1):168–92.

133. Minnen D, Westeyn T, Starner T, Ward JA, Lukowicz P. Performance metrics and evaluation issues for continuous activity recognition. In: Proceedings of the Performance Metrics for Intelligent Systems Workshop; 2006 Aug 21-23; Gaithersburg, MD, USA: NIST; 2006. p. 141–8.

134. Chicco D, Jurman G. The advantages of the Matthews correlation coefficient (MCC) over F1 score and accuracy in binary classification evaluation. BMC Genomics. 2020;21(6):1–13.

135. Banos O, Galvez J-M, Damas M, Pomares H, Rojas I. Window size impact in human activity recognition. Sensors. 2014;14:6474–99.

136. Sarada B, Dandu M, Tarun SK. A comparison of tree based classification and neural network based classification. In: Proceedings of the 21st International Arab Conference on Information Technology; 2020 Nov 28-30; Al Ain University of Science and Technology, Al Ain, UAE: IEEE; 2020. p. 1–3.

137. Bonomi AG, Goris AHC, Yin B, Westerterp KR. Detection of type, duration, and intensity of physical activity using an accelerometer. Med Sci Sports Exerc. 2009;1770–7.

138. Sparks AM, Smith AMS. Accuracy of a lidar-based individual tree detection and attribute measurement algorithm developed to inform forest products supply chain and resource management. Forests 2022;13(3):1-15.

139. Pebesma E, Bivand R, Racine E, Sumner M, Cook I, Keitt T, et al. sf: simple features for R [Internet]. 2021. Available from: https://CRAN.R-project.org/package=sf

140. Prusa J, Khoshgoftaar TM, Dittman DJ, Napolitano A. Using random undersampling to alleviate class imbalance on tweet sentiment data. In: Proceedings of the IEEE 16th International Conference on Information Reuse and Integration; 2015 Aug 13-15; San Francisco, CA, USA: IEEE; 2015.

141. Goyal A, Rathore L, Sharma A. SMO-RF: a machine learning approach by random forest for predicting class imbalancing followed by SMOTE. Mater Today Proc. 2021;

142. Elrahman SMA, Abraham A. A review of class imbalance problem. J Netw Innov Comput. 2013;1:332–40.

143. Westra BL, Dey S, Fang G, Steinbach M, Kumar V, Oancea C, et al. Interpretable predictive models for knowledge discovery from home-care electronic health records. J Healthc Eng. 2011;2(1):55–74.

144. Kamei Y, Monden A, Matsumoto S, Kakimoto T, Matsumoto K. The effects of over and under sampling on fault-prone module detection. In: Proceedings of the First International Symposium on Empirical Software Engineering and Measurement; 2007 Sept; IEEE; 2007. p. 196–204.

145. Dittman DJ, Khoshgoftaar TM, Napolitano A. The effect of data sampling when using random forest on imbalanced bioinformatics data. In: Proceedings of the IEEE 16th International Conference on Information Reuse and Integration; 2015 Aug 13-15; San Francisco, CA, USA: IEEE; 2015. p. 457–63.

146. Li W, Guo Q, Jakubowski MK, Kelly M. A new method for segmenting individual trees from the lidar point cloud. Photogramm Eng Remote Sens. 2012;78(1):75–84.

147. Balsi M, Esposito S, Fallavollita P, Nardinocchi C. Single-tree detection in high-density lidar data from UAV-based survey. Eur J Remote Sens. 2018;51(1):679–92.

148. Eysn L, Hollaus M, Lindberg E, Berger F, Monnet J-M, Dalponte M, et al. A benchmark of lidar-based single tree detection methods using heterogeneous forest data from the alpine space. Forests. 2015;6:1721–47.

149. Dong T, Zhou Q, Gao S, Shen Y. Automatic detection of single trees in airborne laser scanning data through gradient orientation clustering. Forests. 2018;9(219):1–19.

150. Aijazi AK, Checchin P, Malaterre L, Laurent Trassoudaine. Automatic detection and parameter estimation of trees for forest inventory applications using 3D terrestrial lidar. Remote Sens. 2017;9(946):1–24.

151. White JC, Coops NC, Wulder MA, Vastaranta M, Hilker T, Tompalski P. Remote sensing technologies for enhancing forest inventories: a review. Can J Remote Sens. 2016;42(5):619–41.

152. Paziewski J. Recent advances and perspectives for positioning and applications with smartphone GNSS observations. Meas Sci Technol. 2020;31:1–13.

153. Paziewski J, Fortunato M, Mazzoni A, Odolinski R. An analysis of multi-GNSS observations tracked by recent android smartphones and smartphone-only relative positioning results. Meas Sci Technol. 2021;175(109162):1–16.

154. Tomastík J, Chudá J, Tunák D, Chudý F, Kardos M. Advances in smartphone positioning in forests: dual-frequency receivers and raw GNSS data. Forestry. 2021;94:292–310.

155. Darugna F, Wübbena J, Ito A, Wübbena T, Wübbena G, Schmitz M. RTK and PPP-RTK using smartphones: from short-baseline to long-baseline applications. In: Proceedings of the 32nd International Technical Meeting of the Satellite Division of the Institute of Navigation; Miami, FL, USA; 2019. p. 3932–45.

156. Robustelli U, Paziewski J, Pugliano G. Observation quality assessment and performance of gnss standalone positioning with code pseudoranges of dual-frequency android smartphones. Sensors. 2021;21(2125):1–19.

157. Dabove P, DiPietra V, Piras M. GNSS positioning using mobile devices with the android operating system. Int J Geo-Inf. 2020;9(220):1–13.

158. Dabove P, DiPietra V. Towards high accuracy GNSS real-time positioning with smartphones. Adv Space Res. 2019;63:94–102.

Conclusion

The results from the study in Chapter 2 showed pre-treatment stand density metrics only accounting for tree number per unit area, such as trees per hectare (TPH), were poor predictors of resulting surface fuel loads following mechanical fuel treatments with the sampling design and sample size evaluated. TPH prior to treatment was not directly related to the distribution of fuel time-lag classes within the fuel bed, although the percentage of 10-h fuels could be predicted from pre-treatment conditions. However, stand density index (SDI), which accounts for both the relative stem number and DBH of the stand, could be used to predict post-treatment fuel loading across the study area. Further, SDI predicted that as the density of stands increase, a greater percentage of the overall fuel load consisted of 100-h fuels, while 10-h fuels decreased in percentage. Future modeling efforts should continue accounting for stem number and stem size, as stand density alone may not provide the necessary predictive ability. Stand density measures, such as SDI, provide greater insight into stand composition and overall stand biomass, which is significant when predicting fuel load volumes resulting from the physical conversion of standing biomass to mulched surface fuels.

Revisiting the methods discussed in Chapter 2, while taking into account the sampling considerations mentioned, is an important future research opportunity. The growth of LiDAR-derived models to map individual-tree locations and stem characteristics, coupled with onboard GNSS modeling of spatially, explicit, real-time equipment activities, offer the promise of improved high-resolution fuel bed prediction in the immediate future. Future work should address these factors more closely, though the determination of their impacts will likely require sampling at a higher intensity than that performed in this study, or with a sampling design that directly accounts for the spatial resolution at which comminuted material is scattered as a function of localized stand density, treatment prescription, topography, equipment type and size, and the pattern of equipment movements.

The definition of work in forest operations using global navigation satellite system with radio frequency (GNSS-RF) based data and inertial measurement units (IMUs) is becoming increasingly possible. The development of activity recognition models using mobile technologies is an important advancement for digitalization of the forest supply chain. Further, the increasing availability of high resolution products from lidar and other remotely sensed data may further advance the robustness and utility of activity recognition models for research and operational uses.

In Chapter 3, we identified the challenges and limitations of classifying individual cycle elements with high accuracy using spatially explicit data from GNSS-RF devices. However, GNSS-

RF transponders were shown to provide a consumer-available solution for activity recognition for mastication treatments that effectively classified the difference between delay and productive elements over 95% of the time. Despite exposing some challenges and limitations associated with use of consumer-grade GNSS-RF for individual element-level activity recognition, RF enabled components still provide reliable and real-time data sharing capabilities. Recent improvements to GNSS accuracy using real-time correction (RTK) methods, increased sampling rates, and the integration of inertial measurement units (IMUs) address limitations identified in this study. Therefore, GNSS-RF devices should be reconsidered for use in real-time element level activity recognition modelling, particularly models with these improvements.

Continued advances in remote sensing, mobile and GNSS-capable technologies is encouraging a paradigm shift from a stand level, area-based management to a precision forestry and individual tree-centric approach to forest management and operational digitalization. Applying these resources into the planning, implementation and assessment of forest management practices will enable the innovation, growth, and improvements necessary to address current and future challenges of sustainable forest management. Developing consumer-accessible and flexible technological solutions, like the one assessed in chapter 3, may increase the application and utilization of these resources, and provide greater opportunity for contractors, researchers, and land managers to advance their fields and ensure their continued and increased effectiveness.

In Chapter 4, we showed that activity recognition models developed from the sensors on smartphones placed in machine cabs can recognize activities of mechanical fuel treatments in forested stands with balanced accuracies for elements between 87.41% and 97.70%. This is the first known smartphone-based activity recognition study for mechanical forestry equipment. By demonstrating the application of this technology to elemental time studies and production analysis, we have advanced research supporting a ubiquitous smartphone-based activity recognition solution for forestry equipment. Further refining field sampling procedures, model processing and integration of new mobile technologies to enable the collection of sensor and accurate positional data from a single device should be studied in the future. Additional field sampling with varying topographic and stand conditions, operators, and equipment types should also be completed to help quantify the extent to which these factors may impact activity recognition performance.

Forest digitalization and precision forestry is increasingly shaping the future trajectory of natural resource management and forest operations. Increased innovation and adaptation of mobile technologies, remote sensing, and machine learning provide unique opportunities to advance the

processes and resources used to manage forestlands. The research presented in this dissertation provides insight into opportunities to advance the planning, implementation, and assessment of forest operations through the integration of mobile technologies and remotely sensed data. Successful development and deployment of technological solutions to management challenges in forest operations provide the means to improve the efficiency, effectiveness, safety, and sustainability of forest management practices and ensures land managers are equipped with the most advanced resources necessary to meet the needs of forestry in the future.